On the Universal Physics of Smelly Flocks

by

Maxx Miller

A dissertation accepted and approved in partial fulfillment of the
requirements for the degree of
Doctor of Philosophy
in Physics

Dissertation Committee:
Jayson Paulose, Chair
John Toner, Advisor
Ben Farr, Core Member
Marina Guenza, Institutional Representative

University of Oregon
Spring 2025

DISSERTATION ABSTRACT

Maxx Miller

Doctor of Philosophy in Physics

Title: On the Universal Physics of Smelly Flocks

We develop and study the hydrodynamic theory of flocking with autochemotaxis. This describes large collections of self-propelled entities all spontaneously moving in the same direction, each emitting a substance which attracts the others (e.g., ants). The theory combines features of the Keller-Segel model for autochemotaxis with the Toner-Tu theory of flocking. We find that sufficiently strong autochemotaxis leads to an instability of the uniformly moving state (the "flock"), in which bands of different density form moving parallel to the mean flock velocity with different speeds. These bands, which are reminiscent of ant trails, coarsen over time to reach a phase-separated state, in which one high density and one low density band fill the entire system. The same instability, described by the same hydrodynamic theory, can occur in flocks phase separating due to any microscopic mechanism (e.g., attractive interactions). Although in many ways analogous to equilibrium phase separation via spinodal decomposition, the two steady state densities here are determined not by a common tangent construction, as in equilibrium, but by an uncommon tangent construction very similar to that found for motility induced phase separation (MIPS) of disordered active particles. We demonstrate that phase separation in flocks, or ordered polar active fluids, belongs to a new universality class, completely different from that of phase separation in equilibrium fluids. The upper critical dimension for this transition is $d_c = 5$, in contrast to the well-known $d_c = 4$ of equilibrium phase separation. With a dynamical renormalization group analysis, we obtain the large-

distance, long-time scaling laws of the velocity and density fluctuations, which are characterized by universal critical correlation length and order parameter exponents $\nu_\perp$, $\nu_\parallel$ and β respectively. We calculate these to $\mathcal{O}(\epsilon)$ in a $d = 5 - \epsilon$ expansion.

This dissertation includes previously published co-authored material.

CURRICULUM VITAE

NAME OF AUTHOR: Maxx Miller

GRADUATE AND UNDERGRADUATE SCHOOLS ATTENDED:

University of Oregon, Eugene, OR, USA
Embry-Riddle Aeronautical University, Daytona Beach, Florida, USA.

DEGREES AWARDED:

B.S. Space Physics, 2018, Embry-Riddle Aeronautical University
B.S. Aerospace Engineering, 2018, Embry-Riddle Aeronautical University

AREAS OF SPECIAL INTEREST:

Flocks, Nonequilibrium physics, agent-based-modeling, condensed matter

PROFESSIONAL EXPERIENCE:

Graduate Teaching Assistant, University of Oregon, 2019 – 2025

GRANTS, AWARDS AND HONORS:

Weiser Senior Teaching Aware 2023, 2024, 2025

PUBLICATIONS:

M. Miller, J. Toner, Phys. Rev. Lett. 132, 128301 (2024)

M. Miller, J. Toner, Phys. Rev. E 110, 054607 (2024)

M. Miller, J. Toner, Phys. Rev. E 109, 034606 (2024)

ACKNOWLEDGEMENTS

I am thankful to my wife, Isabelle. Our odyssey is already an epic, yet we have just begun. I love you dearly. I could and would fill tomes, but I'll stop here as to not spoil the moment.

I am thankful to my advisor John Toner, to whom I am most grateful for taking me on as his final student. From a technical perspective I have learned a tremendous amount from him. From a personal and professional point of view I have learned to engage with both life and our discipline in a more genuine, curious, kind and joyous way.

I am thankful to my wonderful lap-cat Totoro, whose soothing purring and goofy meows have brought so much light to my life.

I am thankful to my family, my friends, my fellow graduate students and the GTFF for making my success in graduate school possible.

Finally, I am thankful to the billions who toil ceaselessly.

To those who struggle to understand our home.

To those who struggle for those who inhabit it.

To those who struggle through failures, bad days, crushed dreams, imperfect educations and exploitation.

To you, my cherished reader.

TABLE OF CONTENTS

Chapter Page

Chapter Page

LIST OF FIGURES

Figure Page

CHAPTER 1

INTRODUCTION

I'll begin by explaining the title of this work. By "universal physics" I do not mean physics that applies to the entirety of all things. I do mean physics that applies to any system which falls into the category of "smelly flocks". Also, I do not mean that my treatment is universal in the sense it is a totalizing description of "smelly flocks". By "flock" I mean a collection of creatures that have a tendency to follow one another, like a flock. The adjective "smelly" here is used in a complimentary way as a "smelly flock" describes a flock who's constituents are *attracted* to one another through some mechanism (e.g., attractive chemicals emitted by other flockers).

The last two chapters of this work have been published in joint authorship with John Toner.

1.1 This Work

Consider a trail of migrating ants. More specifically, imagine a large collection of ants in a featureless plane traveling in roughly the same direction all aggregated into an ant trail. Most of the plane is devoid of any ants except for the high density band(s) of ants that form the trail. Collectively, these ants form a flock and are an exemplar of a novel phase in flocking.

The purpose of this work is to detail an analytical description of the formation and shape of this novel phase. The scope of our description is limited to the vicinity of the critical point belonging to the phase transition.

Flocking is the collective coherent motion of a large number of organisms [43]. Across the Earth, flocking is ubiquitous. Many motile organisms, across many length scales, flock [45, 31, 14, 19]. Bees swarm, fish school, buffalo herd, ants trail, and birds flock. It is not necessary that flockers are living creatures, as there are synthetic examples of flocks[7]. Any entity, that is capable of moving on its own, with a tendency to follow its neighbors can form a flock with them. A nonzero mean speed of the flock is an example of coherent collective motion. Examples include a flock of birds migrating north and a trail of migrating ants.

Understanding the dynamics of any given flocker can be a very difficult task. After all, any given animal is much more complicated than, say, a point mass bouncing around a given volume. One might be concerned with how muscles move to articulate limbs, how decisions are being made in

the brain, or how sensory organs transmit information. However, as we do in studying, e.g., the dynamics of interacting gas particles in a room at some finite temperature, we can concern ourselves with only the macroscopic behavior and properties of flocks. Much work has already been done to understand the macroscopic properties of flocking. Toner-Tu theory is the hydrodynamic theory of flocking. Just as the hydrodynamics of fluids are described by the Navier-Stokes equations[35], the hydrodynamics of flocks are described by the Toner-Tu equations [43, 46, 42, 44, 41]. In this work we will use Toner-Tu theory to examine the structure and universal properties of flocks as flockers aggregate due to strong attractive interactions.

Continuing with the example of ant trails, autochemotaxis can provide these sufficiently strong attractive interactions. Ants, like nearly all motile organisms [39], utilize chemical gradients to navigate their environment [13, 16]. This behavior is known as "chemotaxis". A graduate student who smells free food and approaches a seminar is an example of chemotaxis. Ants, however, emit a substance to which they themselves and other ants are attracted [13, 16]. This phenomenon is known as "autochemotaxis". Naturally, such a behavior leads to the aggregation of organisms[25, 24, 26, 21, 38]. Flocking ants will follow their neighbors with a bias in the direction of the concentration of the attractive substance. Keller and Segel developed continuum equations that describe the evolution of systems subjected to chemotaxis [25, 24, 26]. The equations can be configured to describe autochemotaxis [20].

There is nothing special about autochemotaxis and its aggregating effects. Any kind of attractive interactions between flockers can lead to aggregation. The work presented here is valid for any mechanism of attraction. However, we will show in great detail how autochemotaxis can provide sufficiently strong interactions.

The phase transition occurs when attractive interactions overcome the flocking analogue of the pressure. That is, it occurs when dense regions of flockers no longer try to spread out, but begin to attract more flockers. When this occurs, the low-density regions become less dense and the high-density regions become more dense. This is what we mean by "sufficiently strong interactions". The result of this transition is to separate space into high and low density regions. In our ant flock example, the high density region corresponds to the ant trail and the low density regions correspond to the open spaces adjacent to the ant trail containing relatively few ants. This is the same mechanism which leads to liquid-gas phase separation in simple fluids [10].

The Questions to be Answered in this Work

The purpose of this text is to answer the following questions:

What does Toner-Tu theory predict if we explore the instability resultant from a negative compressibility? In what way is a homogeneous flock affected by this instability? What is the mechanism that generates divergences? What is the shape of the flock after it phase separates? What is the critical dimension for the linear theory? What are the critical exponents? What are the expansions for the critical exponents for dimensions lower than the critical dimension?

We will elaborate on and answer all of these questions (and more!) in great detail in the subsequent chapters. Before we do so, let us briefly set the stage with some information about the structure of this document.

Introduction to the Structure of this Work

The Notation and Terms used in this Work

The mathematical notation used in this work follows the standard used by the American Physical Society. As a common example of this standard, a vector quantity will be bolded (e.g., $\mathbf{a}$) whereas scalar quantities are unbolded (e.g., a).

Conventions used in this Work

When we preform a Fourier transform in this work we assume all the fields are proportional to $exp[i\mathbf{q}\cdot\mathbf{r} - i\omega t]$. That is for any field $a(\mathbf{r},t)$ we assume the Fourier transform is computed as:

$$a(\mathbf{q},\omega) = \int_t \int_{\mathbf{r}} e^{-i(\mathbf{q}\cdot\mathbf{r}-\omega t)} a(\mathbf{r},t), \tag{1.1.1}$$

where $\int_t \equiv \int dt$ and $\int_{\mathbf{r}} \equiv d^d r$. The inverse is then given by:

$$a(\mathbf{r},t) = \int_\omega \int_{\mathbf{q}} e^{i(\mathbf{q}\cdot\mathbf{r}-\omega t)} a(\mathbf{q},\omega), \tag{1.1.2}$$

where we use the short hand notation $\int_\omega \equiv \int \frac{d\omega}{2\pi}$ and $\int_{\mathbf{q}} \equiv \int \frac{d^d q}{(2\pi)^d}$.

Structure of this Dissertation

The structure of this work is as follows. In this chapter we briefly introduce the reader to Toner-Tu theory. Then we briefly discuss the instability and compare it to equilibrium phase separation. Then we review the results of the dynamical renormalization group calculation.

In the next chapter, we combine the Keller Segel equations with Toner-Tu theory. We show that autochemotaxis in particular and attractive interactions in general can lead to a instability. We explore this instability in detail, we develop an intuitive understanding of the mechanism of aggregation, we construct a phase diagram around the critical point that controls our phase transition and finally we study the resulting steady state shape of the flock after phase separation.

In the final chapter, we include the effect of fluctuations and compute, using the dynamical renormalization group, corrections to the shape of our phase diagram. In addition, we compute several universal scaling features.

The appendix contains a lengthy supplemental calculation for the dynamical renormalization group calculation done in the final chapter.

Introduction to Toner-Tu Theory

A familiar form of motion is the phenomenon of flocking. Flocking is the collective coherent motion of a large number of organisms. Examples include: a school of fish, a swarm of bees, or a flock of birds. Such motion can occur any time creatures exhibit a tendency to follow their neighbors. Strikingly, even purely short ranged interactions prove to be sufficient to generate long-ranged orientational order, even in an arbitrarily large flock, even in two dimensions[43, 46, 42, 44], in contrast to equilibrium systems, in which the development of long-ranged orientational order in a rotation invariant system with purely short-ranged interactions is forbidden by the "Mermin-Wagner-Hohenberg Theorem"[30].

Inspired by the work of Viscek and the historical progression of hydrodynamics, a hydrodynamic theory of flocking was developed by Toner and Tu. [43, 46, 42, 44, 41].

The theory describes a flock composed of active, self-propelled particles moving over a frictional substrate, so that momentum is not conserved and time reversal symmetry is broken. In the jargon of the active matter field, this is called a "dry" flock. The underlying dynamical rules are assumed to be rotation and translation invariant. These symmetries, together with the requirement that

the total number of birds is conserved (that is, we ignore birth and death "on the wing") strongly constrain the form of the theory. In particular, they determine which variables we need to keep in a long-wavelength, long-time theory (which is what we mean by a "hydrodynamic" theory).

In all hydrodynamic theories, it is sufficient to keep only the "slow" variables; that is, the variables which evolve slowly at long length scales. More precisely, this means the variables whose time scales of evolution diverge as the length scale under consideration does.

There are only two generic reasons that a variable will be slow in this sense: it must either be associated with a conserved quantity like boid number, or be a "Goldstone mode" arising from a broken continuous symmetry. For a dry flock as defined above, the only conserved quantity is boid number; the associated hydrodynamic field is the coarse grained number density of boids $\rho(\mathbf{r}, t)$. Since an ordered flock spontaneously breaks the continuous rotational symmetry of the underlying dynamics, the boid velocity field $\mathbf{v}(\mathbf{r}, t)$ (or, more precisely, its components perpendicular to the mean velocity of the ordered state) is a Goldstone mode, and hence, also slow.

The equations of motion for these fields keep all terms that are "relevant", in the renormalization group sense of affecting the scaling of the system at long distances and times, and that are consistent with the symmetry (rotation invariance) and conservation law (boid number) of the system. The requirement of "relevance" is largely met by performing a gradient expansion. As shown by [43, 46, 42, 44], this forces the equations of motion to be of the form:

$$\begin{aligned}
&\partial_t \mathbf{v} + \lambda_1(\mathbf{v}\cdot\nabla)\mathbf{v} + \lambda_2(\nabla\cdot\mathbf{v})\mathbf{v} + \lambda_3\nabla(|\mathbf{v}|^2) = \\
&\quad U(|\mathbf{v}|,\rho)\mathbf{v} - \nabla P_1(|\mathbf{v}|,\rho) - \mathbf{v}(\mathbf{v}\cdot\nabla P_2(|\mathbf{v}|,\rho)) + D_B\nabla(\nabla\cdot\mathbf{v}) + \\
&\quad D_T\nabla^2\mathbf{v} + D_2(\mathbf{v}\cdot\nabla)^2\mathbf{v} + \mathbf{f} \qquad (1.1.3)\\
&\partial_t\rho + \nabla\cdot(\mathbf{v}\rho) = \nabla\cdot\mathbf{f}_\rho \qquad (1.1.4)
\end{aligned}$$

The significance of each of the terms in these equations is as follows:

The terms involving the parameters λ_i are analogs of the convective derivative of the coarse grained velocity field in the Navier-Stokes equations. If our system respected Galilean invariance, we would have $\lambda_1 = 1$ and $\lambda_{2,3} = 0$. However, because our flock is on a frictional substrate, which provides a special reference frame, we have neither Galilean invariance nor momentum conservation.

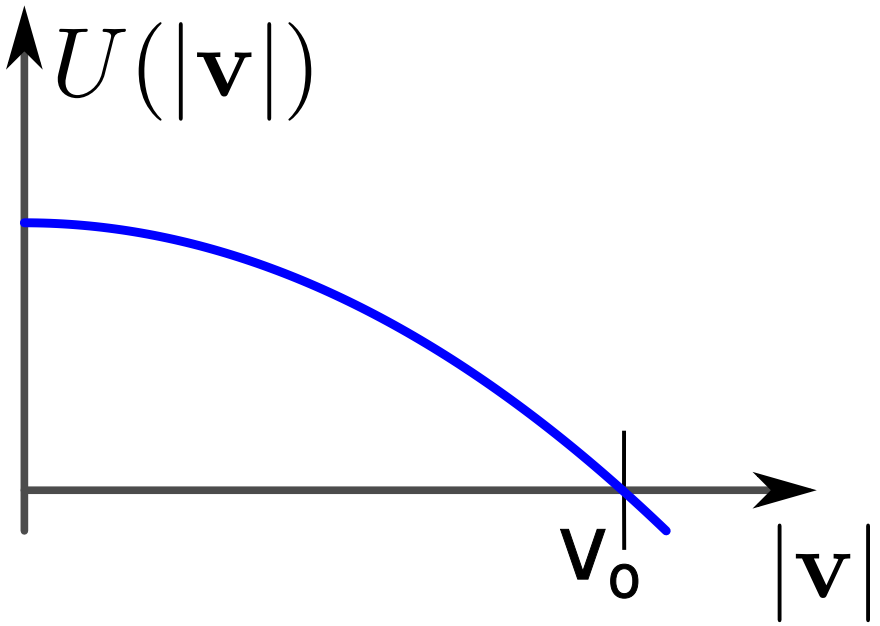

FIGURE 1. A plot of $U(|\mathbf{v}|, \rho)$ for fixed ρ. The effect of this term is to maintain a non-zero speed, v_0, of the flock. Boids will accelerate if their speed is below v_0 and decelerate if their speed is larger than v_0.

Physically these three terms account for the flockers', or boids', tendency to follow and align with one another.

The $U(|\mathbf{v}|, \rho)$ term, which is similar in form to a dissipative term, clearly therefore also breaks both Galilean invariance and momentum conservation. However, because our system is active, $U(|\mathbf{v}|, \rho)$ need not be negative for all $|\mathbf{v}|$. Indeed, if we are to model a system in which the steady state is a *moving* flock, we must take it to have the form illustrated in figure 1. In earlier literature[43, 46, 42, 44, 40], the special choice $U(|\mathbf{v}|, \rho) = \alpha - u|\mathbf{v}|^2$ is often made. This is by no means necessary, however. Therefore, here we will make no assumptions about the precise form of $U(|\mathbf{v}|, \rho)$, other than that it is analytic in $|\mathbf{v}|$ and ρ, and that it has the qualitative shape illustrated in (1). Physically, this term ensures boids tend to maintain some finite and non-zero velocity. Should a boid be traveling slower than the locally preferred speed the boid will increase its speed and vice versa should it be traveling faster than the locally preferred speed. Note that U depends on both $|\mathbf{v}|$ and ρ, so, in general, the locally preferred speed is not uniform across space.

The P_1 term is perfectly analogous to the isotropic pressure in the Navier-Stokes equations. The P_2 term is an "anisotropic pressure", and is allowed because our system breaks rotation invariance

locally, which means that there is no reason that the response to density gradients *along* the local velocity $\mathbf{v}$ should be the same as that to gradients perpendicular to $\mathbf{v}$. Note that this term also breaks Galilean invariance. The anisotropic pressure will not play a significant role in this work. The isotropic pressure term does play significant role in this work. Physically these terms represent a tendency for flockers to flow from high density to low density regions, assuming, of course, they maintain positive coefficients.

The velocity diffusion constants D_B and D_T are precise analogs of the bulk and shear viscosities, respectively, in the Navier-Stokes equations. The diffusion constant D_2 is an anisotropic viscosity which has no analogue in the Navier-Stokes equation, because it violates Galilean invariance. Since we lack Galilean invariance here, it is allowed in our problem. All of these viscosities have the effect of suppressing fluctuations of the velocity away from spatial uniformity.

The quantities $P_{1,2}(|\mathbf{v}|, \rho)$, $U(|\mathbf{v}|, \rho)$, $D_{B,T,2}$, and $\lambda_{1,2,3}$ are in general functions of $|\mathbf{v}|$ and ρ. They can *not* depend of the *direction* of $\mathbf{v}$ due to rotation invariance.

The quantities $\nabla \cdot \mathbf{f}_\rho$ and $\mathbf{f}$ are noise terms. They account for fluctuations, which will always be present in real systems. In order to conserve boid number the divergence of $\mathbf{f}_\rho$ is taken. Later in this work we will assume our noise terms have Gaussian white noise correlations. Should one be motivated to remove the divergence acting on $\mathbf{f}_\rho$ and still want to conserve boid number, one could not assume it has Gaussian white noise correlations.

The Toner-Tu equations admit solutions that describe a flock at some homogeneous density, ρ_0, with a non-zero mean velocity, v_0:

$$\rho(\mathbf{r}, t) = \rho_0, \tag{1.1.5}$$

$$\mathbf{v} = v_0 \hat{x}. \tag{1.1.6}$$

The direction that flock travels is arbitrary due to the rotation invariance of our model. We always choose our coordinate system so that the x-axis is along that direction of spontaneous velocity. We will stop here for now and proceed in different ways later in this work.

Before we continue, we reiterate that Toner-Tu theory is only concerned with long-length and -time scale phenomenon. To avoid having an infinitely complex theory, we had to cut off our gradient expansion. Our platonic ideal of a flock is one which is infinitely large, as it has enough room for *all* long-length and -time scale phenomenon. By large, we mean the ratio of breadth of the flock to

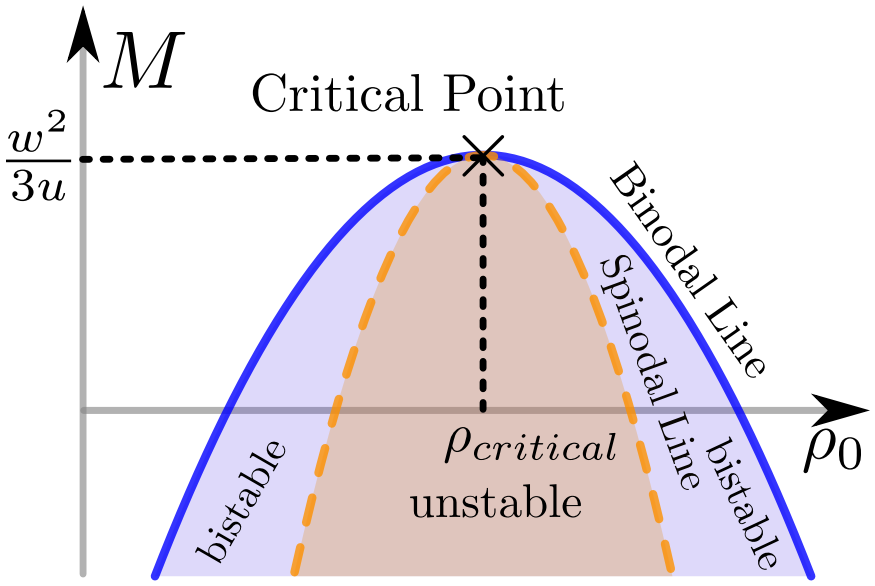

FIGURE 2. Phase diagram of flock phase separation. The solid blue and dashed orange curves are the binodal and spinodal lines respectively. In the orange filled region under the spinodal line, which is labeled "unstable"; only the two-phase state is stable. In the blue region between the spinodal and binodal lines, both the two phase state, and the homogeneous, one phase state, are stable. The analysis we perform in this work is done close to the critical point, where our assumption that density variations are small is valid. Both the binodal and spinodal lines here are parabolas. This is because the analysis that produced this phase diagram ignores fluctuations.

largest microscopic length (e.g., the "mean free path" of a boid). So, a flock of bacteria in a droplet of water could be larger than a flock of locusts in route to unlucky corn field. Real flocks are often not infinitely large, so their long-length and time scale dynamics will unavoidably be influenced by the fast-complex-microscopic motion of the boids; however, as the size of the flock grows our theory will become asymptotically accurate. The Navier-Stokes equation is confined by the same limitation; although, atoms and molecules are much smaller than any real life example of a motile organism.

The Instability

The inclusion of attractive interactions provides a mechanism that can lead to aggregation of boids. This will happen once the pressure forces are overcome by the attractive interactions. Our instability forms out of the homogeneous flock state mentioned in the previous section. Our instability has similarities with equilibrium liquid-vapor phase separation. For example, the phase diagram of flock phase separation, depicted in figure 2, is nearly identical to the phase diagram for equilibrium liquid-vapor systems. We will construct this diagram later in this work.

In this diagram M plays the role of temperature in the analogy to equilibrium phase separation. *In equilibrium phase separation* the left hand region above the binodal line corresponds to a homogeneous vapor state (low density) and the right hand region corresponds to a homogeneous liquid state (high density). Above the critical point the distinction between liquid and vapor vanishes and systems that exist there are known as a supercritical fluid. The region below the spinodal line is unstable to homogeneous fluids and they will spontaneously decompose into a mixture of regions composed of liquid and vapor phases (i.e., phase separation). For example, consider a fixed volume full of water vapor. If we forcefully pump more vapor into our fixed volume a mixed state will eventually form with the nucleation of liquid water. The shape of the those small nucleation sites will be determined by the interfacial tensions between the liquid water and the water vapor (spheres). The regions between the binodal and spinodal lines are, *in equilibrium phase separation*, known as the metastable regions. In this metastable region, mixed states are stable and energetically preferred; however, homogeneous fluids are *locally* stable but finitely-sized "kicks" are capable of leading to decomposition into the mixed state. To prepare a homogeneous state within the metastable region, one must traverse from the stable region into the metastable region. So the current state of the fluid within the metastable region is dependent on the path taken.

In flocks M plays the role of the compressibility of the system, or the balance between the repulsive pressure forces and the attractive interactions. Values of M above the binodal line correspond to a domination of repulsive pressure forces over the attractive interactions. In that region the homogeneous flocking state is stable. Analogous phases to liquid, vapors, and supercritical fluids exist and occupy the same regions as one would expect in the phase diagram. Beneath the spinodal line homogeneous flocks are unstable and will spontaneously decompose into a mixed phase of high and low density regions. The shape of of these regions, as we will show later, will be that of long bands oriented such that they are parallel to the direction of mean flock motion. The shape of the boundary between these regions is set by the balance of attractive interactions and diffusion of boids. The region between the binodal and spinodal lines is a bistable region. Within the bistable region both the homogeneous and mixed phases are locally stable. Since flocks are *nonequilibrium* systems we have no analogous criterion to global free energy minimization available for equilibrium systems to determine which state is "preferred".

The analysis that produces this phase diagram is entirely "mean-field": that is, it ignores fluctuations in the local density and velocity (i.e., noise terms were set to zero). The inclusion of fluctuations shows us that the shape of the spinodal and binodal lines are not parabolas. This is also the case for equilibrium liquid-vapor separation.

The New Universality Class

One of the most important ideas in Condensed Matter Physics is the concept of "universality", which asserts that it is *only* the symmetries and conservation laws describing a given phase of matter, or the transitions between different states, that determine the long-distance, long-time properties of those phases and transitions[10, 27]. The microscopic details of the system in question do not affect these long-distance, long-time properties.

More recently, it has been realized that non-equilibrium systems and phase transitions can belong to *different* universality classes than their equilibrium counterparts.

Fluctuations in the density are well-known[10, 27] to radically change the scaling behavior of the density near the critical point in equilibrium systems. In active polar ordered flocks, fluctuations are even more important, because, in addition to the density field, which has large fluctuations because it is becoming "soft" near (and at) the critical point, the local velocity field of the flock (or, more precisely, its components perpendicular to the mean velocity $\langle \mathbf{v} \rangle$) are Goldstone modes, and so have large fluctuations themselves.

Hence, to understand the true behavior of the system near the critical point in figure 2, and the shape of the phase boundaries themselves there, we therefore clearly must include the effect of fluctuations. We do so in this work, by performing a dynamical renormalization group (DRG) analysis of the hydrodynamic theory of polar ordered active fluids (a.k.a. the "Toner-Tu equations" [43, 46, 42, 44, 40]) near the critical point, in the presence of noise which drives fluctuations.

We have calculated a number of universal exponents characterizing the scaling behavior near the critical point using the DRG in an $\epsilon = 5 - d$ expansion. The first of these is the usual exponent β giving the width $\delta\rho$ of the binodal and spinodal curves in figure 2. Those widths both scale as a power law in the distance $M_c - M$ from the critical point:

$$\delta\rho \propto |M - M_C|^{\beta} , \tag{1.1.7}$$

We find

$$\beta = \frac{1}{2} - \frac{\epsilon}{6} + \mathcal{O}(\epsilon^2)\,. \tag{1.1.8}$$

In addition, we have calculated the correlation length exponent ν. Or, to be more precise, we find *two* correlation length exponents $\nu_{\perp,\parallel}$ for the divergences of the correlation lengths $\xi_{\perp,\parallel}$ perpendicular and parallel to the direction of mean flock motion, respectively. These are defined by

$$\xi_{\perp,\parallel} \propto |M - M_C|^{\nu_{\perp,\parallel}}\,. \tag{1.1.9}$$

We find

$$\nu_\perp = \frac{1}{2} + \frac{\epsilon}{12} + \mathcal{O}(\epsilon^2)\,, \tag{1.1.10}$$

and

$$\nu_\parallel = 1 + \frac{\epsilon}{6} + \mathcal{O}(\epsilon^2)\,. \tag{1.1.11}$$

In addition to this anisotropy in correlation lengths, which does not occur for equilibrium phase separation, the interpretation of the correlation lengths in phase separating flocks is also different. In equilibrium phase separation, the correlation length is the length scale on which density correlations decay exponentially; that is

$$C_{\rho\rho}^{\text{equilibrium}}(\mathbf{r}) \equiv \langle \delta\rho(\mathbf{r}+\mathbf{R})\delta\rho(\mathbf{R})\rangle \propto e^{-r/\xi}, \tag{1.1.12}$$

where $\delta\rho(\mathbf{r},t) \equiv \rho(\mathbf{r},t) - \rho_c$ is the departure of the local number density $\rho(\mathbf{r},t)$ at position $\mathbf{r}$ and time t from its mean value ρ_c.

In contrast, in phase separating flocks, the correlation lengths $\xi_{\perp,\parallel}$ are the length scales at which the density-density correlation function $C_{\rho\rho}(\mathbf{r})$ crosses over from one power law decay to another.

That is

$$C_{\rho\rho}(\mathbf{r}_\perp, r_\parallel = 0) \propto \begin{cases} r_\perp^{2\chi_\perp^c} & , \ r_\perp << \xi_\perp \\ \\ r_\perp^{2\chi_\perp} & , \ r_\perp >> \xi_\perp \end{cases} \tag{1.1.13}$$

for points separated in the direction perpendicular to the direction "($\parallel$)" of mean flock motion, and

$$C_{\rho\rho}(\mathbf{r}_\perp = \mathbf{0}, r_\parallel) \propto \begin{cases} r_\parallel^{2\chi_\parallel^c} & , \ r_\parallel << \xi_\parallel \\ \\ r_\parallel^{2\chi_\parallel} & , \ r_\parallel >> \xi_\parallel \end{cases} \tag{1.1.14}$$

for points separated along the direction of mean flock motion. This behavior is illustrated in figure (3).

Our ϵ-expansion results for the critical "roughness exponents" $\chi^c_{\perp,\parallel}$ in spatial dimensions $d = 5-\epsilon$ are

$$\chi_\perp^c = -2 + \frac{\epsilon}{2} + \mathcal{O}(\epsilon^2) \tag{1.1.15}$$

$$\chi_\parallel^c = -4 + \epsilon + \mathcal{O}(\epsilon^2) \tag{1.1.16}$$

In $5-\epsilon$ dimensions, the *non*-critical roughness exponents are given by

$$\chi_\perp = \frac{3-d}{2} = -1 + \frac{\epsilon}{2} \tag{1.1.17}$$

$$\chi_\parallel = 3 - d = -2 + \epsilon \tag{1.1.18}$$

exactly. However, once the spatial dimension goes below $d = 4$ (which is obviously true for all physically relevant cases), the exact results (1.1.17) and (1.1.18) cease to hold. The χ's that apply then are simply those of the ordered state of a polar active fluid (i.e., a "flock") in that particular dimension of space. These exponents are known only from simulation[28], and are given in three dimensions by

$$\chi_\perp \approx \chi_\parallel \approx -0.62\,, \tag{1.1.19}$$

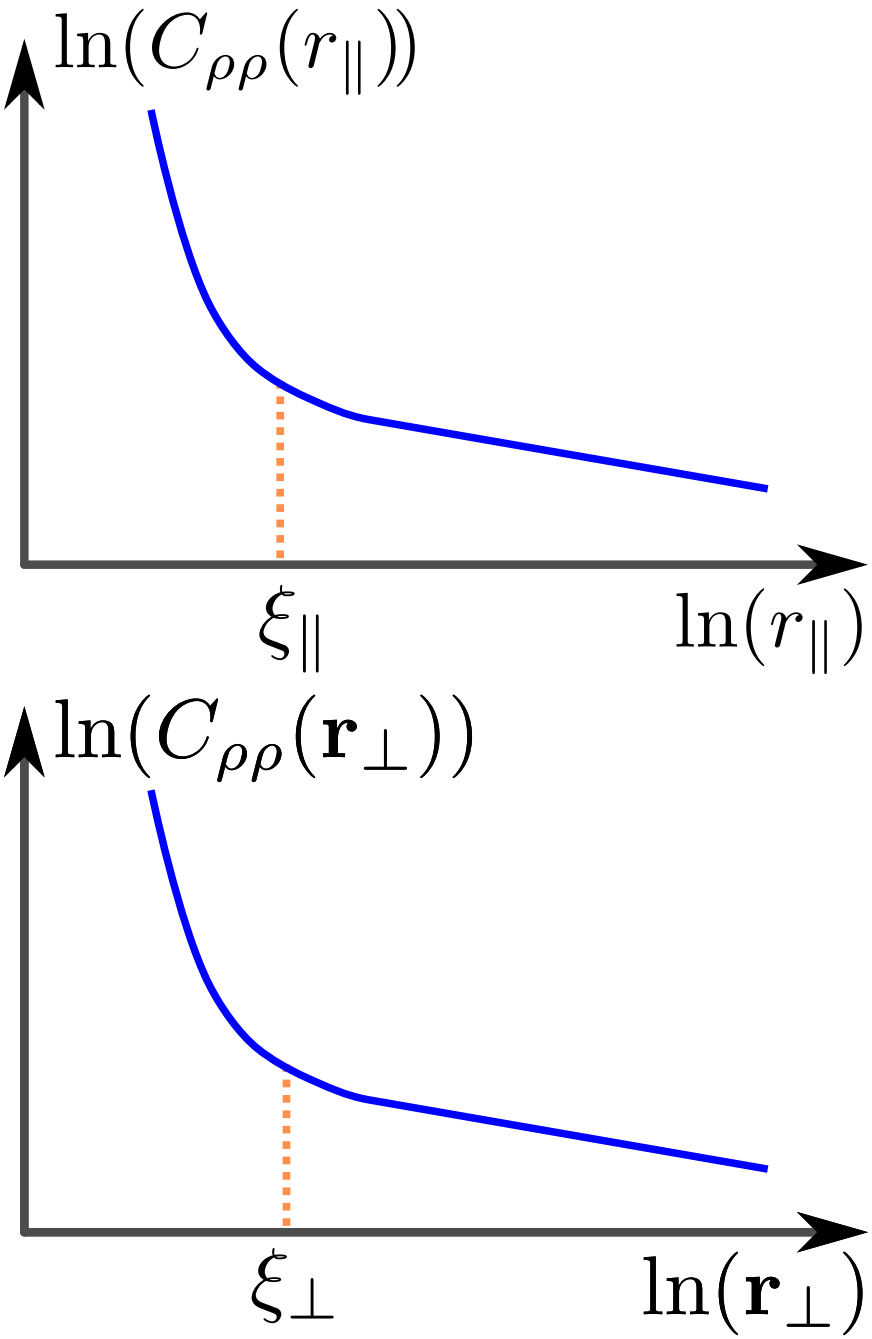

FIGURE 3. Schematic log-log plots of the density autocorrelation functions against distance in the direction of mean flock motion (top), and perpendicular to the mean direction of flock motion (bottom). In contrast to equilibrium phase separation, the density correlation decay does not drop off exponentially for distances greater than the correlation lengths. Instead, the correlation lengths $\xi_{\perp,\parallel}$ separate regions with different power law decays.

and in two dimensions by

$$\chi_\perp \approx \chi_\parallel \approx -0.31\,. \tag{1.1.20}$$

CHAPTER 2

FOLLOWING YOUR NOSE: AUTOCHEMOTAXIS AND OTHER MECHANISM FOR SPINODAL DECOMPOSITION IN FLOCKS

This work was published, in co-authorship with John Toner, in volume 109 of the journal Physical Review E in March 2024.

2.1 Autochemotaxis and Flocking

Two of the principle mechanisms of *ordered* biological motion are "taxis" and "flocking"[47, 43, 46, 42, 44]. "Taxis" is motion in response to an external stimulus. One extremely large class of this type is movement directed preferentially along the gradient of some quantity. Examples include: "thermotaxis" (following temperature gradients)[36] and "phototaxis" (light intensity) [4]. In this chapter, we focus on the extremely common example of "chemotaxis", in which motion is directed along the gradient of the concentration of a chemical substance. Almost all motile organisms perform chemotaxis [39]. Examples include: Escherichia coli[31], spongy moths[14], sperm[19], locusts [45], and ants[13, 16].

Flocking is the collective coherent motion of a large number of organisms: a school of fish, a swarm of bees, or a flock of birds. Such motion can occur any time creatures exhibit a tendency to follow their neighbors; purely short ranged interactions prove to be sufficient to generate long-ranged order, even in an arbitrarily large flock, even in two dimensions[43, 46, 42, 44], in contrast to equilibrium systems ("The Mermin-Wagner-Hohenberg Theorem")[30].

In "autochemotaxis", the chemical substance in question is secreted by the moving creatures themselves. Clearly, this can lead to aggregation of those creatures[25, 24, 26, 21, 38].

Like chemotaxis, flocking can be observed on a large range of length scales from micrometers, as in, (e.g., slime molds [15], to kilometers (e.g., locust plagues) [45]). Locust plagues can contain billions of locusts, can occupy up to a thousand square kilometers, and are capable of causing billions of dollars of damage[45].

Hydrodynamic theories of autochemotaxis without flocking[25, 24, 26, 21, 38] and flocking without autochemotaxis[43, 46, 42, 44, 41] have been successful in quantitatively explaining each of their respective phenomena in isolation. In this chapter, we develop and study a hydrodynamic

theory for systems in which *both* effects are present. We will show the presence of both effects can lead to formation of trails (e.g., ant trails[13]).

Specifically, we consider active self-propelled particles (hereafter called "boids") that move over a frictional substrate, so that momentum is not conserved and time reversal symmetry is broken. The underlying dynamical rules are assumed to be rotation and translation invariant.

We investigate the stability in the presence of autochemotaxis of an "active homogeneous polar ordered state" which spontaneously breaks the underlying rotation invariance by having all of the boids move, on average, in the same direction (i.e., "flock"). The homogeneity of the state means that translation invariance is *not* broken.

The chemotaxic element of the hydrodynamic theory is the same as that of the Keller-Segel model[25, 24, 26, 21]. Specifically, boids release a chemical signal. This chemical signal can be a substance that either repels neighboring boids (i.e., is a "chemo-repellent") or attracts them (i.e., is a "chemo-attractant"). In this chapter, we study the chemo-attractant case, in which, in addition to following their neighbors, each boid also tends to follow the local chemo-attractant concentration gradient. The chemo-attractant diffuses, and decays with a finite lifetime τ.

The "strength" of the autochemotaxis can therefore be increased by increasing any one of three parameters: the chemo attractant lifetime τ, the rate of production of the chemo attractant by the boids γ, or the coupling of their motion to the gradient of the concentration of the chemo-attractant.

The linear stability analysis of the hydrodynamic theory that we perform in this chapter shows that, like disordered active systems undergoing only autochemotaxis [38], the spatially homogeneous state of ordered flocks (or, to use the technical term, "polar ordered active fluids") becomes unstable when the autochemotaxis is sufficiently strong. However, in contrast to this instability in disordered systems, in ordered flocks the instability, near threshold, is extremely anisotropic. Specifically, plane wave modulations of the density with wavevector $\mathbf{q}$ are only unstable in a narrow region of $\mathbf{q}$ space, extended in the direction perpendicular to the direction of flock motion, as illustrated in figure 4.

As a result, the instability is towards forming "bands" in real space running *parallel* to the direction of mean flock motion. This is illustrated in figures 5 and 6.

The instability we find here is completely different from the "banding instability" [5, 41, 34, 41]. The banding instability occurs in a completely different region of parameter space[41], is

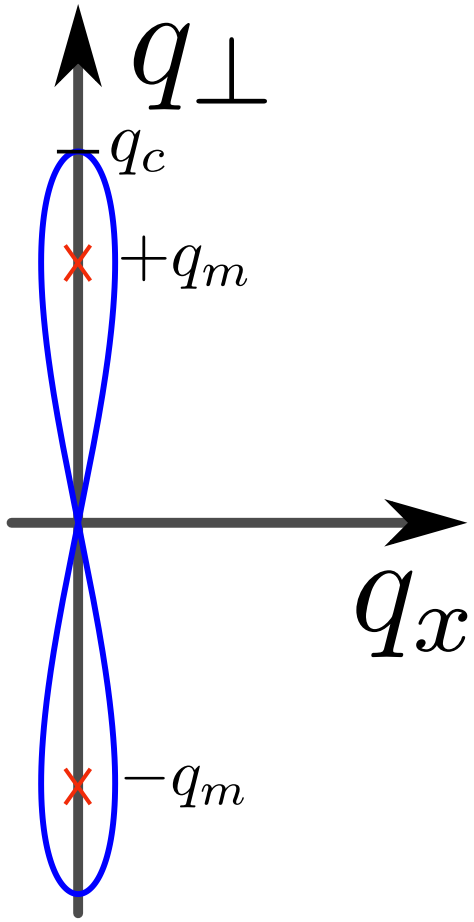

FIGURE 4. The region of instability in $\mathbf{q}$ space, for autochemotaxic systems very close to the instability threshold on the unstable side. Note that the instability only occurs at wavevectors very nearly perpendicular to the mean direction of flock motion, which is the horizontal (x)- axis in this figure. Specifically, the width along q_x of the unstable region scales like ϵ^2, while its length perpendicular to x scales like ϵ, where ϵ is a measure of the distance from the instability threshold (defined more precisely below). As a result, the instability is towards forming "bands" in real space running *parallel* to the direction of mean flock motion, as illustrated in figures 5 and 6.

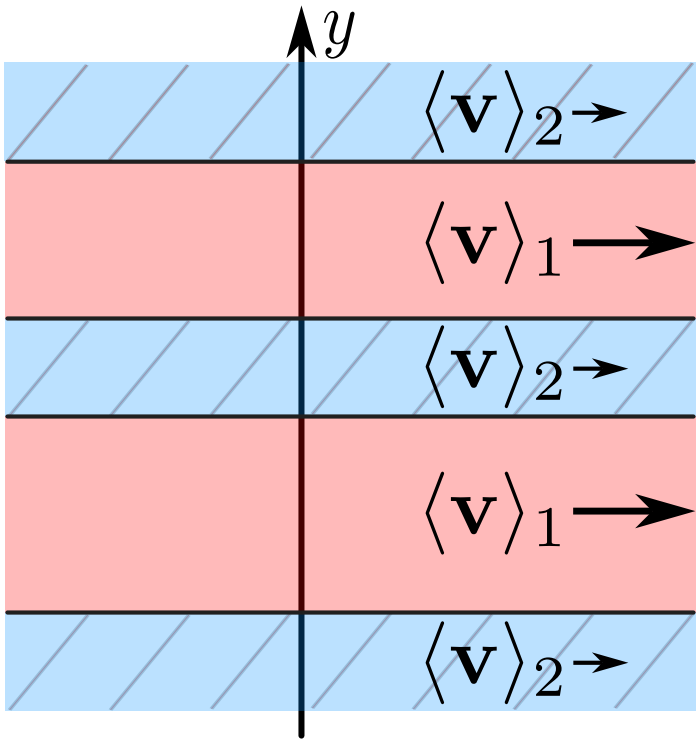

FIGURE 5. The "band" structure of the instability at intermediate times. The density is only modulated along one of the directions (which we call y, and which is indicated in the figure) perpendicular to the direction $\hat{x}$ of mean flock motion. A plot of the modulation of the density along the y-direction (e.g., along the path of the y-axis shown in the figure) is given on 6.

driven by completely different physics[5, 41, 34, 41], and is characterized by the formation of bands *perpendicular* to the direction of mean flock motion.

To investigate what happens once the density and velocity perturbations induced by this instability became too large to be treated by our linear stability analysis, we found both analytic steady-state and numerical time-dependent solutions to our equations of motion. We did so for "one-dimensional" (1d) solutions: that is, solutions in which the fields only depend on time and a single Cartesian coordinate perpendicular to the direction of mean flock motion. This one-dimensional restriction is justified, at least in the early stages, by the aforementioned fact that the instability only occurs for modes with their wavevectors nearly perpendicular to the direction of mean flock motion.

Our numerical solutions show that the these bands fairly quickly evolve into a set of well-separated parallel "plateaus" of almost constant density, as illustrated in figure 6. The evolution then continues via the merger of high density bands with other high density bands and low density bands with other

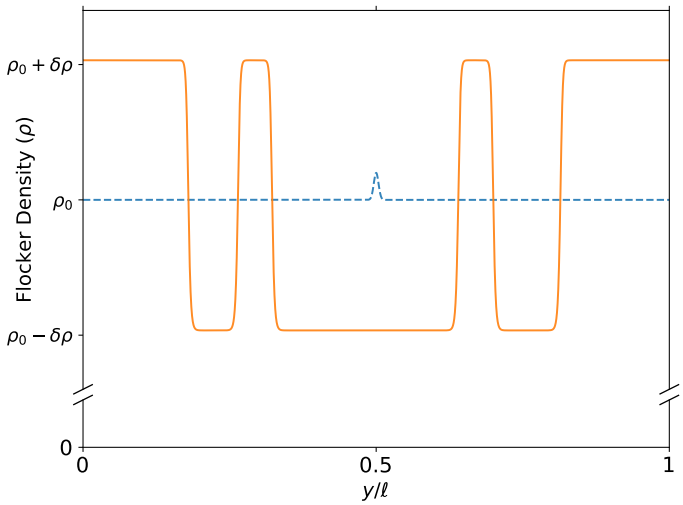

FIGURE 6. A plot of the density for a typical numerical solution of the hydrodynamic equations for 1d configurations, as described in the text, at intermediate times, with weak non-linear terms. The dashed blue curve is the initial condition. The orange curve is the density at the last time step our simulation reached. The density is only modulated along one of the directions (which we call y, and which is indicated in the figure) perpendicular to the direction $\hat{x}$ of mean flock motion. Here ℓ is the linear spatial extent of our system in the y-direction (which is periodic). The parameters used for this solution were $\Gamma, \Lambda = 0.25$, and the solution was iterated for 3000 units of time. The choice of ρ_0 was arbitrary.

low density ones. This suggests that bands of like density are attracted to each other; however, it appears that this interaction falls off quickly with distance, because the merging process gets very slow. Indeed, the mergers become so slow that our 1d simulations simply cannot run long enough (at least in the time we're willing to wait!) to reach what we believe will be the ultimate steady state of the system. That state is predicted by our analytic solution to be phase separation into one high density band and one low density band, moving parallel to each other (and in the direction of the original flock motion) at slightly different speeds. This final geometry is illustrated in figure 7, in which we compare our analytic solution of the steady state equations to the numerical, time-dependent solution at a sufficiently late time.

Our argument for this final state is based on our analytic steady state solution of our equations of motion, which is illustrated in figure 7. This solution, which is asymptotically valid sufficiently close to the analog in our problem of the critical point in equilibrium phase separation, has all of the features of the density profile of an equilibrium system in vapor-liquid coexistence: on the left we have a low density "vapor" phase. As we move to the right, the density increases smoothly through an interface with a well-defined width, until it turns over and plateaus at a higher "liquid" density.

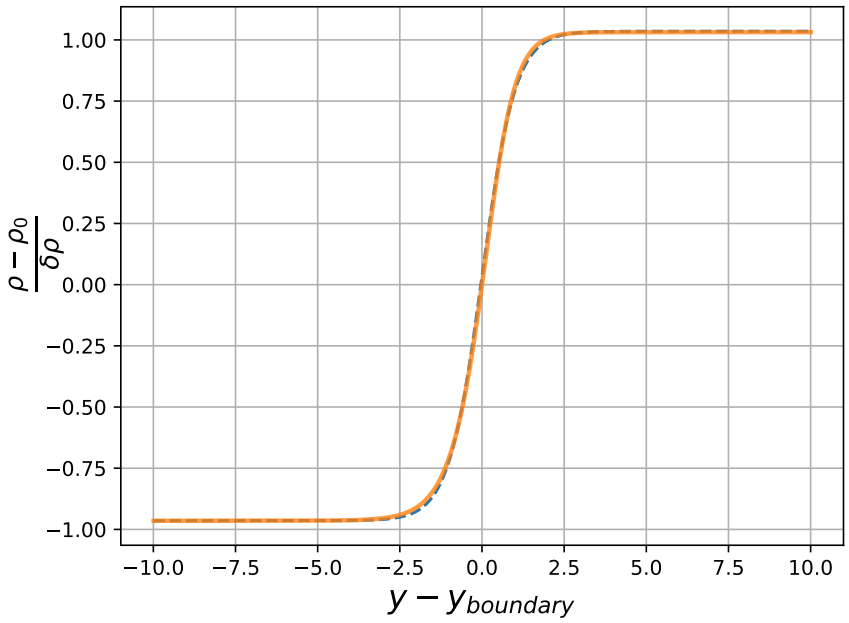

FIGURE 7. The density profile of the final phase separated steady state. The long-time limit of our numerical solution, and our fit curve are both plotted. The solid orange curve is the numerical solution. The dashed blue curve is the fit curve. The fit curve is $\tanh\left(y/\sqrt{1.0263}\right)+0.0355$. Although the form of the fit curve is not derived analytically, its large and small y limits are taken from our analytic theory. As can be seen, the agreement between the analytic theory and the numerical solution is good. The parameters used are $\frac{1}{\rho_0}\sqrt{\frac{m}{u}}, \frac{\lambda}{D_{L\perp}\rho_0}\sqrt{\frac{m}{u}} = 0.25$.

The approach to the liquid density as one moves to the right of the interface, and the approach to the vapor density as one moves to the left, is exponential.

It is this exponential tail - or, more precisely, the overlap of the exponential tail of one high density region with that of one on the other side of an intervening low density region- that leads to the attractive interaction between bands. It is the fact that this interaction falls off exponentially that makes the merger process so slow. Indeed, we expect that the time to reach the fully phase separated state will, in this 1d picture, grow exponentially with the system size. We believe this is the reason the system cannot reach the final phase separated state in our numerical solutions.

However, we also believe that this exponential growth of equilibration time with length scale is an artifact of the 1d nature of the analysis just presented. While we believe this approach is accurate for early times - i.e., times up to and including the formation of the plateaus- we also believe that once the plateaus are formed, their merger will be dominated by processes that are missed in a 1d picture.

Specifically, we expect that what will really happen, once the plateaus form, is that the bands will begin to undulate due to noise in the system, as illustrated in figure 8. These undulations will grow with time until bands begin bumping into their neighbors, at which point the bands can start to merge. The merged region will then rapidly "zipper" along in both directions, merging the two bands. This process will then repeat with the larger bands formed as a result of such mergers, until full phase separation is achieved.

The time scale needed for undulations of the bands to grow large enough to reach neighboring bands probably grows only *algebraically* with the separation between bands - much as the interface fluctuations in the KPZ equation do[23] - rather than exponentially. We therefore expect that the time required for our autochemotaxic instability to completely phase separate a large system will grow only algebraically with system size.

However, to make this idea more precise, a theory of the dynamics of fluctuations of an interface between two flocks of different densities and speeds is needed. No such theory currently exists; its development remains a topic for future research.

Those familiar with the dynamics of equilibrium phase separation will see the similarities with our system, although ours differs from the equilibrium case because of its strong anisotropy, and non-equilibrium effects.

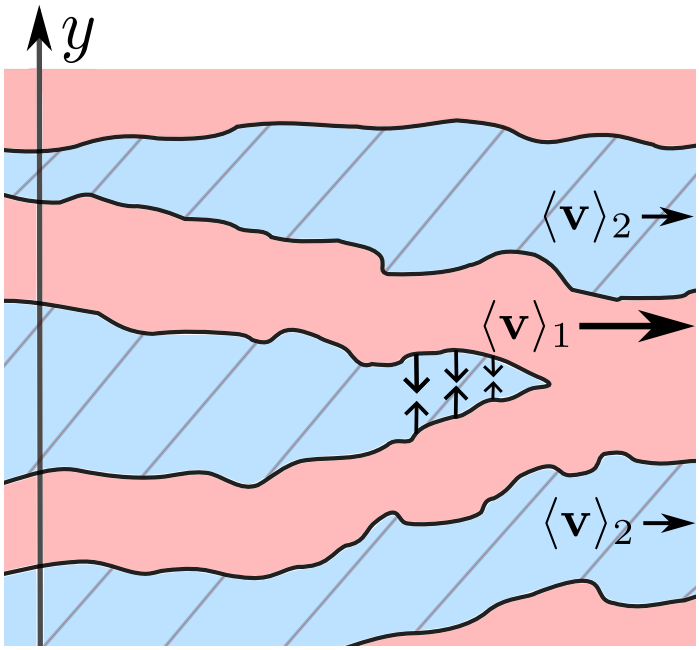

FIGURE 8. Our conjectured picture of the evolution of the density bands at later times. The boundaries fluctuate due to noise in ways that are not captured in the noiseless one dimensional approach. The central blue band is depicted in our conjectured transient "zipper" state.

One manifestation of these non-equilibrium effects is the determination of the values of the two co-existing steady-state densities. In equilibrium, these can be determined by the well-known "common tangent construction"[10]. Our aforementioned analytic steady-state solution shows that in flocks that phase separate, the two coexisting densities are determined by an *uncommon* tangent construction. This is very similar to the behavior found in mobility induced phase separation (MIPS) in *disordered* active systems [9].

More specifically, we find that as one approaches the dynamical critical point, the uncommon tangent construction approaches a common tangent construction - but *only* in this limit. In general, the uncommon tangent construction applies.

Our analytic steady-state solution implies the phase diagram shown in figure 9 and 15, in which the vertical axis is a model parameter defined later which decreases with increasing autochemotaxis , and the horizontal axis is the mean density of the system. This analytic solution is asymptotically valid sufficiently close to the critical point in this figure. In the region above the curve labelled "Binodal line", the uniform state is the only stable steady state of the flock. Below the curve

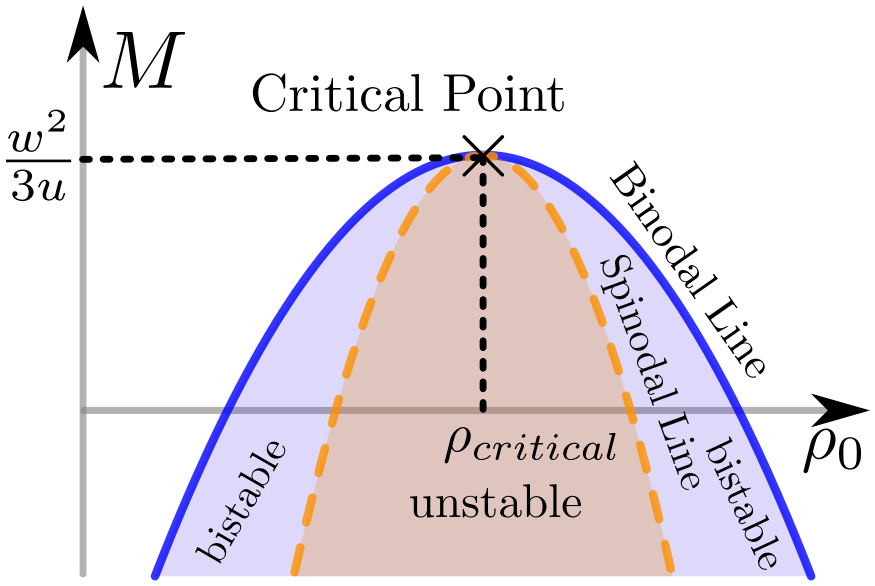

FIGURE 9. Phase diagram of flock phase-separation. Solid blue and dashed orange lines are the binodal and spinodal lines respectively. The orange filled region, labeled "unstable", corresponds to the coexistence of the 'liquid' (high density) and 'gas' (low density) phases. See figure 15 and section V for more details.

labelled "Spinodal line", only the phase separated state is stable. Between these two curves, *either* state can be stable.

When the instability is weak, and when the system is close to the dynamical analog of an equilibrium liquid-gas critical point[10], we can analytically determine the two densities in terms of parameters of the model. This analytic theory agrees extremely well with numerical solutions of our equations of motion, even when the instability is not weak and the system is fairly far from a critical point.

This said, our treatment of this phase separation is entirely "mean-field": that is, it ignores fluctuations in the local density and velocity. Fluctuations in the density are well-known[10, 27] to radically change the scaling behavior of the density near the critical point in equilibrium systems. Furthermore, even stable flocks experience enormous (indeed, divergent) fluctuation corrections to their dynamics[43, 46, 42, 44]. Among other effects, these make the diffusion "constants" no longer constant; they become functions of the wave vector $\mathbf{q}$ under consideration, diverging as $\mathbf{q} \to \mathbf{0}$. Since *both* types of effects - i.e., critical and non-critical fluctuations- are present in our system, we expect the scaling exponents for, e.g., the density difference between the two phase separated

regions, to be quantitatively different from those we find here. Therefore, the effect of fluctuations on the non-equilibrium phase separation we study here is a promising open topic for future research.

Although we have focused in the above discussion on autochemotaxis, the ultimate, longest length and time scale limit of our model, and the results we obtain for it herein, also apply to *any* dry polar ordered active matter system in which *any* microscopic mechanism drives the inverse compressibility negative. There are many other mechanisms one could imagine that could do this: direct attractive interactions between the active agents, for one, would be sufficient. *Any* system in which *any* microscopic mechanism leads to a negative inverse compressibility will be described, at the longest length and time scales, by a Toner-Tu model with a negative inverse compressibility, which is the basis for all of our predictions here. Therefore, , the phenomenology we predict here - in particular, that the phase separation is into bands of alternating higher and lower density form running *parallel* to the direction of mean flock motion, as illustrated in figure 5- will hold for *any* mechanism of phase separation (e.g., sufficiently strong attractive interactions between the boids).

The remainder of this chapter is organized as follows: in section (2.2), we review the Keller-Segel model of autochemotaxis[25, 24, 26, 21, 38]and the hydrodynamic (Toner-Tu) theory of flocking[43, 46, 42, 44, 41]. In section III, we develop the equations of motion for autochemotaxic flocks. In section IV, we linearize the equations of motion, examine their mode structure, and identify the instability. In section V, we analytically and numerically determine the final state to which the instability involves, using a one-dimensional analysis for systems very near a "critical point", analogous to the critical point of phase separating equilibrium systems, that we identify. This proves to be described by a common tangent construction very similar to that for equilibrium systems. In section VI, we demonstrate that further from the critical point, this phase separation is described by an "uncommon tangent construction" quite similar to that found in *disordered* active systems (e.g., motility-induced phase separation (MIPS)[9]. In section VII, we summarize our results, and discuss possible directions for future research.

2.2 Review of Keller and Segel Model of (auto)chemotaxis

In the 1970s, Keller and Segel developed their model of chemotaxis[25, 24, 26, 21, 38]. The general model includes *auto*chemotaxis, which describes a collection of creatures (which we'll call "boids") emitting "chemo-attractant"; i.e., a substance to which they themselves are attracted. The

chemo-attractant then diffuses, and decays with a finite lifetime. The boids diffuse as well, but with a bias in the direction of the gradient of the chemo-attractant concentration. In addition, Keller and Segel in their most general formulation allow for birth and death of the boids, making their system what we would now describe as a "Malthusian flock"[40, 12].

All of these processes (diffusion, chemo-attractant generation and decay) will in general depend on the local number density $\rho(\mathbf{r}, t)$ of boids at position $\mathbf{r}$ and time t, and the local concentration $\eta(\mathbf{r}, t)$ of the chemo-attractant at $(\mathbf{r}, t)$. This reasoning lead Keller and Segel to the following hydrodynamic equations in their most general form:

$$\partial_t \rho = \nabla \cdot \Big(k_1(\rho, \eta) \nabla \rho - k_2(\rho, \eta) \rho \nabla \eta \Big) + k_3(\rho, \eta) \,, \tag{2.2.1}$$

$$\partial_t \eta = D_\eta \nabla^2 \eta + k_4(\rho, \eta) - k_5(\rho, \eta) \eta \,. \tag{2.2.2}$$

In this expression, k_1 is the motility of the boids, k_2 the sensitivity to the chemical signal, k_3 the difference between the boid birth and death rate, and k_4 and k_5 give respectively the production and decay of the chemical signal. [20]

When k_2 is positive, the chemical signal acts as a chemo-attractant. When k_4 is positive and depends on ρ (e.g., $k_4 \propto \rho$), the system is autochemotaxic. We will focus in this chapter on flocks without birth and death, which amounts to taking $k_3 = 0$. Otherwise, we will take the very general form (2.2.2).

2.3 The Hydrodynamic Theory of Autochemotaxic Flocks: Equations of motion

We now wish to develop a hydrodynamic theory of autochemotaxic flocking. This will be a continuum model which takes as its variables the three fields introduced above: the number density of boids $\rho(\mathbf{r}, t)$, the boid velocity field $\mathbf{v}(\mathbf{r}, t)$, and the concentration $\eta(\mathbf{r}, t)$ of the chemical signal (or chemo-attractant/repellent).

Let's begin with our modification of equation (2.2.2) for the dynamics of the chemo-attractant, η, in the Keller-Segel model . First, our model is not "Malthusian"; that is, we will not consider birth and death of the boids. Therefore, we set $k_3 = 0$ in the equation of motion (2.2.1) for the boid density.

In addition, because of the coherent motion of the flock, we need to supplement the terms in the density equation of motion (2.2.1) with the convective $\nabla \cdot (\mathbf{v}\rho)$ term in the Toner-Tu equation of motion (1.1.4) for the boid density. A similar term, but with a non-unit coefficient, can also appear in the chemo-attractant equation of motion. Analogs of the "convective derivative" terms with coefficients $\lambda_{1,2,3}$ that appear in the velocity equation of motion (1.1.3) are allowed in the chemo-attractant equation of motion as well. We also need to allow for *anisotropic* diffusive terms (i.e., anisotropic versions of the $k_{1,2}$ terms) in the density equation, and similar terms in the chemo-attractant equation of motion, in much the way we introduced the anisotropic pressure P_2 in the velocity equation of motion (1.1.3) in the Toner-Tu model.

In addition, all of the k_i's can now depend on the local speed $|\mathbf{v}|$, as well as on ρ and η.

The coupling of the chemo-attractant concentration η to the velocity dynamics must, by symmetry, be embodied entirely by making the pressures $P_{1,2}$, and the phenomenological coefficients U, $D_{B,T,2}$, and $\lambda_{1,2,3}$, depend on η as well as $|\mathbf{v}|$ and ρ. It is the dependence of the isotropic pressure on η that leads to the instability we find, as we'll show below.

This reasoning leads to the following equations of motion for the boid density ρ, chemo-attractant concentration η, and the velocity $\mathbf{v}$[1]:

[1]The velocity field in our field equations is *not* the "true", or "full", velocity field. The true velocity field is defined as the velocity that satisfies $\mathbf{J} = \rho\mathbf{v}$. The velocity field that we employ is, instead, a proxy for the polarization field of the flock $\hat{\mathbf{p}}$, defined as $\mathbf{v} = v_0\hat{p}$. Where $\hat{\mathbf{p}}$ is the local "polarization"; that is, a unit vector along the direction in which the local flockers are pointing, and v_0 is the speed of the boids in a uniform state. By "pointing" here, we mean the direction along which the "motors" with which the flockers are propelling themselves are acting. Because there are many other effects that can lead to a net current of the flockers aside from their self-propulsion (e.g., pressure forces, Brownian noise, etc.), the net current $\mathbf{J}$ can get additional contributions that are *not* simply given by $\rho\mathbf{v}$, *with this definition of* $\mathbf{v}$. This fact then requires that we include the symmetry allowed k_1, k_{1a}, k_2 and k_{2a} terms in the equation of motion III.2. Note that even if we *had* defined the velocity field via $\mathbf{J} = \rho\mathbf{v}$, that exact relation would still have broken down once we coarse grained, since coarse graining means that we have averaged out some of the short-wavelength components of the velocity. The remaining components therefore no longer constitute the full velocity field, and so, in general, will not obey $\mathbf{J} = \rho\mathbf{v}$. Operationally, this fact is manifested by the generation of the k_1, k_{1a}, k_2 and k_{2a} terms by coarse graining (i.e., by the dynamical RG), even if those terms are absent in the original (bare) model

$$\partial_t \mathbf{v} + \lambda_1(\mathbf{v}\cdot\nabla)\mathbf{v} + \lambda_2(\nabla\cdot\mathbf{v})\mathbf{v} + \lambda_3\nabla(|\mathbf{v}|^2) = U(|\mathbf{v}|,\rho,\eta)\mathbf{v} - \nabla P_1(|\mathbf{v}|,\rho,\eta)$$
$$-\mathbf{v}(\mathbf{v}\cdot\nabla P_2(|\mathbf{v}|,\rho,\eta)) + D_B\nabla(\nabla\cdot\mathbf{v}) + D_T\nabla^2\mathbf{v} + D_2(\mathbf{v}\cdot\nabla)^2\mathbf{v}\,, \tag{2.3.1}$$
$$\partial_t\rho = \nabla\cdot\Big(k_1(|\mathbf{v}|,\rho,\eta)\nabla\rho - k_2(|\mathbf{v}|,\rho,\eta)\rho\nabla\eta + k_{1a}(|\mathbf{v}|,\rho,\eta)\mathbf{v}(\mathbf{v}\cdot\nabla\rho) - k_{2a}(|\mathbf{v}|,\rho,\eta)\rho\mathbf{v}(\mathbf{v}\cdot\nabla\eta)\Big)$$
$$-\nabla\cdot(\mathbf{v}\rho)\,, \tag{2.3.2}$$
$$\partial_t\eta = {}_\eta\nabla^2\eta + k_6(|\mathbf{v}|,\rho,\eta) - \lambda_{\eta1}(\mathbf{v}\cdot\nabla)\eta - \lambda_{\eta2}(\nabla\cdot\mathbf{v})\eta - \zeta_\eta\nabla\cdot(\mathbf{v}\rho) + D_{\eta\rho}\nabla^2\rho + D_{\eta v}\nabla^2|\mathbf{v}|$$
$$+D_{\eta a}\nabla\cdot[\mathbf{v}(\mathbf{v}\cdot\nabla)\eta] + D_{\eta\rho a}\nabla\cdot[\mathbf{v}(\mathbf{v}\cdot\nabla)\rho] + D_{\eta v a}\nabla\cdot[\mathbf{v}(\mathbf{v}\cdot\nabla)|\mathbf{v}|], \tag{2.3.3}$$

where we've defined

$$k_6(|\mathbf{v}|,\rho,\eta) \equiv k_4(|\mathbf{v}|,\rho,\eta) - k_5(\rho,\eta)\eta\,. \tag{2.3.4}$$

As just discussed, we connect the concentration of the auto-attractant to the velocity equation by coupling them through the equations of state of the pressures $P_{1,2}$.

We have also introduced anisotropic analogs k_{1a} and k_{2a} of the boid mobility k_1 and response to the chemotactant k_2, since we expect the response *along* the direction of the flock velocity $\mathbf{v}$ to be different in general from the response perpendicular to that direction.

2.4 Derivation of the Chemo-Attractant Instability

The homogeneous polar fluid state

We begin by identifying the steady state solution of our equations of motion that corresponds to a homogeneous moving flock. In a homogeneous state, all of our fields are constants, so we have

$$\rho(\mathbf{r},t) = \rho_0\,, \tag{2.4.1}$$
$$\eta(\mathbf{r},t) = \eta_0\,, \tag{2.4.2}$$
$$\mathbf{v} = v_0\hat{x}\,. \tag{2.4.3}$$

Note that the direction of $\mathbf{v}$ is completely arbitrary, due to the rotation invariance of our model. We will henceforth choose our coordinate system so that the x-axis is the direction of the spontaneous velocity.

Inserting these constant ansätze (2.4.1), (2.4.2) and (2.4.3), into our equations of motion (2.3.1), (2.3.2) and (2.3.3), it is clear that all terms involving spatial or temporal derivatives vanish. It is easy to see that this implies that the density equation (2.3.2) is automatically satisfied. The chemo-attractant concentration equation in a steady, homogeneous state then reads

$$k_6(\rho_0, \eta_0) = 0\,, \tag{2.4.4}$$

while the velocity equation reduces to

$$U(v_0, \rho_0, \eta_0) = 0\,. \tag{2.4.5}$$

This amounts to two scalar algebraic equations with three unknowns. We clearly need one more condition. This can be obtained by fixing the number N of boids contained in the volume V of our system (in spatial dimension $d = 3$) (or the area in $d = 2$). Once we do so, we have, in a uniform system, fixed the density ρ_0 everywhere to be $\rho_0 = N/V$ or $\rho_0 = N/\text{Area}$. Inserting that value of ρ_0 into (2.4.4) then in principle determines η_0. (We will assume (2.4.4) has a unique solution for η_0 for any value of ρ_0.)

With these values of ρ_0 and η_0 in hand, we can then in principle use (2.4.5) to determine the steady-state speed v_0. We will also assume that the solution of (2.4.5) is unique, which it clearly will be if $U(v_0, \rho_0, \eta_0)$ looks like figure 1.

Linearization

Having found a steady state solution to our equations of motion that corresponds to a spatially homogeneous and uniformly moving flock, we now will determine the stability of this state. To do so, we begin by linearizing our equations of motion about our steady state solution. That is, we will write

$$\rho(\mathbf{r}, t) = \rho_0 + \delta\rho(\mathbf{r}, t), \tag{2.4.6}$$

$$\eta(\mathbf{r}, t) = \eta_0 + \delta\eta(\mathbf{r}, t), \tag{2.4.7}$$

$$\mathbf{v}(\mathbf{r}, t) = v_0\hat{x} + \delta\mathbf{v}(\mathbf{r}, t) = (v_0 + \delta v_x(\mathbf{r}, t))\hat{x} + \mathbf{v}_\perp(\mathbf{r}, t), \tag{2.4.8}$$

and then expand our equations of motion to linear order in the fluctuations $\delta\rho(\mathbf{r},t)$, $\delta\eta(\mathbf{r},t)$, and $\delta\mathbf{v}(\mathbf{r},t)$ of the fields $\rho(\mathbf{r},t)$, $\eta(\mathbf{r},t)$, and $\mathbf{v}(\mathbf{r},t)$.

The process of linearization begins by expanding all of the $|\mathbf{v}|$, ρ, and η dependent parameters in the equations of motion to sufficiently high order in the fluctuations $\delta\rho(\mathbf{r},t)$, $\delta\eta(\mathbf{r},t)$, and $\delta\mathbf{v}(\mathbf{r},t)$ of the fields $\rho(\mathbf{r},t)$, $\eta(\mathbf{r},t)$, and $\mathbf{v}(\mathbf{r},t)$ to obtain all terms in the equation of motion to linear order in $\delta\rho(\mathbf{r},t)$, $\delta\eta(\mathbf{r},t)$, and $\delta\mathbf{v}(\mathbf{r},t)$. This gives us

$$
\begin{aligned}
k_1 &= D_{_C}\,, && (2.4.9)\\
k_2 &= D_{_C}\mu\,, && (2.4.10)\\
k_3 &= 0\,, && (2.4.11)\\
k_6 &= \gamma\delta\rho - \frac{\delta\eta}{\tau} + \alpha\delta|\mathbf{v}|\,, && (2.4.12)\\
P_{1,2}(|\mathbf{v}|,\rho,\eta) &= \text{constant} + \sigma_{1,2}\delta\rho - \kappa_{1,2}\delta\eta + \nu_{1,2}\delta|\mathbf{v}|\,, && (2.4.13)\\
U(|\mathbf{v}|,\rho,\eta) &= -A\delta|\mathbf{v}| + \bar{B}\delta\rho + C\delta\eta\,, && (2.4.14)
\end{aligned}
$$

where $D_{_C}$, μ, γ, τ, $\sigma_{1,2}$, $\kappa_{1,2}$, A, $\bar{B}$, and C are all phenomenological constants. We remind the reader that boids are not being born and dying "on the wing". This means that the boid birth and death rate term k_3 is zero. Most of the other parameters in the model can have either sign, but κ_1 and A are both positive definite. The positivity of A can be seen from figure 1 , since A is just -1 times the slope of $U(v)$ as it crosses the v axis. The positivity of κ_1 means that the chemical signal *attracts* the boids (i.e., that it *is* a chemo-*attractant*), which is the case we wish to consider here. As we will see, it is this attraction that destabilizes the spatially uniform flocking state.

Note that we also have $\bar{B} > 0$ for systems in which the mean speed v_0 increases with increasing density, as it does for, e.g., the Vicsek model[47].

The parameters γ and τ respectively set the sensitivity of the production rate and decay rate of the chemo-attractant.

Making the substitutions (2.4.8) and (2.4.9-2.4.14) in our equations of motion (2.3.1-2.3.3), and keeping only terms to linear order in $\delta\rho$, $\delta\eta$, and $\delta\mathbf{v}$, we obtain our linearized equations of motion:

$$\frac{\partial \delta\rho}{\partial t} = D_{_C}\nabla^2\delta\rho - \mu D_{_C}(\rho_0\nabla^2\delta\eta) - \rho_0\partial_x\delta v_x - \rho_0\nabla_\perp\cdot\mathbf{v}_\perp - v_0\partial_x\delta\rho$$
$$+ D_{ca}v_0^2\partial_x^2\delta\rho - D_{ca}\mu_a v_0^2\partial_x^2\delta\eta\,, \tag{2.4.15}$$
$$\frac{\partial \delta\eta}{\partial t} = D_\eta\nabla^2\delta\eta - \frac{\delta\eta}{\tau} + \gamma\delta\rho + \alpha\delta v_x - v_0\zeta_\eta\partial_x\delta\rho - \lambda_{\eta 1}v_0\partial_x\delta\eta$$
$$- (\lambda_{\eta 2}\eta_0 + \zeta_\eta\rho_0)[\partial_x\delta v_x + \nabla_\perp\cdot\mathbf{v}_\perp] + D_{\eta\rho}\nabla^2\delta\rho + D_{\eta v}\nabla^2\delta v_x$$
$$+ D_{\eta\rho a}v_0^2\partial_x^2\delta\rho + D_{\eta a}v_0^2\partial_x^2\delta\eta + D_{\eta v a}v_0^2\partial_x^2\delta v_x\,, \tag{2.4.16}$$
$$\frac{\partial \delta v_x}{\partial t} = v_0(-A\delta v_x + \bar{B}\delta\rho + C\delta\eta) - (\lambda_1+\lambda_2+2\lambda_3)v_0\partial_x\delta v_x - \lambda_2 v_0(\nabla_\perp\cdot\mathbf{v}_\perp)$$
$$- (\sigma_1 + v_0^2\sigma_2)\partial_x\delta\rho + (\kappa_1 + v_0^2\kappa_2)\partial_x\delta\eta - (\nu_1 + v_0^2\nu_2)\partial_x\delta v_x$$
$$+ D_B[\partial_x(\nabla_\perp\cdot\mathbf{v}_\perp) + \partial_x^2\delta v_x] + D_T\nabla^2\delta v_x + D_2 v_0^2\partial_x^2\delta v_x\,, \tag{2.4.17}$$
$$\frac{\partial \mathbf{v}_\perp}{\partial t} = -\lambda_1 v_0\partial_x\mathbf{v}_\perp - 2\lambda_3 v_0\nabla_\perp\delta v_x - \nabla_\perp(\sigma_1\delta\rho - \kappa_1\delta\eta + \nu_1\delta v_x)$$
$$+ D_B\nabla_\perp[\nabla_\perp\cdot\mathbf{v}_\perp + \partial_x\delta v_x] \; + D_T\nabla_\perp^2\mathbf{v}_\perp + D_x\partial_x^2\mathbf{v}_\perp\,. \tag{2.4.18}$$

where $D_x \equiv D_T + D_2 v_0^2$.

We'll now use the equations to investigate the stability of the uniform steady state.

Demonstration that $\delta\eta$ and δv_x are Fast Variables, and their elimination

We begin by observing that the fields δv_x and $\delta\eta$ are "fast" in the sense that their time derivatives do not vanish in the limit of extremely slowly spatially varying fields. In contrast, the fields ρ and $\mathbf{v}_\perp$ are "slow", or, to use another word, "hydrodynamic": that is, their time derivatives *do* vanish in the limit of extremely slowly spatially varying fields.

As a result, if we are considering the most slowly evolving modes in the system at the longest wavelengths, the "fast" fields δv_x and $\delta\eta$ will, on the time scale of those slowest modes, relax very quickly back to values determined entirely by the slow fields. This means that those fast variables become effectively "enslaved" to the hydrodynamic variables in the problem - in this case the boid density ρ. By "enslaved", we mean that its value at any point in space and time is determined entirely by the instantaneous value of ρ at the same point in space and time. It is this sort of "enslavement" that enables hydrodynamic theories in general to eliminate "fast" variables - that is,

variables that do not relax infinitely slowly as the length scale under consideration goes to infinity- and work only with the "slow" hydrodynamic variables.

To see how this works in our problem, note that, in the hydrodynamic limit of long wavelengths and large time scales, derivatives of the fluctuations of the fields are small compared to terms that contain the fluctuation with no derivatives. We will therefore expand the equations of motion for the fast fields η and δv_x in derivatives by writing

$$\delta\eta = \delta\eta_0 + \delta\eta_1 \quad , \quad \delta v_x = \delta v_x^{(0)} + \delta v_x^{(1)} \,, \tag{2.4.19}$$

where

$$\delta\eta_0 \,, \delta v_x^{(0)} = O(\delta\rho) \;,\; \delta\eta_1 \,, \delta v_x^{(1)} = O(\partial_t \delta\rho, \nabla\delta\rho, \nabla\cdot\mathbf{v}_\perp) \,. \tag{2.4.20}$$

Note that $\nabla \cdot v_\perp \ll \delta\rho$, as can be seen by the following argument: In order to satisfy Eq (IV.15), $\nabla\cdot v_\perp$ must be of order $(\partial_t\rho)$ or $\partial_x\delta\rho$ (the only other term in (IV.15), namely $\partial_x\delta v_x$, is clearly much smaller than $\nabla\cdot v_\perp$, since x-derivatives are much smaller than $\perp$ derivatives in the unstable regime (where $q_x \ll \mathbf{q}_\perp$), and δv_x is $\ll \mathbf{v}_\perp$, since the former is massive). Therefore, $\nabla\cdot v_\perp$ is of order a *derivative* of $\delta\rho$, and hence much less than $\delta\rho$, as we asserted.

Therefore, to leading order in a hydrodynamic expansion, we can drop all terms with derivatives from the equations of motion (2.4.16) and (2.4.17). Dropping those terms, equations (2.4.16) and (2.4.17) become:

$$0 = -\frac{\delta\eta_0}{\tau} + \gamma\delta\rho + \alpha\delta v_x^{(0)} \,, \tag{2.4.21}$$

$$0 = v_0(-A\delta v_x^{(0)} + \bar{B}\delta\rho + C\delta\eta_0) \,. \tag{2.4.22}$$

These equations can trivially be solved to relate the "fast" variables δv_x and $\delta\eta$ to the "slow" variable $\delta\rho$:

$$\delta v_x^{(0)} = \left(\frac{\bar{B}+\tau\gamma C}{A-\alpha\tau C}\right)\delta\rho = K_v\delta\rho, \,, \tag{2.4.23}$$

$$\delta\eta_0 = \left(\frac{(A\gamma+\alpha\bar{B})\tau}{A-\alpha\tau C}\right)\delta\rho = K_\eta\delta\rho \,, \tag{2.4.24}$$

where we've defined

$$K_v \equiv \frac{\bar{B} + \tau\gamma C}{A - \alpha\tau C} \quad , \quad K_\eta \equiv \frac{(A\gamma + \alpha\bar{B})\tau}{A - \alpha\tau C} \, . \tag{2.4.25}$$

The only important point to be noted about these rather complicated expressions is that both K_v and K_η are monotonically *increasing* functions of the chemo-attractant release rate γ, provided A and C are positive. As pointed out earlier, A definitely is positive. Strictly speaking, C could, in principle, have either sign. However, we expect intuitively that increasing the chemo-attractant concentration should *increase* the speed of the boids (since most critters move faster when they smell food!). If this is the case, then C will be positive as well.

We'll show later that the fact that both K_v and K_η are monotonically *increasing* functions of the chemo-attractant release rate γ implies that the system will always eventually become unstable if we increase the chemo-attractant release rate γ without bound.

The alert reader will notice that K_v and K_η both diverge as $A \to \alpha\tau C$ from above. The physics of this instability is simply that, when the denominator vanishes, the decay rate of one of the "fast" modes vanishes. This can be seen by noting that the denominator in question is nothing but the determinant of the dynamical matrix for the fast fields if we set the slow field $\rho = 0$. That determinant is simply the product of the two eigen-decay rates. While this instability would clearly be an interesting topic for future research, we will not discuss it further here. Instead, we will focus our attention on the parameter regime $A > \alpha\tau C$, where this particular instability does not occur.

Inserting (2.4.23) and (2.4.24) into the linearized equation of motion (2.4.17) for δv_x, and gathering terms proportional to one derivative (either spatial or temporal) of the hydrodynamic variables $\delta\rho$ and $\mathbf{v}_\perp$, gives

$$v_0(-A\delta v_x^{(1)} + C\delta\eta_1) = K_v\partial_t\delta\rho + G_v\partial_x\delta\rho + \lambda_2 v_0 \nabla\cdot\mathbf{v}_\perp \, , \tag{2.4.26}$$

where

$$\begin{aligned} G_v \quad \equiv \quad & \sigma_1 + v_0^2\sigma_2 + K_v(\nu_1 + \nu_2 v_0^2 + (\lambda_1 + \lambda_2 + 2\lambda_3)v_0) \\ & -K_\eta(\kappa_1 + v_0^2\kappa_2) \, . \end{aligned} \tag{2.4.27}$$

Likewise, inserting (2.4.23) and (2.4.24) into the linearized equation of motion (2.4.15) for $\delta\eta$, and gathering terms proportional to one derivative (either spatial or temporal) of the hydrodynamic variables $\delta\rho$ and $\mathbf{v}_\perp$, gives

$$-\frac{\delta\eta_1}{\tau} + \alpha\delta v_x^{(1)} = K_\eta \partial_t \delta\rho + (\lambda_{\eta 2}\eta_0 + \zeta_\eta \rho_0)\nabla\cdot\mathbf{v}_\perp + G_\eta \partial_x \delta\rho\,, \tag{2.4.28}$$

where

$$G_\eta \equiv \lambda_{\eta 1} v_0 K_\eta + \lambda_{\eta 2}\eta_0 K_v + v_0\zeta_\eta\,. \tag{2.4.29}$$

Solving these two simple linear equations (2.4.26) and (2.4.28) for $\delta v_x^{(1)}$ and $\delta\eta_1$ gives

$$\delta v_x^{(1)} = -K_{v1}\partial_t\delta\rho - G_{v1}\partial_x\delta\rho - H_v\nabla\cdot\mathbf{v}_\perp \tag{2.4.30}$$

where

$$K_{v1} \equiv \frac{v_0 C\tau K_\eta + K_v}{v_0(A-\alpha C\tau)}\,, \tag{2.4.31}$$

$$G_{v1} \equiv \frac{G_v + C\tau v_0 G_\eta}{v_0(A-\alpha C\tau)}\,, \tag{2.4.32}$$

$$H_v \equiv \frac{\lambda_2 + (\lambda_{\eta 2}\eta_0 + \zeta_\eta\rho_0)C\tau}{A-\alpha C\tau}\,, \tag{2.4.33}$$

and

$$\delta\eta_1 = -K_{\eta 1}\partial_t\delta\rho - G_{\eta 1}\partial_x\delta\rho - H_\eta\nabla\cdot\mathbf{v}_\perp\,, \tag{2.4.34}$$

where

$$K_{\eta 1} \equiv \frac{v_0 A\tau K_\eta + \alpha\tau K_v}{v_0(A-\alpha C\tau)}\,, \tag{2.4.35}$$

$$G_{\eta 1} \equiv \frac{\tau(\alpha G_v + A v_0 G_\eta)}{v_0(A-\alpha C\tau)}\,, \tag{2.4.36}$$

$$H_\eta \equiv \frac{\tau(\alpha\lambda_2 + (\lambda_{\eta 2}\eta_0 + \zeta_\eta\rho_0)A)}{A-\alpha C\tau}\,. \tag{2.4.37}$$

Where K_{v1} and $K_{\eta 1}$ give the linear response of $\delta v_x^{(1)}$ and $\delta\eta_1$ to the time rate of change of the local density, $\delta\rho$. Likewise, the G_{v1} and $G_{\eta 1}$ give the linear response to the spatial change in the

direction of flock motion to the local density, $\delta\rho$. Finally, H_ν and H_η give the linear response to the divergence of the local velocity that is perpendicular to the direction of flock motion, $\Delta \cdot \mathbf{v}_\perp$.

Having eliminated the fast variables η and δv_x in favor of the slow variable $\delta\rho$, we can now write a set of closed equations of motion for the density fluctuation $\delta\rho$ and perpendicular velocity field $\mathbf{v}_\perp$ by substituting equations (2.4.23), (2.4.24), (2.4.30) and (2.4.34) into our equations of motion (2.4.15) and (2.4.18). This gives:

$$\begin{aligned}\frac{\partial \delta\rho}{\partial t} =& D_{\rho\perp}\nabla_\perp^2\delta\rho + D_{\rho x}\partial_x^2\delta\rho - v_\rho\partial_x\delta\rho - \rho_0\nabla_\perp\cdot\mathbf{v}_\perp \\ &+ D_{\rho v}\partial_x(\nabla_\perp\cdot\mathbf{v}_\perp) + \phi\partial_t\partial_x\delta\rho\,, \qquad (2.4.38)\\ \frac{\partial \mathbf{v}_\perp}{\partial t} =& -v_v\partial_x\mathbf{v}_\perp - \left(\frac{B}{\rho_0}\right)\nabla_\perp\delta\rho + D_{BR}\nabla_\perp(\nabla\cdot\mathbf{v}_\perp) + D_T\nabla_\perp^2\mathbf{v}_\perp \\ &+ D_x\partial_x^2\mathbf{v}_\perp + \nu_x\partial_x\nabla_\perp\delta\rho + \nu_t\partial_t\nabla_\perp\delta\rho\,, \qquad (2.4.39)\end{aligned}$$

where we have defined:

$$\begin{aligned} v_\rho &\equiv \rho_0 K_v + v_0\,, && (2.4.40)\\ D_{\rho\perp} &\equiv D_C(1-\mu K_\eta\rho_0)\,, && (2.4.41)\\ D_{\rho x} &\equiv D_C + D_{Ca}v_0^2 - D_C\mu\rho_0 K_\eta - D_{Ca}\mu_a v_0^2\rho_0 K_\eta + \rho_0 G_{v1}\,, && (2.4.42)\\ D_{\rho v} &\equiv \rho_0 H_v\,, && (2.4.43)\\ \phi &\equiv \rho_0 K_{v1}\,, && (2.4.44)\\ v_v &\equiv \lambda_1 v_0\,, && (2.4.45)\\ D_{BR} &\equiv D_B + (2\lambda_3 v_0 + \nu_1)H_v + \kappa_1 H_\eta\,, && (2.4.46)\\ \nu_x &\equiv \kappa_1 G_{\eta 1} + D_B K_v + (2\lambda_3 v_0 + \nu_1)G_v\,, && (2.4.47)\\ \nu_t &\equiv \kappa_1 K_{\eta 1} + (2\lambda_3 v_0 + \nu_1)K_{v1}\,, && (2.4.48)\end{aligned}$$

and, most importantly, the "inverse compressibility"

$$\begin{aligned} B &\equiv \rho_0[\sigma_1 - K_\eta\kappa_1 + (2\lambda_3 v_0 + \nu_1)K_v] \\ &= \rho_0\left(\sigma_1 - \left[\frac{\kappa_1(A\gamma + \alpha\bar{B})\tau - (2\lambda_3 v_0 + \nu_1)(\bar{B} + \gamma\tau C)}{A - \alpha\tau C}\right]\right). \end{aligned} \tag{2.4.49}$$

This last expression is the most important result of this analysis, since it shows that autochemotaxis can make the inverse compressibility negative. One way this can be done is by increasing the parameter κ_1, which governs the sensitivity of the isotropic pressure to the chemo-attractant concentration. As can been by inspection of (2.4.49), increasing κ_1 without bound while holding all other parameters fixed will inevitably make B become negative, provided only that

$$\frac{(A\gamma + \alpha\bar{B})\tau}{A - \alpha\tau C} > 0\,, \tag{2.4.50}$$

which clearly is a very large portion of the parameter space of our hydrodynamic model.

Likewise, increasing the chemo-attractant production rate γ with all other parameters held fixed will also unavoidably drive the inverse compressibility B negative, provided that

$$\frac{(\kappa_1 A + (2\lambda_3 v_0 + \nu_1)C)\tau}{A - \alpha\tau C} > 0\,. \tag{2.4.51}$$

Finally, increasing the chemo-attractant lifetime τ with all other parameters held fixed will also certainly drive the inverse compressibility B negative if, for example, all of the parameters α, $\bar{B}$, C, and the combination $2\lambda_3 v_0 + \nu_1$ are all positive. Indeed, in this case, B is guaranteed to turn negative as τ is increased from zero for some $\tau < \frac{A}{\alpha C}$.

The forms of the equations of motion (2.4.38) and (2.4.39) are *identical* to the linearized equations of motion obtained in [41] for stable flocks without chemotaxis. This was inevitable, since the symmetries and conservation laws of our model are the same as those of an ordinary, stable flock. The only long-wavelength effect of the autochemotaxis is to provide a mechanism to drive the inverse compressibility B negative, as discussed above. Any attractive interaction, which is sufficiently strong to drive the inverse compressibility negative, will obey the same hydrodynamic description put forward in this chapter. In the next section, we will show that when B does become negative, the homogeneous phase of the flock becomes unstable.

Mode Structure

To investigate the mode structure of our linearized model, we proceed exactly as in [43, 46, 42, 44, 41], by seeking solutions of the linearized equations of motion (2.4.38) and (2.4.39) for plane-wave normal modes, in which all fields are proportional to $\exp[i\boldsymbol{q}\cdot\boldsymbol{r} - i\omega t]$. Doing so, the equations of motion then read:

$$\Big[-i(\omega - v_\rho q_x) + D_{\rho\perp}q_\perp^2 + D_{\rho x}q_x^2 - \phi\omega q_x\Big]\delta\rho = -i\rho_0 \mathbf{q}_\perp\cdot\mathbf{v}_\perp - D_{\rho v}q_x(\mathbf{q}_\perp\cdot\mathbf{v}_\perp)\,, \tag{2.4.52}$$

$$\Big[-i\omega + iv_v q_x + D_T q_\perp^2 + D_x q_x^2\Big]\mathbf{v}_\perp + D_{BR}\mathbf{q}_\perp(\mathbf{q}_\perp\cdot\mathbf{v}_\perp) = \Big[-i\frac{B}{\rho_0} + \nu_t\omega - \nu_x q_x\Big]\mathbf{q}_\perp\delta\rho\,. \tag{2.4.53}$$

We decouple these by projecting (2.4.53) perpendicular to and along $\mathbf{q}_\perp$. That is, we write

$$\mathbf{v}_\perp = v_L\hat{q}_\perp + \mathbf{v}_T\,, \tag{2.4.54}$$

with the "transverse" components $\mathbf{v}_T$, by definition, perpendicular to $\mathbf{q}_\perp$ (that is, $\mathbf{v}_T\cdot\hat{q}_\perp = 0$), while the single "longitudinal" component $v_L = \frac{\mathbf{q}_\perp\cdot\mathbf{v}_\perp}{|q_\perp|}$ is the projection of $\mathbf{v}_\perp$ onto $\mathbf{q}_\perp$.

This split decouples $\delta\rho$ and v_L from the $d-2$ transverse modes $\mathbf{v}_T$, as can be seen by inserting the decomposition (2.4.54) into the ρ equation of motion (2.4.52), and projecting the velocity equation of motion (2.4.53) in the transverse and longitudinal directions (i.e., along and perpendicular to $\mathbf{q}_\perp$). This gives:

$$\Big[-i(\omega - v_\rho q_x) + \Gamma_\rho(\mathbf{q}) - \phi\omega q_x\Big]\delta\rho = -i\rho_0 q_\perp v_L - D_{\rho v}q_x q_\perp v_L, \tag{2.4.55}$$

$$\Big[-i(\omega - v_v q_x) + \Gamma_L(\mathbf{q})\Big]v_L = \Big[-i\frac{B}{\rho_0} + \nu_t\omega - \nu_x q_x\Big]q_\perp\delta\rho, \tag{2.4.56}$$

$$\Big[-i(\omega - v_v q_x) + \Gamma_T(\mathbf{q})\Big]\mathbf{v}_T = \mathbf{0}\,. \tag{2.4.57}$$

Here we've defined $\Gamma_T = D_T q_\perp^2 + D_x q_x^2$, $\Gamma_L = D_{L\perp}q_\perp^2 + D_x q_x^2$, $D_{L\perp} = D_T + D_{BR}$, and $\Gamma_\rho = D_{\rho\perp}q_\perp^2 + D_{\rho x}q_x^2$.

Altogether we have d frequencies to determine. Since the transverse modes are decoupled, we can immediately write down the transverse dispersion relation implied by equation (2.4.57):

$$\omega = -i\Gamma_T + v_v q_x \tag{2.4.58}$$

All these $d-2$ modes decay, provided $D_T q_\perp^2 + D_x q_x^2 > 0$. Thus, there is no instability in these modes, even when the inverse compressibility B becomes negative (unsurprisingly, since B does not enter the transverse equations of motion).

The instability arises from the coupled density ρ and longitudinal velocity v_L modes, as can be seen from equations (2.4.55) and (2.4.56), which can be rewritten:

$$\begin{aligned} -i\omega\delta\rho =& - D_{\rho\perp} q_\perp^2 \delta\rho - D_{\rho x} q_x^2 \delta\rho - i v_\rho q_x \delta\rho - i\rho_0 q_\perp v_L \\ & - D_{\rho v} q_x q_\perp v_L + \phi\omega q_x \delta\rho \,, \end{aligned} \tag{2.4.59}$$

$$\begin{aligned} -i\omega v_L =& - i v_v q_x v_L - i\left(\frac{B}{\rho_0}\right) q_\perp \delta\rho - D_{L\perp} q_\perp^2 v_L - D_x q_x^2 v_L \\ & - \nu_x q_x q_\perp \delta\rho + \nu_t \omega q_\perp \delta\rho \,. \end{aligned} \tag{2.4.60}$$

As shown in [43, 46, 42, 44, 41], the eigenfrequencies of these equations, to linear order in q, are

$$\omega_\pm = \frac{1}{2}\Big[q_x v_\rho + q_x v_v \pm \Delta\Big], \tag{2.4.61}$$

$$\Delta = \sqrt{(v_v - v_\rho)^2 q_x^2 + 4B q_\perp^2}\,. \tag{2.4.62}$$

In contrast to prior work, however, we now know that autochemotaxis can drive the inverse compressibility B negative. When this happens, it is clear from (2.4.62) that modes whose wavevectors $\mathbf{q}$ lie in the region in which

$$(v_v - v_\rho)^2 q_x^2 + 4B q_\perp^2 < 0\,, \tag{2.4.63}$$

will be unstable, thereby destabilizing the spatially uniform flocking state. This implies the instability lies in the region

$$|q_x| < \frac{2\sqrt{|B|}}{|v_v - v_\rho|}|\mathbf{q}_\perp| = \epsilon|\mathbf{q}_\perp|\,, \tag{2.4.64}$$

where we've defined:

$$\epsilon \equiv \frac{2\sqrt{|B|}}{|v_v - v_\rho|}\,. \tag{2.4.65}$$

(Recall that in the unstable region $B < 0$). If we are near the instability on the unstable side, $|B| \ll (v_v - v_\rho)^2$, and so (2.4.64) implies $\epsilon << 1$, and so the unstable wavevectors satisfy $|q_x| \ll |\mathbf{q}_\perp|$, as claimed in the introduction.

The window (2.4.64) gives the region in which, at sufficiently small $\mathbf{q}$, the flock becomes unstable with a growth rate that is *linear* in $q \equiv |\mathbf{q}|$. Small $\mathbf{q}$'s that lie outside this region, however, are not necessarily stable. This is because, for $|q_x| > \epsilon|\mathbf{q}_\perp|$, the eigenfrequencies ω *to linear order in* q, are real, as can be seen by inspection of equation 2.4.61. Since the stability or instability is determined entirely by the *imaginary* part of ω, we must therefore, for $\mathbf{q}$'s in the regime $|q_x| > \epsilon|\mathbf{q}_\perp|$, work to higher (in fact, second) order in $\mathbf{q}$ in order to determine the absolute instability limit. This proves, as we shall see, to be have a larger opening angle at small $\mathbf{q}$ than the limit (2.4.64), but the new limit has the same $\sqrt{|B|}$ scaling with B. In contrast to equation (2.4.64), however, the instability is only limited to a narrow window if $|v_v - v_\rho|$ exceeds some finite threshold. See equation (2.4.77) for more details.

It is instructive to rewrite the dispersion relation (2.4.62) in terms of two complex, direction dependent sound speeds $c_\pm(\theta_\mathbf{q})$:

$$\omega = c_\pm(\theta_\mathbf{q})q\,, \tag{2.4.66}$$

where $q \equiv |\mathbf{q}|$, and $\theta_\mathbf{q}$ is the angle between the $\mathbf{q}$ and the $\hat{x}$ direction (i.e., the direction of mean flock motion $\langle\mathbf{v}\rangle$). Using $q_x = q\cos\theta$ and $q_\perp = q\sin\theta$ in (2.4.62), we obtain the expression of references [43, 46, 42, 44, 41] for $c_\pm(\theta_\mathbf{q})$:

$$c_\pm(\theta_\mathbf{q}) = \frac{1}{2}\left[(v_\rho + v_v)\cos(\theta_\mathbf{q}) \pm \sqrt{(v_v - v_\rho)^2\cos^2(\theta_\mathbf{q}) + 4B\sin^2(\theta_\mathbf{q})}\right]. \tag{2.4.67}$$

from this expression, we can see that ω_+ acquires a positive imaginary part, signaling instability, for directions of propagation $\theta_\mathbf{q}$ near $\pm\pi/2$; i.e., perpendicular to the direction of mean flock motion.

Specifically, the instability occurs for

$$|\theta \pm \pi/2| < \frac{2\sqrt{|B|}}{|v_v - v_\rho|}\,. \tag{2.4.68}$$

For directions of propagation $\theta_{\mathbf{q}}$ between 0 and $\frac{\pi}{2}$, this condition is equivalent to

$$\theta_{\mathbf{q}} > \theta_c \equiv \frac{\pi}{2} - \frac{2\sqrt{|B|}}{|v_v - v_\rho|}\,. \tag{2.4.69}$$

This result holds only for very small q. As noted earlier, even at very small q, it only gives the region in which the instability growth rate is *linear* in q; the possibility of an $O(q^2)$ instability outside this small angular window still exists. Furthermore, at larger $\mathbf{q}$, higher order terms in the equation of motion become important. As a result, even $\mathbf{q}$'s whose directions lie in the narrow angular wedge (2.4.68) do not remain unstable out to arbitrarily large $|\mathbf{q}|$.

To investigate both of these possibilities, we'll now go beyond leading order in q for systems close to the instability threshold. Assuming that we continue to have $q_x \sim \epsilon|\mathbf{q}_\perp|$ with $\epsilon \ll 1$, we can greatly simplify the eigenvalue conditions (2.4.38) and (2.4.39). We'll also assume, and verify *a posteriori*, that the typical unstable wavevector satisfies $|\mathbf{q}_\perp| \propto \epsilon$. Then the various terms in (2.4.59) scale as follows:

$$\begin{gathered}
i\omega\delta v_x^{(1)} \sim \epsilon^2\delta v_x^{(1)} \quad , \quad D_{\rho\perp}q_\perp^2\delta v_x^{(1)} \sim \epsilon^2\delta v_x^{(1)}\,, \\
D_{\rho x}q_x^2\delta v_x^{(1)} \sim \epsilon^4\delta v_x^{(1)} \quad , \quad iv_\rho q_x\delta v_x^{(1)} \sim \epsilon^2\delta v_x^{(1)}\,, \\
i\rho_0 q_\perp v_L \sim \epsilon v_L \quad , \quad D_{\rho v}q_x q_\perp v_L \sim \epsilon^3 v_L\,, \\
\phi\omega q_x\delta v_x^{(1)} \sim \epsilon^4\delta v_x^{(1)}\,.
\end{gathered}$$

Thus, as we approach the transition, so that $\epsilon \to 0$, we can neglect the terms $D_{\rho x}q_x^2\delta\rho$ and $\phi\omega q_x\delta\rho$ relative to $\omega\rho$, and also drop the $D_{\rho v}q_x q_\perp v_L$ term relative to the $v_\rho q_x\delta\rho$ term. Doing so reduces our $\delta\rho$ equation of motion (2.4.59) to the far more manageable form:

$$[-i(\omega - v_\rho q_x) + D_{\rho\perp}q_\perp^2]\delta\rho + i\rho_0 q_\perp v_L = 0\,. \tag{2.4.70}$$

Performing this sort of power counting on the v_L equation of motion (2.4.60) gives:

$$\begin{aligned} i\omega v_L \sim \epsilon^2 v_L \quad , \qquad & v_v q_x v_L \sim \epsilon^2 v_L \, , \\ B q_\perp \delta v_x^{(1)} \sim \epsilon^3 \delta v_x^{(1)} \quad , \quad & D_{L\perp} q_\perp^2 v_L \sim \epsilon^2 v_L \, , \\ D_x q_x^2 v_L \sim \epsilon^4 v_L \quad , \quad & \nu_x q_x q_\perp \delta v_x^{(1)} \sim \epsilon^3 \delta v_x^{(1)} \, , \\ \nu_t \omega q_\perp \delta v_x^{(1)} \sim \epsilon^3 \delta v_x^{(1)} \, , & \end{aligned}$$

which shows that we can drop the $D_x q_x^2$ term in the v_L equation of motion (2.4.60) relative to the $D_{L\perp} q_\perp^2$ term. Doing so gives:

$$[-i(\omega - v_v q_x) + D_{L\perp} q_\perp^2] v_L + \left[- i \frac{|B|}{\rho_0} q_\perp + \nu_x q_x q_\perp - \nu_t \omega q_\perp \right] \delta\rho = 0 \, . \tag{2.4.71}$$

These simplified equations of motion (2.4.70) and (2.4.71) can be combined into a single vector equation:

$$\boldsymbol{M}(\omega) \begin{bmatrix} \delta\rho \\ \\ v_L \end{bmatrix} = \begin{bmatrix} 0 \\ \\ 0 \end{bmatrix} \, , \tag{2.4.72}$$

where the matrix $\boldsymbol{M}$ is given by:

$$\boldsymbol{M} = \begin{pmatrix} [-i(\omega - v_\rho q_x) + D_{\rho\perp} q_\perp^2] & i\rho_0 q_\perp \\ \left[- i \frac{|B|}{\rho_0} q_\perp + \nu_x q_x q_\perp - \nu_t \omega q_\perp \right] & [-i(\omega - v_v q_x) + D_{L\perp} q_\perp^2] \end{pmatrix} .$$

The eigenvalue condition that determines the eigenfrequencies ω is clearly simply

$$\det \boldsymbol{M}(\omega) = 0 \, , \tag{2.4.73}$$

which leads to

$$\begin{aligned} & -\omega^2 + \omega[(v_v + v_\rho) q_x - i(D_{L\perp} + D_{\rho\perp} - \rho_0 \nu_t) q_\perp^2] - |B| q_\perp^2 \\ & \quad + i(v_\rho D_{L\perp} + v_v D_{\rho\perp} - \rho_0 \nu_x) q_x q_\perp^2 + D_{L\perp} D_{\rho\perp} q_\perp^4 - v_\rho v_v q_x^2 = 0 \, . \end{aligned} \tag{2.4.74}$$

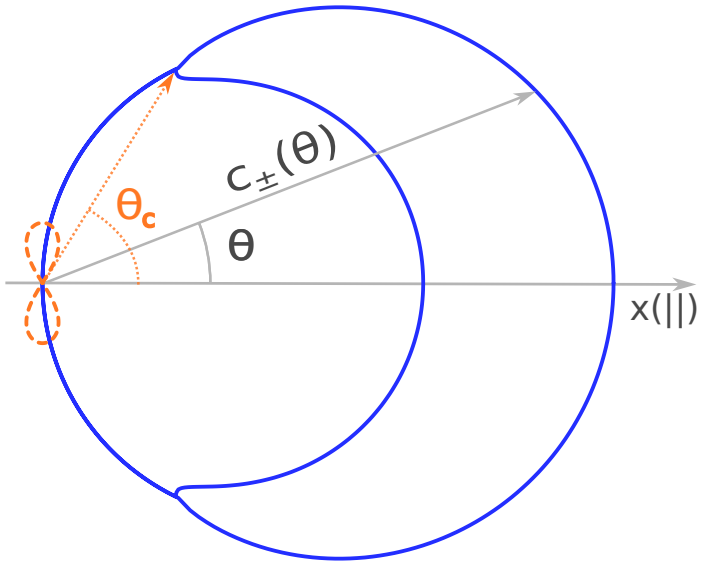

FIGURE 10. Polar plot of the direction dependent sound speed $c_{\pm}(\theta)$ from equation (2.4.67) ($B = -0.025,\ v_\rho = 1.50,\ v_v = 1$ (all units arbitrary).). The horizontal axis, $x(\|)$, is the mean direction of the flock's motion. The solid blue line is the real part of the sound speed. The dashed orange line is the imaginary part of the sound speed. Wavevectors with non-zero imaginary speed values are unstable. This instability region is highly anisotropic, with all of the unstable wavevectors very nearly perpendicular to $y(\|)$. Note that the bifurcation of the real part coincides with the opening angle of the imaginary part , θ_c.

We'll first determine the instability boundary. Instability occurs for those $\mathbf{q}$'s for which the imaginary part $\mathrm{Im}\,\omega(\mathbf{q})$ of $\omega(\mathbf{q})$ is positive ; modes with $\mathrm{Im}\,\omega(\mathbf{q})$ negative are stable. Therefore, the boundary between stable and unstable regions of $\mathbf{q}$ must be the locus on which $\mathrm{Im}\,\omega(\mathbf{q}) = 0$; i.e., the locus on which ω is purely real. We can determine this locus by first taking the imaginary part of (2.4.74) when $\mathrm{Im}\,\omega(\mathbf{q}) = 0$. This implies

$$-(D_{L\perp} + D_{\rho\perp} - \nu_t\rho_0)q_\perp^2\omega + (v_v D_{\rho\perp} + v_\rho D_{L\perp} - \rho_0\nu_x)q_\perp^2 q_x = 0\,, \tag{2.4.75}$$

which can be trivially solved for the value ω_{inst} of ω at which the instability occurs:

$$\omega_{inst} = \left(\frac{v_v D_{\rho\perp} + v_\rho D_{L\perp} - \rho_0\nu_x}{D_{L\perp} + D_{\rho\perp} - \rho_0\nu_t}\right) q_x\,. \tag{2.4.76}$$

Plugging this value of ω into the *real* part of (2.4.74) then leads to a linear equation for q_x^2, whose solution is

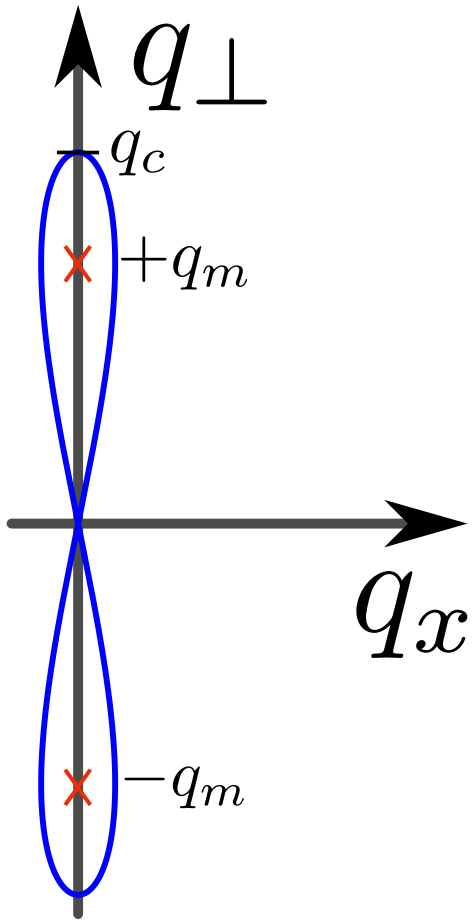

FIGURE 11. A plot of the highly anisotropic instability region in q-space. There are unstable modes at all $\mathbf{q}$'s inside the two loops of this lemniscate. The largest unstable wavevector q_c is marked with a black dash at the highest point on the instability boundary. The wavevectors q_m with the fastest growing modes are identified with red crosses.

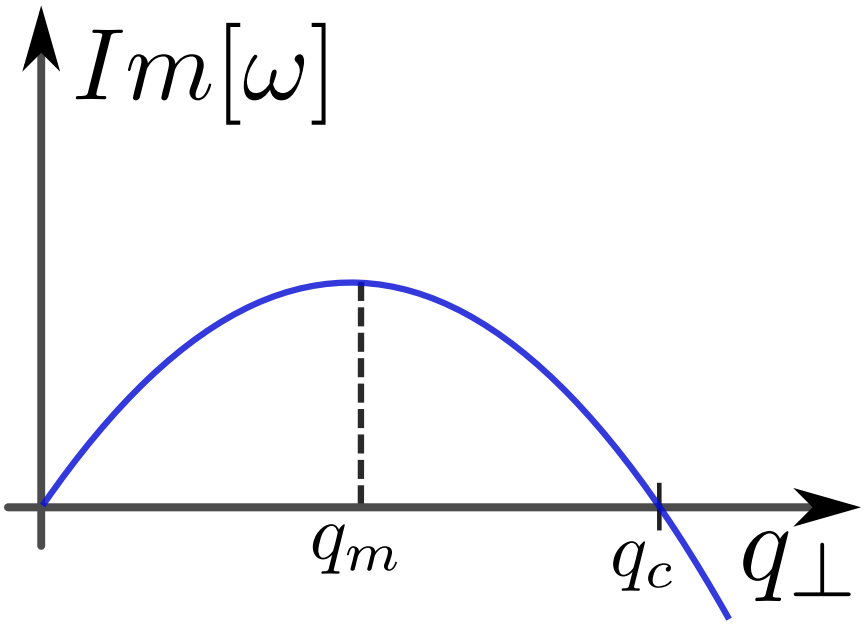

FIGURE 12. Plot of the growth rate (2.4.89). All wave vectors beyond q_c decay. The fastest growth occurs at wavevector $q_\perp = q_m$, the position of the maximum of this curve.

$$q_x^2 = \frac{|B| q_\perp^2 - D_{\rho\perp} D_{\scriptscriptstyle L\perp} q_\perp^4}{V^2} \,, \tag{2.4.77}$$

where we've defined

$$D_3 \equiv D_{\scriptscriptstyle L\perp} + D_{\rho\perp} - \rho_0 \nu_t \,, \tag{2.4.78}$$

$$D_6 \equiv \frac{4}{v_4}(v_\rho D_{\scriptscriptstyle L\perp} + v_v D_{\rho\perp} - \nu_x \rho_0) - 2D_3 \,, \tag{2.4.79}$$

$$V^2 \equiv \left[\frac{(v_v - v_\rho)^2}{4} - \frac{D_6^2 (v_v + v_\rho)^2}{16 D_3^2}\right] . \tag{2.4.80}$$

The alert reader will recognize (2.4.77) as the shape of the stability boundary in wavevector space, as depicted in figure 4 , which we present again here, with a new caption, as figure 11.

Note that the maximum value q_c of $|\mathbf{q}_\perp|$ in the unstable region is the value

$$q_c = \sqrt{\frac{|B|}{D_{\scriptscriptstyle L\perp} D_{\rho\perp}}} \tag{2.4.81}$$

of $|\mathbf{q}_\perp|$ at which the right hand side of (2.4.77) vanishes. This is the justification for the preceding scaling argument, which assumed that $|q_\perp| \lesssim \epsilon$.

Having found the instability boundary, we'd now like to determine the wavevector of the fastest growing mode. As a first step, we'll solve (2.4.74) for ω:

$$\omega = \frac{1}{2}\left[v_4 q_x - iD_3 q_\perp^2 \pm \sqrt{S}\right] \tag{2.4.82}$$

$$S = (v_\rho - v_v)^2 q_x^2 - D_5^2 q_\perp^4 - 4|B|q_\perp^2 + iv_4 D_6 q_x q_\perp^2 \tag{2.4.83}$$

where we've defined

$$v_4 \equiv v_\rho + v_v, \tag{2.4.84}$$

$$D_5^2 \equiv D_3^2 - 4D_{L\perp} D_{\rho\perp}. \tag{2.4.85}$$

Let's first maximize the imaginary part of this over q_x. Note that all of the q_x dependence of the imaginary part comes from the square root. Therefore, we need only maximize the imaginary part of that square root. This implies we want to find the value of q_x at which $\frac{\partial \mathrm{Im}\sqrt{S}}{\partial q_x} = 0$. This condition is equivalent to saying that $\frac{\partial \sqrt{S}}{\partial q_x} = \frac{1}{2\sqrt{S}}\left(\frac{\partial S}{\partial q_x}\right)$ is real. Squaring both sides of this condition implies that $\frac{1}{S}\left(\frac{\partial S}{\partial q_x}\right)^2$ is also real. Hence, at the wavevector of the fastest growing mode,

$$\frac{\left(\frac{\partial a}{\partial q_x}\right)^2 - \left(\frac{\partial b}{\partial q_x}\right)^2 + 2i\left(\frac{\partial a}{\partial q_x}\right)\left(\frac{\partial b}{\partial q_x}\right)}{S} = \text{real}\,, \tag{2.4.86}$$

where $a \equiv (v_\rho - v_v)^2 q_x^2 - D_5^2 q_\perp^4 - 4|B|q_\perp^2$ and $b \equiv D_6 q_x q_\perp^2$ are the real and imaginary parts of S respectively. Calculating the required partial derivatives and performing this algebra, we can rewrite this condition as:

$$4(v_\rho - v_v)^2 \left(\frac{(v_\rho - v_v)^2 q_x^2 - \left(\frac{D_6^2}{4(v_\rho - v_v)^2}\right) q_\perp^4 + iD_6 q_x q_\perp^2}{(v_\rho - v_v)^2 q_x^2 - D_5^2 q_\perp^4 - 4|B|q_\perp^2 + iD_6 q_x q_\perp^2}\right) = \text{real} \tag{2.4.87}$$

Note that the imaginary parts of the numerator and denominator of the parenthetical term in (2.4.87) are equal. Therefore the condition can only be satisfied in two ways: either

1) the real parts of the numerator and denominator are also equal, or

2) the imaginary parts of the numerator and denominator both vanish.

Note that condition 2) implies $q_x = 0$. (We can't have $q_\perp = 0$ and $q_x \neq 0$, since $q_x \ll q_\perp$ in the unstable region.) This proves to be the condition at the maximum.

We will prove that condition 2) must hold by showing that condition 1) is impossible. Assuming condition 1) is satisfied leads to the following constraint on $q_\perp$:

$$\left(- D_5^2 + \frac{D_6^2}{4(v_v - v_\rho)^2} \right) q_\perp^2 = 4|B|. \tag{2.4.88}$$

This condition can never be satisfied in the unstable region, at least for small $\nu_{x,t}$. To see this, note that when ν_x and ν_t are both zero, the coefficient of $q_\perp^2$ on the left hand side of (2.4.88) vanishes, as can be seen from the expressions (2.4.85) and (2.4.80) for $D_{5,6}$ evaluated for $\nu_{x,t} = 0$. This means that for small ν_x and ν_t, the the coefficient of $q_\perp^2$ on the left hand side of (2.4.88) is guaranteed to be small compared to $D_{L\perp} D_{\rho\perp}$. That in turn implies that $|\mathbf{q}_\perp| >> \sqrt{\frac{|B|}{D_{L\perp} D_{\rho\perp}}} = q_c$. However, such wavevectors lie outside the unstable region, in which $|\mathbf{q}_\perp| < q_c$. Hence, this solution is not acceptable, at least for small ν_x and ν_t. This is the limit on which we will henceforth focus. In this limit, we must therefore have $q_x = 0$ at the wavevector of fastest growth.

Setting $q_x = 0$ in our expression (2.4.82) for ω greatly simplifies that expression. Taking Im ω gives the growth rate

$$\text{Im } \omega = -D_3 q_\perp^2 + \sqrt{4|B| q_\perp^2 + D_5^2 q_\perp^4}. \tag{2.4.89}$$

Maximizing this over $q_\perp$ gives, after a little algebra, a quadratic equation for the square of the value q_m of $q_\perp$ at which the growth rate is maximized:

$$\left(\frac{D_5^2}{D_{L\perp} D_{\rho\perp}} \right) q_m^4 + 4 q_c^2 q_m^2 - q_c^4 = 0\,, \tag{2.4.90}$$

whose only real solutions are

$$q_m = \pm q_c \left(\frac{1}{D_5} \sqrt{D_{L\perp} D_{\rho\perp} \left[\sqrt{4 + \left(\frac{D_5^2}{D_{L\perp} D_{\rho\perp}} \right)} - 2 \right]} \right), \tag{2.4.91}$$

whose magnitude the reader can verify for herself is always less than q_c, as it must be.

Intuitive explanation for the anisotropy of the instability

Why is the instability we just found restricted to modes with their wavevectors $\mathbf{q}$ almost perpendicular to the mean velocity $\langle \mathbf{v} \rangle$? The explanation is the competition between convection and pressure forces.

By convection, we mean the v_ρ and v_v terms in equations (2.4.38) and (2.4.39) respectively. These would, in the absence of other effects, cause any instantaneous local configuration of $\rho(\mathbf{r}, t)$ or $\mathbf{v}(\mathbf{r}, t)$ to simply be transported along the direction of flock motion at speeds v_ρ and v_v respectively. Naively, one might have expected v_ρ and v_v to both simply equal the speed of the flock $|\langle \mathbf{v} \rangle|$ itself, since this would simply correspond to the fluctuations moving along with the flock as it moves. However, as explained in reference [43], due to the lack of Galilean invariance in our system, there is no reason that either of these speeds should be equal to $|\langle \mathbf{v} \rangle|$, since the flock itself does not provide the only observable Galilean reference frame in the problem; there is also the frictional substrate. Nor is there any reason that v_ρ and v_v should be equal to each other. Indeed, their *inequality* plays a crucial role in limiting the instability, as can be seen from, e.g., the expression (2.4.65) for ϵ, which shows that $\epsilon \to \infty$ if $v_\rho = v_v$. That is, the window of instability would have an opening angle that covers all space, making all wavevectors unstable.

To understand why the inequality of v_ρ and v_v is so crucial, consider the evolution of a small fluctuation in which both the density and velocity depart from their mean values in a band perpendicular to the direction of mean flock motion, as illustrated in figure 13. This corresponds to a fluctuation with wavevectors making an angle $\theta_{\mathbf{q}} = 0$ with the mean velocity $\langle \mathbf{v} \rangle$. The fluctuation in the density creates a pressure gradient, which, because the inverse compressibility B is negative, causes the velocity field to increase in the direction that tends to *increase* the fluctuation in the density. That is, if the density is *higher* in our band, the pressure forces tend to increase the velocity *into* the band, making the density grow even more. The opposite will happen if the density is lower than average in our band: pressure forces will tend to make the velocity flow *out*, carrying boids out of the band and reducing the density even further.

It is this positive feedback mechanism that is responsible for the familiar instability of negative compressibility equilibrium systems. In *our* system, however, this mechanism must compete against

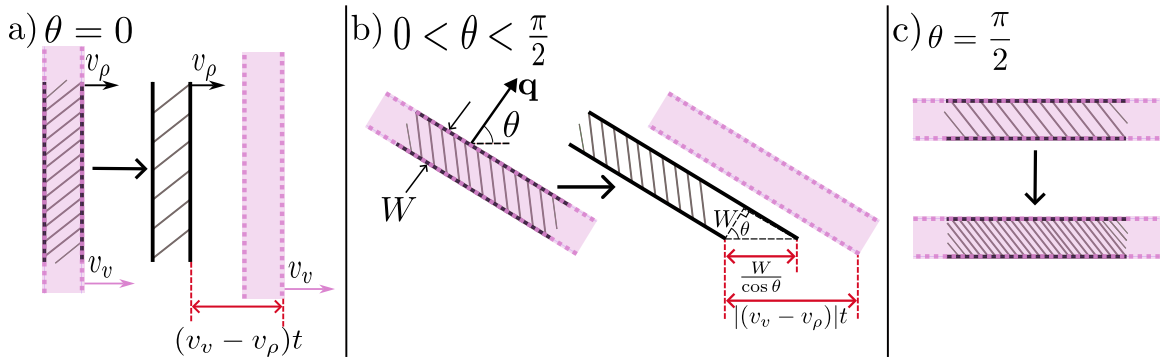

FIGURE 13. Three density and velocity fluctuations are depicted at different angles θ relative to the mean motion of the flock. The density fluctuation is depicted as a short rectangular region with cross hatching. The density of the hash marks indicates the density in that region. The velocity fluctuation is depicted as a long pink rectangular region with dashed edges. Both regions propagate to the right, which is the in mean direction of motion of the flock in all three panels, but at different speeds v_ρ and v_v respectively, and extend infinitely in the directions parallel to their depicted boundary. a) $\theta = 0$, $c_+ = v_v > v_\rho = c_-$. The velocity fluctuation separates from the density fluctuation. The density fluctuation begins to decay by diffusion, and the system is stable against such fluctuations. b) $0 < \theta < \frac{\pi}{2}$,the velocity and density bands still separate over time, but by an a distance that's reduced by a factor of $\cos(\theta)$ when projected along the normal to the bands. As a result, if $\theta > \theta_c$, the bands do not fully separate before the instability sets in, and those fluctuations therefore grow, destablizing the system. c) $\theta = \pi/2$. The density and velocity fluctuations both propagate parallel to the band itself, so they continue to overlap for all time. This is therefore the *most* unstable direction.

the aforementioned convection. For the band direction just discussed, convection stabilizes the system by separating the band of perturbed velocity from the band of perturbed density, because they propagate at different speeds. This is illustrated in figure 13a.

Once the velocity fluctuation is separated from the density fluctuation, both simply decay away by diffusion. Therefore, this orientation of the bands is stable.

Now consider the other extreme case, in which the band runs *parallel* to the direction of mean flock motion, as illustrated in figure 13c. Now the relative displacement of the velocity and density fluctuations makes no difference: the two bands of each still overlap, since the bands are infinitely extended in the direction of that relative motion. Hence, the velocity fluctuation continues to sit right on top of the density fluctuation, allowing the pressure induced instability to occur.

We can even derive the critical instability angle θ_c by this argument. To see this, consider a fluctuation in which the initial band now runs at an angle θ to the vertical, (which corresponds to the component wavevectors $\mathbf{q}$ making an angle θ with the horizontal (i.e., with the x-axis)), as illustrated in 13b. Now the bands will again separate by a distance $|v_v - v_\rho|t$ from each other in a

time t, but that separation *is in the x-direction*. The *projection* of that displacement *perpendicular* to the bands (which is what determines when the bands actually separate, of course) is therefore only $|v_v - v_\rho| t \cos\theta|$.

How long do these bands have to separate before the instability sets in? Well, roughly speaking, the instability growth rate is $\sqrt{|B|}q$, where the wavenumber $q \sim 1/W$, with W the width of the band. Hence, the characteristic time for the instability to grow is the inverse of this rate; i.e., $t \sim \frac{W}{\sqrt{|B|}}$. In this time, the bands will separate perpendicular to the bands by a distance

$$|v_v - v_\rho| t \cos\theta \sim \frac{|v_v - v_\rho| \cos\theta W}{\sqrt{|B|}} \,. \tag{2.4.92}$$

Requiring that this distance be greater than the width W itself leads to the condition:

$$\frac{|v_v - v_\rho| W |\cos\theta|}{\sqrt{|B|}} > W \tag{2.4.93}$$

or, cancelling off the common factor of the band width W,

$$\frac{|v_v - v_\rho| |\cos(\theta)|}{\sqrt{|B|}} > 1 \,. \tag{2.4.94}$$

This is the condition for stability, because only if this condition is satisfied will the bands separate before the fluctuation grows. This condition can be rewritten

$$|\cos(\theta)| > \frac{\sqrt{|B|}}{|v_v - v_\rho|} \,. \tag{2.4.95}$$

For small $|B|$ (i.e., near the instability), the right hand side of this inequality becomes very small, so that we can expand the cosine on the left hand side for θ near $\pm\frac{\pi}{2}$. This leads to the *stability* condition

$$|\theta \pm \pi/2| > \frac{\sqrt{|B|}}{|v_v - v_\rho|} \,, \tag{2.4.96}$$

which the alert reader will recognize as equivalent to the *instability* condition (2.4.68), up to a factor of 2, which one wouldn't expect to get correctly from an argument as crude as this one.

Summary of the stability analysis

In summary, we have shown in this section that autochemotaxis can make the inverse compressibility negative. Next, we demonstrated that *any* negative inverse compressibility, no matter how small, always destabilizes the uniform homogeneous flock. However, in contrast to disordered systems, ordered flocks near this instability are only unstable in a narrow region of region of $\mathbf{q}$ space, very near the direction perpendicular to the direction of flock motion, as illustrated in figure 4. Furthermore, the wavevector of the *most* unstable mode is precisely perpendicular to the mean direction of flock motion.

Finally, we note that the unstable wavevectors are all necessarily small near the threshold of the instability (i.e., when the inverse compressibility B is negative, but its magnitude $|B|$ is small).

We will use all of the above facts in the next section to help us determine the final steady state the system near, but on the unstable side of, the instability threshold.

2.5 The Final state: Phase separation

Formulation

We'd now like to determine the final steady state of the system when the instability found in the last section occurs. We will show in this section that, as claimed in the introduction, this state is "phase separated": the system separates into two macroscopic bands running parallel to the mean velocity, with essentially constant density within each. The interface between these two bands has a width ℓ that is independent of the system width w. Therefore, the ratio $\frac{\ell}{w}$ of the interface width to the system width vanishes as system size $w \to \infty$. The interface width ℓ itself diverges as the system approaches a non-equilibrium "critical point" that we will determine.

Since the instability is sharply focused in the directions perpendicular to the bulk motion, we will seek solutions of our equations of motion that depend only on one Cartesian component of position, by which we mean configurations in which all of the fields depend *on only one of the* $d-1$ *Cartesian coordinates* perpendicular to $\hat{x}$ (d being the dimension of space). We'll call this direction y.

In addition, since the instability was in a mode in which only the "longitudinal" component of the perpendicular velocity $\mathbf{v}_\perp$ (i.e., the component v_L along the direction of the projection of the wavevector of the instability perpendicular to the mean flock velocity vector $\langle \mathbf{v} \rangle$) was non-zero,

we will seek solutions in which only that component of $\mathbf{v}_\perp$ - which, in this geometry, means the y-component- is non-zero.

Note that in addition there is a fluctuating and position dependent component of the velocity in the $\hat{x}$ direction. This is due to the density dependence of $U(|\mathbf{v}|, \rho)$, which, as the reader may recall, maintains the non-zero speed of the flock.

Specifically, we'll search for solutions of the form

$$\mathbf{v}_\perp = v_y(y,t)\hat{y} \quad , \quad \rho = \rho_{ref} + \Delta\rho(y,t)\,, \tag{2.5.1}$$

where ρ_{ref} is some reference density. Because we wish to consider the effect of changing the mean density ρ_0 of the system, we will chose this reference density to in general differ from ρ_0.

The chemically sensitive reader will notice that we have not included the chemo-attractant concentration η in the above analysis. This is because, as we did when we linearized our equations of motion in section IV, we can eliminate this field. We can similarly eliminate the fluctuating component of the velocity along $\langle\mathbf{v}\rangle$. See section IV for more details.

This approach is justified whenever the solutions we are studying vary slowly in space and time. Since we are looking for *steady-state* solutions, slow variation in time is guaranteed (*no* variation is as slow as you can get!). We will verify *a posteriori* that the solutions we find do indeed vary slowly in space, for parameters near a non-equilibrium "critical point". We will identify this "critical point" as we proceed.

As discussed in the introduction, our system proves to be closely analogous to equilibrium phase separation. In particular, it proves, as the analytic solution we'll present below shows, to have the analog of the liquid-vapor critical point[10] of equilibrium phase separation. We will choose our reference density ρ_{ref} to be close to the critical density of our non-equilibrium critical point. This justifies our expansion in powers of $\Delta\rho$, since, as we'll see, it implies that the density $\rho(\mathbf{r})$ is never very far from ρ_{ref} at any point in space in the phase separated state, provided that the mean density ρ_0 is close to ρ_{ref}.

We will not go through the process of eliminating the fast variables in detail here. We will content ourselves with noting that the resultant equations of motion *must* be of the form of the Toner-Tu equations (1.1.3) and (1.1.4). This is an inevitable result of the fact that the symmetries

and conservation laws of our problem are the same as those considered in the formulation of the Toner-Tu model.

Note that, in contrast to the stability analysis of the previous section, we will *not* linearize our equations of motion. However, we will still truncate them to *quadratic* order in the fluctuations $v_y(y)$, to *cubic* order in $\Delta\rho(y)$, and to *bilinear* order in $v_y\Delta\rho$. This will be sufficient if $v_y(y)$ and $\Delta\rho(y)$ are small, as we will again verify they are *a posteriori*.

We will further gradient expand our model. In particular, terms involving 2 derivatives of any type (x, $\perp$, or t) will be expanded only to *linear* order in the fields. This is justified by our expectation that, near the critical point, the density varies very slowly in space and time. We will verify this assumption *a posteriori*.

The resultant equations read[1]:

$$\begin{aligned}\partial_t \mathbf{v}_\perp + v_v \partial_x \mathbf{v}_\perp + \lambda\left(\mathbf{v}_\perp \cdot \nabla_\perp\right)\mathbf{v}_\perp &= -g_1 \Delta\rho \partial_x \mathbf{v}_\perp - g_2 \mathbf{v}_\perp \partial_x \Delta\rho \\ &- \nabla_\perp P_1 + D_B \nabla_\perp (\nabla_\perp \cdot \mathbf{v}_\perp) + D_T \nabla_\perp^2 \mathbf{v}_\perp + D_x \partial_x^2 \mathbf{v}_\perp \\ &+ \nu_x \partial_x \nabla_\perp \Delta\rho + \nu_t \partial_t \nabla_\perp \Delta\rho \,, \end{aligned} \tag{2.5.2}$$

$$\begin{aligned}\partial_t \Delta\rho + \rho_{ref} \nabla_\perp \cdot \mathbf{v}_\perp + \nabla_\perp \cdot (\mathbf{v}_\perp \Delta\rho) + v_\rho \partial_x \Delta\rho &= D_{\rho x} \partial_x^2 \Delta\rho \\ &+ D_{\rho\perp} \nabla_\perp^2 \Delta\rho + D_{\rho v} \partial_x \left(\nabla_\perp \cdot \vec{v}_\perp\right) + \phi \partial_t \partial_x \Delta\rho \\ &+ w_2 \partial_x (\Delta\rho^2) + \frac{\rho_{ref}}{2 v_0} \partial_x (|\vec{v}_\perp|^2) \,, \end{aligned} \tag{2.5.3}$$

where we've defined $\lambda \equiv \lambda_1(\rho_{ref}, v_0)$.

Inserting our one-dimensional ansätze (2.5.1) into the Toner-Tu equations (2.5.2) and (2.5.3), and dropping terms of higher than quadratic order in $v_y(y)$ and higher than cubic order in $\Delta\rho(y)$ leads to PDE's for the one-dimensional evolution:

$$\partial_t v_y + \lambda v_y \partial_y v_y = D_{L\perp} \partial_y^2 v_y - \partial_y P_1 + \nu_t \partial_t \partial_y \Delta\rho, \tag{2.5.4}$$

$$\partial_t \Delta\rho = D_C \partial_y^2 \Delta\rho - \rho_{ref} \partial_y v_y - \partial_y (v_y \Delta\rho), \tag{2.5.5}$$

where we've defined

$$D_{L\perp} \equiv D_B + D_T \quad , \quad D_C \equiv D_{\rho\perp} \,. \tag{2.5.6}$$

In the steady-state, these reduce to two coupled ODE's:

$$\lambda v_y \frac{dv_y}{dy} = D_{L\perp} \frac{d^2 v_y}{dy^2} - \frac{dP_1}{dy}, \tag{2.5.7}$$

$$D_C \frac{d^2 \Delta\rho}{dy^2} - \rho_{ref} \frac{dv_y}{dy} - \frac{d}{dy}(v_y \Delta\rho) = 0 \,. \tag{2.5.8}$$

We will begin by using equations (2.5.7) and (2.5.8) to analytically determine the steady state solution. To validate our solution, we numerically solved the dynamical equations (2.5.4) and (2.5.5), and allowed them to evolve for long times.

In the previous sections we demonstrated the uniform state with $\rho(\mathbf{r}) = \rho_0$ and $v_y = 0$ becomes unstable when the inverse compressibility B changes sign. In order to find a stable steady state, it is therefore necessary to extend our expansion of the isotropic pressure P_1 to third order in $\Delta\rho$:

$$P_1 = P_0 + M\Delta\rho + w\Delta\rho^2 + u\Delta\rho^3 \,. \tag{2.5.9}$$

Recall that, in the linear theory, we found that the inverse compressibility B appearing in the linearized equations of motion become negative for sufficiently strong attractive autochemotaxis. It is therefore clear that the expansion coefficient M in the above expansion will likewise be driven from positive to negative values by increasing autochemotaxis.

We will therefore treat M as an experimentally controllable parameter, which can be decreased by increasing the chemotaxis. The other experimentally controllable parameter at our disposal is the mean density ρ_0.

The experimental situation is thus very similar to studying equilibrium phase separation by tuning both the system's mean density ρ_0 and the temperature, with, in our problem, chemotaxis - or its proxy M- playing the role of temperature. We will therefore determine the "phase diagram" of our system in the ρ_0-M plane.

Stability boundary: the "spinodal" line

We'll begin by determining the *stability boundary* in this ρ_0-M plane. As shown in the last section, the instability occurs when the inverse compressibility vanishes; that is, when

$$B \equiv \left(\frac{dP_1}{d\rho} \right) \Big|_{\rho_0} = 0 \,. \tag{2.5.10}$$

We will define the value of M that satisfies this condition to be $M_{spinodal}$, since it is the precise analog of the spinodal line in equilibrium phase separation: that is, the line on which the uniform density state becomes unstable.

Inserting our expansion (2.5.9) into the condition (2.5.10) gives

$$M_{\text{spinodal}} + 2w(\rho_0 - \rho_{ref}) + 3u(\rho_0 - \rho_{ref})^2 = 0 \,, \tag{2.5.11}$$

which can easily be solved for the spinodal line:

$$M_{\text{spinodal}} = M_c - 3u(\rho_0 - \rho_c)^2 \,, \tag{2.5.12}$$

where we've defined the "critical" value M_c of M as

$$M_c \equiv \frac{w^2}{3u} \,, \tag{2.5.13}$$

and the "critical density"

$$\rho_c \equiv \rho_{ref} - \frac{w}{3u} \,. \tag{2.5.14}$$

The critical values M_c and ρ_c of M and ρ prove to be the analogs of the critical temperature and critical density of an equilibrium phase separating system.

Using (2.5.14), we can rewrite (2.5.7) and (2.5.8) in terms of the critical density ρ_c and a new density variable ρ' defined as the difference between the local density and the *critical* density:

$$\rho' = \rho - \rho_c \,. \tag{2.5.15}$$

Those equations read:

$$\lambda v_y \frac{dv_y}{dy} = D_{L\perp} \frac{d^2 v_y}{dy^2} - \frac{dP_1}{dy}, \tag{2.5.16}$$

$$D_C \frac{d^2\rho'}{dy^2} - \rho_c \frac{dv_y}{dy} - \frac{d}{dy}(v_y \rho') = 0\,. \tag{2.5.17}$$

Two-phase coexistence boundary: the "binodal" line and the common tangent construction

Now we turn to the question of the phase separated state of the system. In discussing this, it is useful to define the analog $F(\rho)$ of an equilibrium free energy for our system. We can do so by defining

$$P_1 = \frac{dF(\rho)}{d\rho}\,, \tag{2.5.18}$$

which is readily seen to imply

$$F(\rho) = F_0 + P_0 \Delta\rho + \frac{M}{2}\Delta\rho^2 + \frac{w}{3}\Delta\rho^3 + \frac{u}{4}\Delta\rho^4\,. \tag{2.5.19}$$

We will show below that the two densities into which the system ultimately phase separates in the steady state are determined, *sufficiently close to the critical point*

$$M = M_c \quad , \quad \rho = \rho_c\,, \tag{2.5.20}$$

by the familiar "common tangent construction" of equilibrium statistical mechanics, applied to the "free energy" (2.5.19). This is illustrated in figure 14.

This analogy to equilibrium statistical mechanics *only* applies close to the critical point (2.5.20). We will also show below that, as we move away from the critical point, the densities are determined by an *"uncommon tangent construction"*: the slope of the free energy (2.5.19) remains the same at both coexisting densities, but the tangents to the free energy curve at those two densities do *not* coincide, as illustrated in figure 14.

As pointed out earlier, our calculation here is very similar to Landau theory for equilibrium liquid-gas phase separation[10]. In particular, as in equilibrium Landau theory, our truncation of the expansion of the pressures in powers of $\Delta\rho$ at third order is only justified very near the "critical

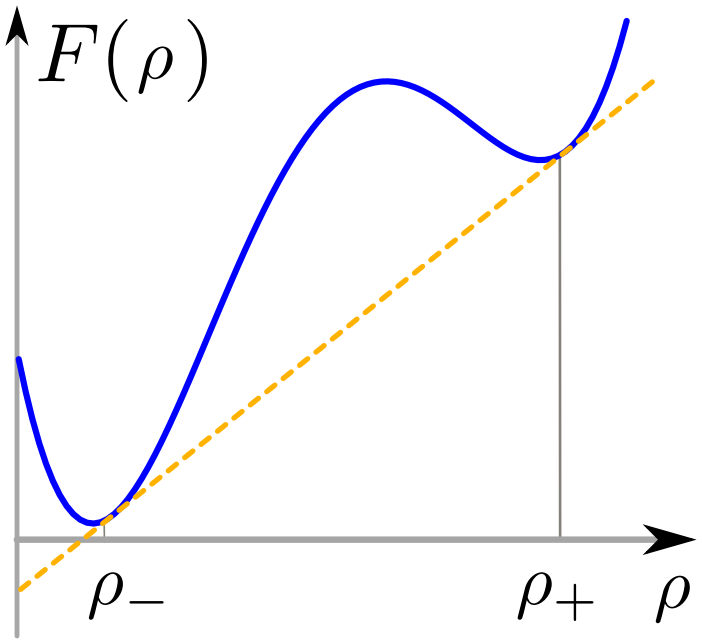

FIGURE 14. Illustration of the common tangent construction. The densities of the high and low density regions are the points that share a common tangent line. In equilibrium physics, each phase has the same thermodynamic pressure and chemical potential.

point" (2.5.20) for our system, and only if the critical density ρ_c is close to the reference density ρ_{ref} around which we did our expansion. Of course, since we are free to choose the reference density ρ_{ref} to be anything we want, we can *always* choose it to be close to the critical density ρ_c. Indeed, we *could* have chosen it to be *equal* to ρ_c; with that choice, we would have had $w = 0$. Hence, if our reference density ρ_{ref} is close to the critical density, w will be small. We will also restrict our discussion to the vicinity of the critical point (2.5.20), which implies that M is small as well. We will therefore make liberal use of the assumption of small M and w in all of the analysis that follows.

All of these assumptions are precisely the same as those usually made in the Landau theory analysis of an equilibrium critical point for phase separation[10]. We therefore expect that our analytic results obtained below to be as reliable as those obtained from equilibrium Landau theory: that is, valid (in the absence of fluctuation effects) sufficiently close to the critical point.

For computational convenience, we will shift variable from $\Delta\rho$ to the new density variable ρ' defined in (2.5.15) as the difference between the local density and the *critical* density. Using our expression (2.5.14) for the critical density, we see that

$$\Delta\rho = \rho' - \frac{w}{3u}\,. \tag{2.5.21}$$

This shift eliminates the quadratic term in the pressure, or, equivalently, the cubic term in the free energy, (2.5.19), enabling us to write

$$P_1(\rho') = \frac{dF(\rho')}{d\rho'} \tag{2.5.22}$$

with

$$F(\rho') = P_0\rho' - \frac{1}{2}m\rho'^2 + \frac{1}{4}u\rho'^4 + \text{constant}\,, \tag{2.5.23}$$

where we've defined

$$m \equiv \frac{w^2}{3u} - M\,. \tag{2.5.24}$$

We have not bothered evaluating the constant in (2.5.23), since it drops out of the equation of motion (2.5.16).

Note also that since we are limiting our analysis to small M and w, m is also small. We will make use of this fact in the perturbation theory we develop for the non-equilibrium phase separation later.

With the expansion (2.5.23) in hand, we now further simplify (2.5.16) and (2.5.17) by rescaling to dimensionless coordinates and variables, as follows:

$$s \equiv \frac{y}{\ell} \quad , \quad \tilde{v} \equiv \frac{v_y}{v_s} \quad , \quad \tilde{\rho} \equiv \frac{\rho'}{\rho_s}\,. \tag{2.5.25}$$

with the characteristic length ℓ, speed v_s, and density ρ_s given by

$$\ell = \sqrt{\frac{D_{L\perp}D_C}{\rho_c m}}\,, \tag{2.5.26}$$

$$v_s = \frac{m\sqrt{D_C}}{\sqrt{D_{L\perp}\rho_c u}}\,, \tag{2.5.27}$$

$$\rho_s = \sqrt{\frac{m}{u}}\,. \tag{2.5.28}$$

We'll see shortly that the length ℓ is roughly the width of the interface between phase separated regions, while the difference between the densities of the two phase separated regions is roughly ρ_s.

In terms of these new coordinates and variables, our dimensionless steady-state equations of motion (2.5.16) and (2.5.17) read:

$$\frac{d^2\tilde{v}}{ds^2} = \frac{d}{ds}\left(\frac{d\tilde{F}(\tilde{\rho})}{d\tilde{\rho}}\right) + \Lambda\tilde{v}\frac{d\tilde{v}}{ds}\,, \tag{2.5.29}$$

$$\frac{d^2\tilde{\rho}}{ds^2} = \frac{d\tilde{v}}{ds} + \Gamma\frac{d}{ds}(\tilde{\rho}\tilde{v})\,, \tag{2.5.30}$$

where we've defined the dimensionless parameters:

$$\Lambda = \frac{\lambda D_c}{D_{L\perp}\rho_c}\sqrt{\frac{m}{u}} = \frac{\lambda D_c \rho_s}{D_{L\perp}\rho_c}\,, \tag{2.5.31}$$

$$\Gamma = \frac{1}{\rho_c}\sqrt{\frac{m}{u}} = \frac{\rho_s}{\rho_c}\,, \tag{2.5.32}$$

and the dimensionless free energy

$$\tilde{F}(\tilde{\rho}) \equiv \frac{\ell}{\rho_s v_s D_{L\perp}} F(\rho' = \rho_s\tilde{\rho}) = \tilde{P}_0\tilde{\rho} - \frac{1}{2}\tilde{\rho}^2 + \frac{1}{4}\tilde{\rho}^4\,. \tag{2.5.33}$$

In (2.5.33), we've defined the dimensionless pressure

$$\tilde{P}_0 \equiv \frac{P_0\ell}{D_{L\perp}v_s}\,. \tag{2.5.34}$$

In doing this rescaling, we have implicitly assumed that m is positive ($m > 0$), as it obviously will be for $M < M_c$ (see equation (2.5.24).

Note that, because m is small near the critical point, both of our dimensionless parameters Γ and Λ are also small near the critical point. Therefore, to leading order near the critical point, we can set them to zero. Doing so gives, for the steady state,

$$\frac{d^2\tilde{v}}{ds^2} = \frac{d}{ds}\left(\frac{d\tilde{F}(\tilde{\rho})}{d\tilde{\rho}}\right)\,, \tag{2.5.35}$$

$$\frac{d^2\tilde{\rho}}{ds^2} = \frac{d\tilde{v}}{ds}\,. \tag{2.5.36}$$

Differentiating (2.5.36) with respect to s and using equation (2.5.35) in the result gives

$$\frac{d^3\tilde{\rho}}{ds^3} = \frac{d}{ds}\left(\frac{d\tilde{F}(\tilde{\rho})}{d\tilde{\rho}}\right). \tag{2.5.37}$$

Integrating this once with respect to s then gives

$$\frac{d^2\tilde{\rho}}{ds^2} = \left(\frac{d\tilde{F}(\tilde{\rho})}{d\tilde{\rho}}\right) + \mu\,, \tag{2.5.38}$$

where μ is a constant of integration. Multiplying both sides of (2.5.38) by $\frac{d\tilde{\rho}}{ds}$ and integrating with respect to s again reveals that this equation has a conserved first integral of motion. That is, the quantity

$$E \equiv -\frac{1}{2}\left(\frac{d\tilde{\rho}}{ds}\right)^2 + \tilde{F}(\tilde{\rho}) + \mu\tilde{\rho} \tag{2.5.39}$$

is a constant (independent of position s).

Assuming that the density profile in the steady state consists of a set of "plateaus" - i.e., regions of essentially constant density - we can calculate the possible plateau densities, which we'll call $\tilde{\rho}_\pm$ (with $\tilde{\rho}_-$ being the smaller of the two), from equations (2.5.38) and (2.5.39). The result, as we'll now show, is identical to the familiar "common tangent construction" of equilibrium phase separation.

On a plateau, all spatial derivatives must vanish. Hence, (2.5.38) implies

$$\left.\frac{d\tilde{F}}{d\tilde{\rho}}\right|_{\tilde{\rho}_\pm} = -\mu\,. \tag{2.5.40}$$

That is, at the plateau densities, the derivatives of the effective free energy $\tilde{F}$ must be equal. Since $\tilde{F}$ and $\tilde{\rho}$ are linearly related to to our dimensionful free energy $F(\rho)$ and ρ, this condition clearly also applies to the derivatives of F with respect to ρ.

Now setting derivatives equal to zero in (2.5.39), and using the fact that the "energy" E must be the same on both plateaus, we obtain a relation between the values of $\tilde{F}$ itself (as opposed to its derivatives) on the plateaus:

$$\tilde{F}(\tilde{\rho}_+) + \mu\tilde{\rho}_+ = \tilde{F}(\tilde{\rho}_-) + \mu\tilde{\rho}_-\,. \tag{2.5.41}$$

This expression can be reorganized to read

$$\tilde{F}(\tilde{\rho}_+) = \tilde{F}(\tilde{\rho}_-) - \mu(\tilde{\rho}_+ - \tilde{\rho}_-)\,. \tag{2.5.42}$$

Using the fact that (2.5.40) implies that $\frac{d\tilde{F}}{d\tilde{\rho}}|_{\tilde{\rho}_\pm} = -\mu$, we see immediately that (2.5.40) and (2.5.42) taken together imply the "common tangent construction": a tangent to a plot of $\tilde{F}(\tilde{\rho})$ at one of the plateau densities $\tilde{\rho}_\pm$ must also be tangent to the plot at the other plateau density. As for the common slope relation, here too, this relation must apply to the original, unrescaled density ρ and free energy F as well.

This common tangent construction is illustrated in figure 14.

To solve for these two steady state densities, it is most convenient to define a new "pseudo-Gibbs free energy" G via

$$G(\tilde{\rho}) \equiv \tilde{F} + \mu\tilde{\rho} = (\tilde{P}_0 + \mu)\tilde{\rho} - \frac{1}{2}\tilde{\rho}^2 + \frac{1}{4}\tilde{\rho}^4\,. \tag{2.5.43}$$

Keep in mind that μ is an as yet undetermined constant of integration, which we must adjust in order to obtain plateaus in the density.

With the definition (2.5.43), we see that the condition (2.5.40) on the slope of the effective free energy $\tilde{F}$ at the plateau densities becomes the simpler condition

$$\left.\frac{dG}{d\tilde{\rho}}\right|_{\tilde{\rho}_\pm} = 0\,, \tag{2.5.44}$$

i.e., G must be minimized (or maximized) at $\tilde{\rho}_\pm$.

Furthermore, the condition (2.5.41) implies

$$G(\tilde{\rho}_+) = G(\tilde{\rho}_-)\,. \tag{2.5.45}$$

Taking the conditions (2.5.44) and (2.5.45) together implies that the arbitrary constant of integration μ must be chosen so that G has two *degenerate* minima. Inspection of (2.5.43) makes it fairly obvious what choice of μ will accomplish this:

$$\mu = -\tilde{P}_0\,. \tag{2.5.46}$$

With this choice, we have

$$G(\tilde{\rho}) = -\frac{1}{2}\tilde{\rho}^2 + \frac{1}{4}\tilde{\rho}^4\,, \tag{2.5.47}$$

which clearly has two degenerate minima at

$$\tilde{\rho}_\pm = \pm 1\,. \tag{2.5.48}$$

Undoing the rescaling (2.5.25) and the shift (2.5.15), we see that this implies the two plateau densities $\rho_\pm$ are given by

$$\rho_\pm = \rho_c \pm \rho_s = \rho_c \pm \sqrt{\frac{m}{u}}\,. \tag{2.5.49}$$

Note that, for small m (i.e., close to the critical point), these densities are close to the critical density ρ_c, which justifies our expansion in $\Delta\rho$.

However, the two phase separated states only become accessible if the mean density ρ_0 lies between these two phase separated densities:

$$\rho_+ > \rho_0 > \rho_- \quad . \tag{2.5.50}$$

Otherwise, conservation of particle number forbids going to a phase separated state (since both plateaus would have either have a *lower* density than the mean density ρ_0, or a higher density). In either case, there is no way that one can achieve the mean density ρ_0 by putting part of the system in a plateau at ρ_+, and the remainder in a plateau of density ρ_-. It is only in the regime (2.5.50) that such a separation can lead to the mean density ρ_0.

Using our result (2.5.49) for $\rho_\pm$, we see that the condition (2.5.50) is equivalent to

$$\sqrt{\frac{m}{u}} > |\rho - \rho_c|\,. \tag{2.5.51}$$

Using our expression (2.5.24) relating m and the parameter M in our expansion (2.5.9) for the isotropic pressure P_1, we see that this condition can be written as

$$M < \frac{w^2}{3u} - u(\rho - \rho_c)^2 \equiv M_{\text{binodal}}\,. \tag{2.5.52}$$

Note that $M_{\text{binodal}} > M_{\text{spinodal}}$ for all ρ. In fact, the ratio

$$\frac{(M_{\text{spinodal}} - M_c)}{(M_{\text{binodal}} - M_c)} = 3 \tag{2.5.53}$$

is universal for all ρ sufficiently close to the critical point.

The result (2.5.52), along with our earlier result (2.5.12) for the "spinodal" value M_{spinodal} of M at which the uniform state becomes unstable, can be summarized by the "phase diagram" in the ρ_0-M plane illustrated in figure 15. For all M above the "binodal" parabola, which is the upper parabola in 15, the system can only be in the uniform state, which is stable. For values of M between the two parabolae (the blue and orange curves in figure 15) - that is, for $M_{\text{binodal}} > M > M_{\text{spinodal}}$, with M_{spinodal} and M_{binodal} given by (2.5.12) and (2.5.52), both the two phase state, and the homogeneous, one phase state, are stable. Finally, for $M < M_{\text{spinodal}}$, only the phase separated state is stable.

The strong similarity between our results and equilibrium liquid-vapor phase separation is apparent from this phase diagram, which is identical to that for an equilibrium liquid-vapor system, with M playing the role of temperature. Recall that M can be increased (decreased) experimentally by decreasing (increasing) the strength of the chemotaxis, or, more generally, by tuning the strength of whatever attractive interactions in the flock reduce the inverse compressiblity.

Note there is an important difference between our results and equilibrium liquid-vapor phase separation. In *equilibrium* systems, a homogeneous density state is only *meta*-stable in the region between the binodal and spinodal curves. The homogeneous state exists at a *local* minimum in the free energy; the *global* minimum is the phase separated state. In the presence of sufficiently large fluctuations, the homogeneous phase will overcome this energy barrier through droplet nucleation[10], which leads to phase separation. Since flocks are *non-equilibrium* systems, we do not have any reason to believe that the global minimum of our pseudo-energy (G) corresponds to a "preferred" stable state. All we can determine is the *local* stability of each phase between the binodal and spinodal curves. Between these two curves, both states are locally stable. We therefore refer to this region as the bistable region.

We turn now from the plateau densities to the form of the interface between different plateaus. We will determine this using equation (2.5.39). Using our earlier result that $\mu = -\tilde{P}_0$, and evaluating

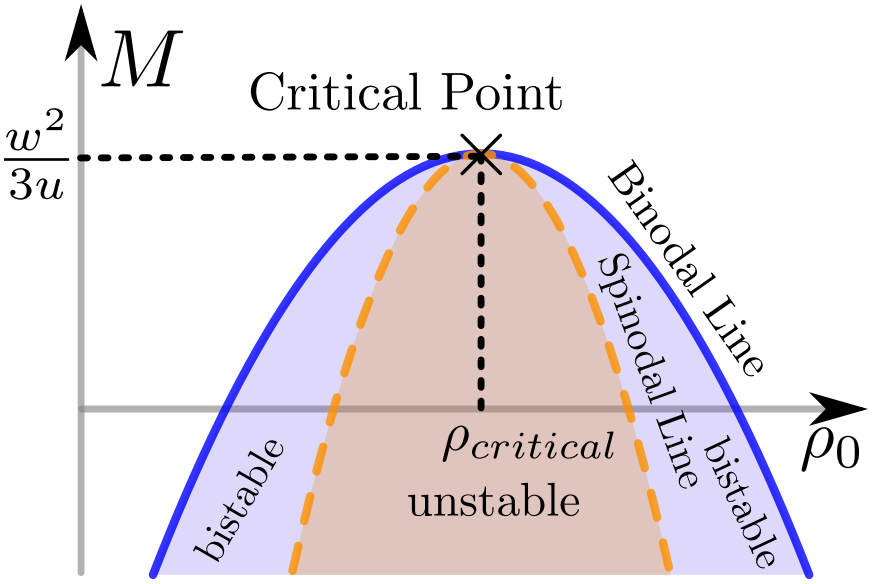

FIGURE 15. Phase diagram of flock phase separation. The solid blue and dashed orange curves are the binodal and spinodal lines respectively , analytic expressions for which are given by equations (2.5.52) and (2.5.12). Note that those expressions are only valid close to the critical point. In the orange filled region under the spinodal line, which is labeled "unstable", only the two-phase state is stable. In the blue region between the spinodal and binodal lines, both the two phase state, and the homogeneous, one phase state, are stable. The analysis we perform in this chapter is done close to the critical point, where our assumption that density variations are small is valid.

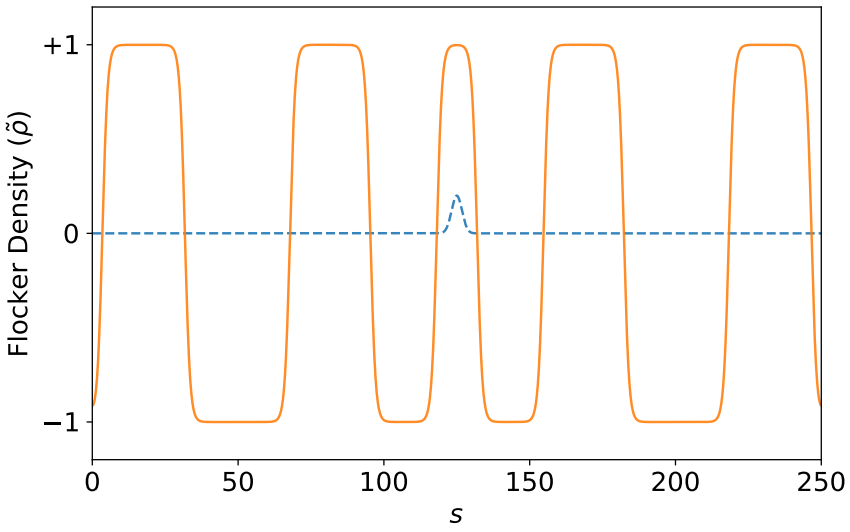

FIGURE 16. A result from evolving equation (2.5.29) and (2.5.30) for a long time, in a periodic space. The dashed blue curve is the initial condition, and the orange curve is the final state. This solution was iterated for 3000 units of time and $\Lambda, \Gamma = 0$. The plateaus are very weakly attracted to one another. The long time steady state solution in a periodic space would consist one a single high density region and a single low density region.

the right hand side of (2.5.39) on a plateau, where $\tilde{\rho} = \pm 1$ and $\frac{d\tilde{\rho}}{ds} = 0$, we see that

$$E = -\frac{1}{4}\,. \tag{2.5.54}$$

Using this in (2.5.39), we can solve that equation for $\frac{d\tilde{\rho}}{ds}$:

$$\frac{d\tilde{\rho}}{ds} = \pm\sqrt{\frac{1}{2}(\tilde{\rho}^4 - 2\tilde{\rho}^2 + 1)} = \pm\frac{1}{\sqrt{2}}(1-\tilde{\rho}^2)\,, \tag{2.5.55}$$

where the plus sign corresponds to the transition region from the low density plateau at $\tilde{\rho} = -1$ on the left to the high density plateau at $\tilde{\rho} = 1$ on the right, and the minus sign to the opposite case. Solving this first order ODE by separation of variables, we find the interface structure:

$$\tilde{\rho}(s) = \pm\tanh\left(\frac{s-s_0}{\sqrt{2}}\right)\,, \tag{2.5.56}$$

where the constant of integration s_0 simply gives the position of the interface.

Undoing our various shifts (2.5.21) and rescalings (2.5.25), we can use this to write the density profile of the interface in terms of the physical variable ρ and the physical coordinate y:

$$\rho(y) \;\;=\;\; \rho_{ref} - \frac{w}{3u} \pm \sqrt{\frac{\frac{w^2}{3u} - B}{u}}\tanh\left(\frac{y-y_0}{\ell\sqrt{2}}\right)\,, \tag{2.5.57}$$

where as before the plus sign describes the case in which the low density plateau is on the left (i.e., as $y \to -\infty$) and the high density on the right, while the minus sign describes the opposite case.

Note that, as claimed earlier, the characteristic width of these interfaces is of order ℓ, and hence diverges like $m^{-1/2}$ as we approach the critical point $m = 0$, as can be seen from equation (2.5.26).

Having found the density ρ, we can now also determine the velocity field $\mathbf{v}$. The y-component follows from equation (2.5.36), which can be integrated once to give

$$\tilde{v} = \frac{d\tilde{\rho}}{ds} + \text{constant} = \pm\frac{1}{\sqrt{2}\cosh^2\left(\frac{s-s_0}{\sqrt{2}}\right)} + \text{constant}\,. \tag{2.5.58}$$

The constant of integration in this expression is readily seen to be zero, since, as can be seen from our full time-dependent 1d equations of motion (2.5.7) and (2.5.8) the volume integral of $\tilde{v}$ is conserved.

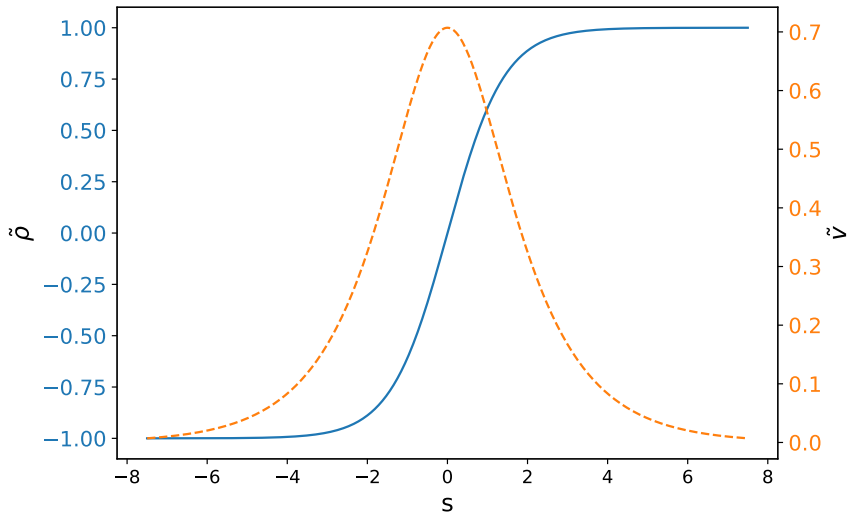

FIGURE 17. Interface density and velocity profile, as described by plus variants of (2.5.56) and (2.5.59), where $s_0 = 0$. The blue line is the density fluctuation. The dashed orange line is the velocity field. Boids accelerate from a low density region (on the left) and move rightward to the high density region. They reach their maximum velocity halfway through the interface and begin to decelerate as they move deeper into the plateau. This accumulation of boids is balanced with diffusion from the high density region to the low density region.

This volume integral was zero initially, because we started with a system moving uniformly in the x-direction, so $v_y(y, t = 0) = 0$ for all y. Hence, this volume integral must be zero in the final state, as it will be if we choose the constant of integration in (2.5.58) to be zero (note that a system with periodic boundary conditions must have equal numbers of "up" and "down" interfaces, so the small contributions to $\int dy v_y(y)$ coming from these regions will cancel).

Thus we have

$$\tilde{v} = \pm \frac{1}{\sqrt{2}\cosh^2\left(\frac{s-s_0}{\sqrt{2}}\right)} \,. \tag{2.5.59}$$

Undoing our rescaling (2.5.25), we see that the true y-component of the velocity is given by

$$v_y(y) = \pm \frac{v_s}{\sqrt{2}\cosh^2\left(\frac{y-y_0}{\ell\sqrt{2}}\right)} \,, \tag{2.5.60}$$

which shows that the velocity is localized to within a distance ℓ of the interface, and that its characteristic velocity scale v_s vanishes like m as the critical point is approached. The density and the velocity profiles (2.5.56) and (2.5.59) are plotted in figure 17.

The steady state profile of the interface is stabilized by a balance between the velocity field (2.5.60), which convectively carries boids from the low density region to the high density region, and diffusion (controlled by $D_{\rho\perp}$) which carries boids from the high density region to the low density region.

Finally, we note that the x-component of the velocity must also become position dependent; in particular, it must take on different values in the plateaus. This is true simply because, in general, the mean local speed of the flock should depend on the local density. Since that density is different in the two plateaus, the speeds in each plateau should be different as well.

This can be verified by looking at the x-component of the Toner-Tu-Keller-Segel equations (2.3.1-2.3.3) in each plateau. In a plateau, all spatial derivatives must vanish. In addition, in the steady state, time derivatives must vanish as well. Hence, the x-component of the Toner-Tu-Keller-Segel equations reduces to

$$U(|\mathbf{v}|, \rho, \eta) = 0\,. \tag{2.5.61}$$

This is an implicit equation relating the speed $|\mathbf{v}|$ to the density ρ and chemo-attractant concentration η. Since $v_y = 0$ in the plateaus (as we just saw), $|\mathbf{v}| = v_x$ there. Hence, v_x will be a function of ρ and η. And since ρ and η take on different values in the plus and minus plateaus, the speed v_x will take on different values as well.

For example, in models like the Vicsek model, in which the speed is an increasing function of ρ, the birds in the high density plateaus will be moving (parallel to the plateau boundaries) *faster* than those in the low density plateaus. For systems exhibiting jamming-like behavior, in which the local speed is a *decreasing* function of the local density, the opposite will be true.

All of the above predictions for the final steady state of the system are fully borne out by numerical solution of the time-dependent equations (2.5.29) and (2.5.30) in a periodic space, as illustrated in figure 16, and in the animation Movie 1, in the supplemental materials.

All of our numerical solutions started with initial conditions in which the departure from a uniform state was small. Furthermore, we performed the analog of a "critical quench" in an equilibrium system, by choosing our mean density to be the critical density ρ_c.

These simulations all show that at small times, the system quickly forms multiple well-defined plateaus, with density and velocity profiles that agree well with our analytic solution. Adjacent

plateaus merge quickly, while distant plateaus do not merge on time scales numerically accessible to our numerical solution (and patience).

This slowing down is a consequence of the exponential approach to the uniform plateau state of both the density (as shown by equation (2.5.56)) and the velocity (as shown by equation (2.5.59)). It is only the overlap of these exponential tails that leads to any interaction at all between neighboring interfaces. As a result, the attraction between neighboring interfaces falls off exponentially with their separation. Hence, the time for neighboring domains of high density to merge also grows exponentially with their separation, which is why the merger slows down so dramatically once the near-lying plateaus have merged.

We believe that this slowing down is an artifact of both the one-dimensionality of our numerical solutions, and the fact that they are noiseless. As discussed in the introduction, we expect that what will really happen, once the plateaus form, is that the bands will begin to undulate due to noise in the system, as illustrated in figure 8. These undulations will grow with time until bands begin bumping into their neighbors, at which point the bands can start to merge. The merged region will then rapidly "zipper" along in both directions, merging the two bands. This process will then repeat with the larger bands formed as a result of such mergers, until full phase separation is achieved.

Again reiterating our discussion in the introduction, we expect the size of these undulations to grow algebraically with time, as the interface fluctuations in the KPZ equation do[23]. Therefore, the time scale needed for undulations of the bands to grow large enough to reach neighboring bands will grow only *algebraically* with the separation between bands, rather than exponentially. We therefore expect that the time required for our autochemotaxic instability to completely phase separate a large system will grow only algebraically with system size.

To make these ideas precise, a theory of the dynamics of fluctuations of an interface between two flocks of different densities and speeds. This would be an excellent topic for further research.

Indeed, a quantitative comparison of our analytical result, (2.5.56) and (2.5.57), for the shape of the interfaces and plateau densities fits the final steady state of these numerical solutions extremely well.

Two-phase coexistence boundary further from the critical point: the *Uncommon* Tangent Construction

The previous section's analysis neglected all non-linearities in the equations of motion except for those in the isotropic pressure P_1. As we saw, this reduces the statics of the problem to those of the equilibrium system.

While, as we also saw in the previous section, it is asymptotically exact to neglect those other non-linearities as we approach the critical point, it must also be the case that all non-equilibrium effects, at least on the plateau densities and the binodal and spinodal curves, must come from those neglected non-linearities. To see those effects, we must therefore go beyond the leading order behavior near the critical point, and include the extra non-linearities Λ and Γ in equations (2.5.29) and (2.5.30).

Recall that we are always limited in any event to analyzing the system close to the critical point, just as one is in equilibrium, because only near the critical point are the density variations small enough to justify our expansion (2.5.9) of the isotropic pressure. Therefore, we will continue to assume that we're close to the critical point, where Λ and Γ are small. This justifies treating Λ and Γ as small perturbations to the problem, and calculating their effects perturbatively.

We will now do such a perturbation theory, and show that the effect of those terms is to change the *common* tangent construction of the previous section to an *uncommon* tangent construction: the condition that the *slopes* of our effective free energy at the two plateau densities be equal survives, but the tangent at either of these no longer intersects the free energy curve at the other.

A very similar "uncommon" tangent construction was found[9] for "motility induced phase separation", which occurs in some *disordered* active systems.

In the steady state, our full equations (2.5.29) and (2.5.30) can be rewritten:

$$\frac{d^2\tilde{v}}{ds} = \frac{d}{ds}\left(\partial_{\tilde{\rho}}\tilde{F}(\tilde{\rho})\right) + \frac{\Lambda}{2}\frac{d\tilde{v}^2}{ds}\,, \tag{2.5.62}$$

$$\frac{d^2\tilde{\rho}}{ds^2} = \frac{d\tilde{v}}{ds} + \Gamma\frac{d}{ds}(\tilde{\rho}\tilde{v})\,, \tag{2.5.63}$$

where $\tilde{F}(\tilde{\rho})$ is the effective free energy we introduced in equation (2.5.33).

Just as in the common tangent construction, we take the derivative of the second equation (2.5.63), and substitute the first equation (2.5.63) into it. This gives

$$\frac{d^3\tilde{\rho}}{ds^3} = \frac{d}{ds}\left(\partial_{\tilde{\rho}}\tilde{F} + \frac{\Lambda}{2}\tilde{v}^2\right) + \Gamma\frac{d^2}{ds^2}(\tilde{\rho}\tilde{v})\,. \tag{2.5.64}$$

Next, we rearrange this equation, keeping the new nonlinearities on the right hand side. Each term is a derivative with respect to s, so we'll integrate once, obtaining

$$\left[\frac{d^2\tilde{\rho}}{ds^2} - \partial_{\tilde{\rho}}\tilde{F}(\tilde{\rho})\right] = \frac{\Lambda}{2}\tilde{v}^2 + \frac{d}{ds}\left(\Gamma(\tilde{\rho}\tilde{v})\right) + \mu\,, \tag{2.5.65}$$

where μ is a constant of integration. Next, we multiply each side by $\frac{d\tilde{\rho}}{ds}$. This enables us to rewrite (2.5.65) in the form

$$\frac{d}{ds}\left[\frac{1}{2}\left(\frac{d\tilde{\rho}}{ds}\right)^2 - G(\tilde{\rho})\right] = \frac{\Lambda}{2}\left(\frac{d\tilde{\rho}}{ds}\right)\tilde{v}^2 + \Gamma\left(\frac{d\tilde{\rho}}{ds}\right)\frac{d}{ds}\left(\tilde{\rho}\tilde{v}\right), \tag{2.5.66}$$

where G is our "pseudo-Gibbs free energy", given by equation (2.5.43); that is $G(\tilde{\rho}) = \tilde{F}(\tilde{\rho}) + \mu\tilde{\rho}$.

Note that if we set the non-linear coefficients Λ and Γ to zero, this recovers our earlier result that the term in square brackets on the left hand side of (2.5.66) is a constant. That constancy then leads directly to the common tangent construction of the last section.

Now we wish to work to next order in the non-linear coefficients Λ and Γ. We'll do this by writing

$$\tilde{\rho} = \tilde{\rho}_1 + \tilde{\rho}_2, \tag{2.5.67}$$

$$\tilde{v} = \tilde{v}_1 + \tilde{v}_2. \tag{2.5.68}$$

where $\tilde{\rho}_1$ and $\tilde{v}_1$ are the common tangent solutions (2.5.56) and (2.5.59) found in the previous section, and $\tilde{\rho}_2$ and $\tilde{v}_2$ are small perturbations to those solutions; that is

$$\tilde{\rho}_1 = \pm\tanh\left(\frac{s - s_0}{\sqrt{2}}\right), \tag{2.5.69}$$

$$\tilde{v}_1 = \pm\frac{1}{\sqrt{2}\cosh^2\left(\frac{s-s_0}{\sqrt{2}}\right)}. \tag{2.5.70}$$

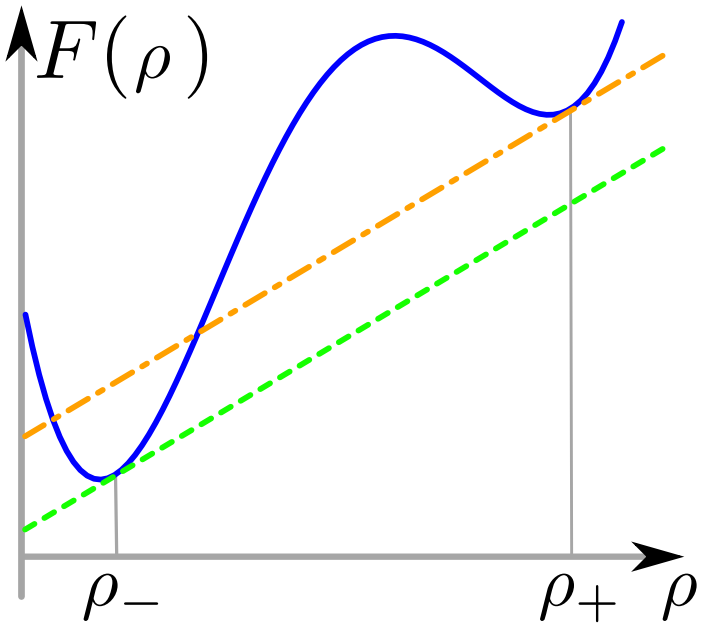

FIGURE 18. Illustration of the uncommon tangent construction. The *slope* of the pseudo-Free energy $F(\rho)$ is the same at both plateau densities $\rho_\pm$, but the two tangents are distinct, rather than being the same line, as they are in equilibrium. It is only in the limit as the system approaches the critical point that the common tangent construction is recovered.

We'll assume, and verify *a posteriori*, that $\tilde{\rho}_2$ and $\tilde{v}_2$ are of order Λ and Γ; $\tilde{\rho}_1$ and $\tilde{v}_1$ are, obviously, zeroeth order in Λ and Γ.

In light of this perturbative hierarchy, we can, to next order in Λ and Γ, replace $\tilde{\rho}$ and $\tilde{v}$ with $\tilde{\rho}_1$ and $\tilde{v}_1$ on the right hand side of (2.5.66). Doing so, using $\tilde{v}_1 = \partial_s \tilde{\rho}_1$, and integrating over s from a low density plateau to a high density one, and remembering once again that within a plateau, $\frac{d\tilde{\rho}}{ds} = 0$, gives

$$\begin{aligned} G(\tilde{\rho}_+) - G(\tilde{\rho}_-) = &-\frac{\Lambda}{2}\int_{-\infty}^{\infty}\left(\frac{d\tilde{\rho}_1}{ds}\right)^3 ds \\ &-\Gamma\int_{-\infty}^{\infty}\left(\frac{d\tilde{\rho}_1}{ds}\right)\frac{d}{ds}\left(\tilde{\rho}_1\left(\frac{d\tilde{\rho}_1}{ds}\right)\right)ds\,. \end{aligned} \tag{2.5.71}$$

Plugging (2.5.69) into this expression, and performing the resulting elementary integrals, we find:

$$G(\tilde{\rho}_+) - G(\tilde{\rho}_-) = 2\tilde{P}_0 + 2\mu = -\frac{4}{15}[\Lambda + \Gamma] \tag{2.5.72}$$

$$\mu = -\tilde{P}_0 - \frac{2}{15}[\Lambda + \Gamma]. \tag{2.5.73}$$

Since we are working in the limit in which the nonlinear coefficients are all small, we see that (2.5.73) implies that $\mu + \tilde{P}_0$ is small. We will make use of this fact in a moment.

Next, we evaluate equation (2.5.65) deep in the density plateaus, where all spatial derivatives vanish. This implies:

$$-\frac{\partial \tilde{F}(\tilde{\rho}_\pm)}{\partial \tilde{\rho}} = -\tilde{P}_0 + \rho_\pm - \rho_\pm^3 = \mu \,. \tag{2.5.74}$$

We define $\delta_\pm = \tilde{\rho}_\pm \mp 1$ as the small deviation of these densities from those we obtained earlier by ignoring these "new" non-linearities. From equation (2.5.73), we see that these obey

$$-(\pm 1 + \delta_\pm) + (\pm 1 + \delta_\pm)^3 = -\mu - \tilde{P}_0 \,, \tag{2.5.75}$$

which is easily solved to linear order in the small quantities $\delta_\pm$ to give

$$\delta_\pm = -\left(\frac{\mu + \tilde{P}_0}{2}\right) = \frac{1}{15}[\Lambda + \Gamma] \,. \tag{2.5.76}$$

Counter-intuitively, the shift is the same for the low and high density plateaus. We strongly suspect that this does not hold to higher orders in perturbation theory, although we have not attempted such a calculation.

Figure 19 shows the excellent agreement between the analytically predicted offset (2.5.76) and the results of simulating the time dependent equation of motion for a long time.

An uncommon tangent construction much like that we find here is also found in phase separation in *disordered* active systems (e.g., "Motility Induced Phase Separation" ("MIPS") [9]). It thus appears that this uncommon construction is, paradoxically, quite common in active systems.

2.6 Conclusion

We have shown that a dry active autochemotaxic flock, or, more generally, *any* flock with sufficiently strong attractive interactions between the flockers, can become unstable to the formation of density bands parallel to the mean direction of motion of the flock. The attractive interactions must drive the inverse compressibiliy negative. This behavior may be connected to the formation of, e.g., unidirectional ant trails. The instability is caused by the autochemotaxic "pressure" or

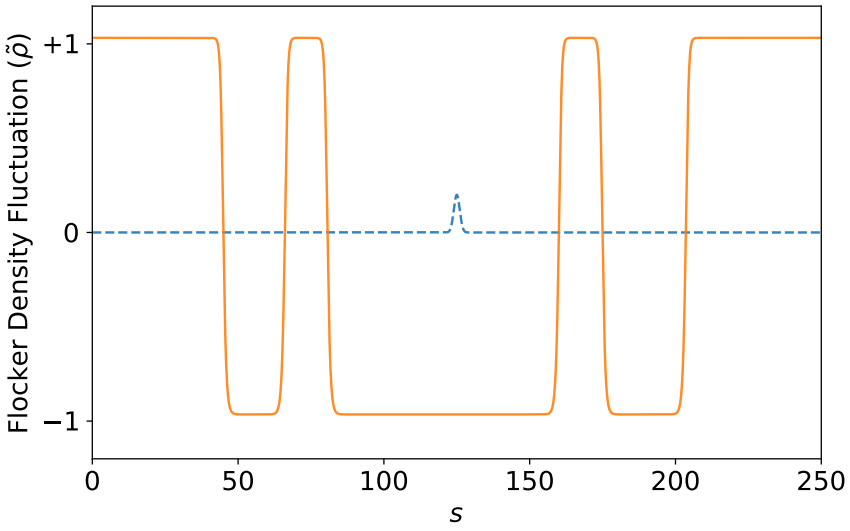

FIGURE 19. The result of evolving equations (2.5.62) and (2.5.63) for a long time in a periodic space. The dashed blue curve is the initial state of the numerical solution. The orange curve is the density profile once the final time step is reached. We retain the plateau structure but it is shifted upwards. The predicted offset $\delta_{\pm}$ differs from the result obtained by direct numerical solution of the equations of motion, (2.5.16) and (2.5.17), by less than 6%. The parameters used for this numerical solution were $\Gamma, \Lambda = 0.25$ and it was iterated for 3000 units of time.

other attractive mechanism overcoming the usual repulsive isotropic pressure, causing the inverse compressibility B of the flock to be negative. We investigated that instability, and specifically demonstrated that:

- The instability is anisotropic. The direction of maximum growth rate is *perpendicular* to the mean flock motion. This initially causes the formation of a growing wavelike modulation of the local density *parallel* to mean flock motion. The maximum growth rate Im $\omega_{max} \propto \sqrt{|B|}$.
- This modulation quickly grows into a "phase separated" flock consisting of high density plateaus separated by low density plateaus. The boundaries of the plateaus are weakly attracted to one another. Our analytical results predict the final state of the system will consist of a single high density plateau and a single low density plateau.
- The approach to this final state is extremely (exponentially) slow in our 1D numerical solutions. However, this one dimensional picture is almost certainly incorrect for the late stage dynamics. We believe that noise, and the wandering of the band boundaries noise induces, will considerably accelerate these coarsening dynamics. In particular, two high density bands may collide and "zip up", as illustrated in figure 8. We speculate that this process will make

the time required to reach the final state of one high density band "coexisting" with one low density band grow algebraically, rather than exponentially, with system size.

- Sufficiently near the "critical point" of this non-equilibrium phase separation, the coexisting plateau densities can be determined by a "common tangent construction" quite like that used in equilibrium phase separation. Further from the critical point, however, this becomes an "*un*common tangent construction", with the effective free energy having the same slope at both plateau densities, but with the tangents at those two densities being distinct, as illustrated in figure 18.

- Our system exhibits both binodal and spinodal lines, just as in equilibrium phase separation, as illustrated in figure 15.

- We have analytically determined the plateau densities, and the profile of both the density and the velocity at the interfaces between plateaus, in a perturbation theory asymptotically valid close to the critical point. This analytic theory compares extremely well with our long-time numerical solutions, even far from the critical point.

Our work has focused on a linear analysis of a noiseless, polar ordered, dry, active autochemotaxic flock. The next step we haven taken is to include fluctuation effects. This inclusion changes the shape of the binodal and spinodal boundaries just as a non-zero temperature changes the shape of the binodal and spinodal boundaries in equilibrium phase separation. In the next chapter, we use the dynamical renormalization group to compute corrections to these curves.

CHAPTER 3

A NEW UNIVERSALITY CLASS

This work was published, in co-authorship with John Toner, in volume 110 of the journal Physical Review E in November 2024.

3.1 Introduction

One of the most important ideas in Condensed Matter Physics is the concept of "universality", which asserts that it is *only* the symmetries and conservation laws describing a given phase of matter, or the transitions between different states, that determine the long-distance, long-time properties of those phases and transitions[10, 27]. The microscopic details of the system in question do not affect these long-distance, long-time properties.

More recently, it has been realized that non-equilibrium systems and phase transitions can belong to *different* universality classes than their equilibrium counterparts. A dramatic demonstration of this difference is provided by the phenomenon of "flocking", in which a large collection of self-propelled entities, which could be macroscopic living creatures[45], microorganisms[15], or even intra-cellular components[40], spontaneously all move in the same direction. Synthetic examples of such "flocks" also abound[7].

A more technical term for such a "flock" is a "polar ordered active fluid": "polar" because a particular direction is picked out (namely, the direction of the mean flock velocity vector $\langle \mathbf{v} \rangle$), "ordered" because this direction is the same throughout an arbitrarily large flock (i.e., the flock has "long-ranged order"), "active" because the "boids" are self-propelled, which consumes energy locally, and "fluid", because we assume that translational symmetry is *not* broken: we are considering flying *fluids*, not flying crystals.

We consider flocks *without* momentum conservation (i.e., "dry" flocks). As a result, the only conservation law in our system is boid number: boids are not being born and dying "on the wing". Both "Malthusian" flocks[40, 12], in which boid number is *not* conserved, and "wet" flocks[37, 29], in which momentum *is* conserved, exhibit very different hydrodynamic behavior, which we will not discuss further here.

The underlying symmetry of the dynamics of flocking is the same as ferromagnetism: rotation invariance[10, 27]. Likewise, the nature of the symmetry *breaking* is the same: by spontaneously choosing a direction to move, a flock is breaking the underlying rotation invariance of the dynamics, in precisely the same way that a ferromagnet spontaneously breaks the underlying rotation invariance of the spin dynamics.

Despite these similarities, the fundamentally non-equilibrium nature of flocking makes it very different from ferromagnetism. In particular, flocks can spontaneously break rotation invariance even in spatial dimension $d = 2$ [47, 43, 18, 11]. Such spontaneous symmetry breaking is forbidden in equilibrium systems by the "Mermin-Wagner-Hohenberg Theorem")[30]. Flocks also exhibit "anomalous hydrodynamics" [43, 42, 44] even in spatial dimensions $d > 2$. By "anomalous hydrodynamics", we mean that the long-wavelength, long-time behavior of these systems can *not* be accurately described by a linear theory; instead, non-linear interactions between fluctuations must be taken into account, even to get the correct scaling laws. Indeed, it is the anomalous hydrodynamics in $d = 2$ that makes the existence of long-ranged order possible [43, 42, 44].

Flocks are also known to exhibit a variety of phase transitions; see, e.g., [22].

One of these transitions is phase separation[32, 33]. This occurs when the individual components of the flock attract each other, and is characterized by the separation of a large flock into one high density band, and one low density band, both moving parallel to each other at different speeds, as illustrated in figure 20. This "band structure" is reminiscent of ant trails. This is not a coincidence; rather, it a consequence of how ants move collectively, as we'll now explain.

Ants, like nearly all motile organisms, utilize chemical gradients to navigate[39]. More specifically, ants exhibit "autochemotaxis": each ant emits a "chemo-attractant"; i.e., a substance to which they themselves (and the other ants in the colony) are attracted. This is known to be the mechanism for the formation of ant trails[13].

We therefore considered in [32, 33] a flock in which the members of the flock (which we'll call "boids") emit a chemo-attractant, which then diffuses, and decays with a finite lifetime. The boids "flock" - that is, follow their neighbors, but with a bias in the direction of the gradient of the chemo-attractant concentration.

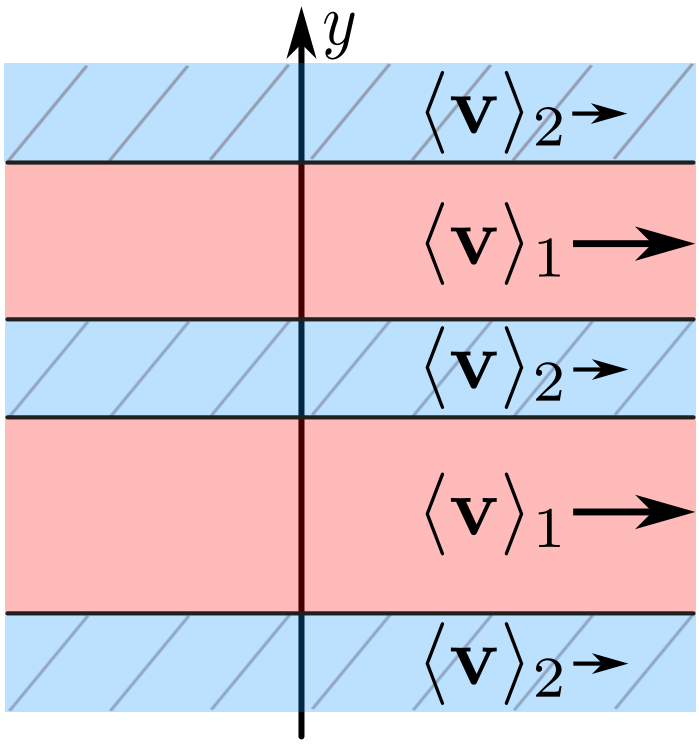

FIGURE 20. The "band" structure of the instability at intermediate times. The density is only modulated along one of the directions (which we call y, and which is indicated in the figure) perpendicular to the direction $\hat{x}$ of mean flock motion.

Of course, many other mechanisms besides autochemotaxis can generate attractions between the boids. Any such mechanism could lead to the phase separation in a polar ordered active fluid considered in [32, 33] and here.

The treatment of this phase separation in [32, 33] revealed a phase diagram qualitatively identical to that found for equilibrium phase separation, as illustrated in figure 21. Here the vertical axis M could be any experimentally tunable parameter that decreases with increasing strength of the attractive interactions. Increasing the strength of the autochemotaxis in an autochemotactic system, for example, which could be accomplished by increasing the strength of the boids' response to the chemical signal, or its emission rate, or the chemo-attractant lifetime, would have this effect.

The horizontal axis is the number density of boids per unit volume (or area, in a two dimensional system).

This "phase diagram" (figure 21) is to be interpreted as follows. For all M above the "binodal" parabola, which is the upper parabola in 21, the system can only be in the uniform state, which is stable. For values of M between the two parabolae (the blue and orange curves in figure 21) - that is, for $M_{\text{binodal}} > M > M_{\text{spinodal}}$ both the two phase state, and the homogeneous, one phase state, are stable. Finally, for $M < M_{\text{spinodal}}$, only the phase separated state is stable. See [33] for a detailed discussion and derivation of this phase diagram.

The strong similarity between these results and equilibrium liquid-vapor phase separation is apparent from this phase diagram, which is identical to that for an equilibrium liquid-vapor system, with M playing the role of temperature. Recall that M can be increased (decreased) experimentally by decreasing (increasing) the strength of the chemotaxis, or, more generally, by tuning the strength of whatever attractive interactions in the flock reduce the inverse compressibility.

Note there is an important difference between these results and equilibrium liquid-vapor phase separation. In *equilibrium* systems, a homogeneous density state is only *meta*-stable in the region between the binodal and spinodal curves. The homogeneous state exists at a *local* minimum in the free energy; the *global* minimum is the phase separated state. In contrast, since flocks are *non-equilibrium* systems, there is no criterion that we know of analogous to the equilibrium global minimization principle to decide which of the two locally stable states is "preferred". Instead, all we can determine is the *local* stability of each phase between the binodal and spinodal curves. Between

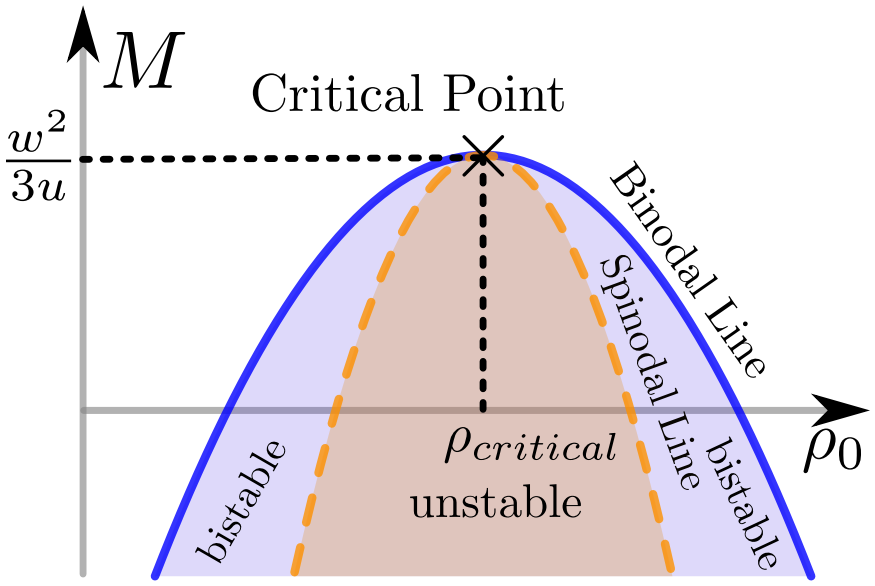

FIGURE 21. Phase diagram of flock phase separation. The solid blue and dashed orange curves are the binodal and spinodal lines respectively. In the orange filled region under the spinodal line, which is labeled "unstable", only the two-phase state is stable. In the blue region between the spinodal and binodal lines, both the two phase state, and the homogeneous, one phase state, are stable. The analysis we perform in this chapter is done close to the critical point, where our assumption that density variations are small is valid.

these two curves, both states are locally stable. We therefore refer to this region as the bistable region.

The treatment of this phase separation in [32, 33] is entirely "mean-field": that is, it ignores fluctuations in the local density and velocity. That is to say, noise terms were ignored. Fluctuations in the density are well-known[10, 27] to radically change the scaling behavior of the density near the critical point in equilibrium systems. In active polar ordered flocks, fluctuations are even more important, because, in addition to the density field, which has large fluctuations because it is becoming "soft" near (and at) the critical point, the local velocity field of the flock (or, more precisely, its components perpendicular to the mean velocity $\langle \mathbf{v} \rangle$) are Goldstone modes, and so have large fluctuations themselves.

Hence, to understand the true behavior of the system near the critical point in figure 21, and the shape of the phase boundaries themselves there, we therefore clearly must include the effect of fluctuations. We do so in this chapter, by performing a dynamical renormalization group (DRG) analysis of the hydrodynamic theory of polar ordered active fluids (a.k.a. the "Toner-Tu equations" [43, 46, 42, 44, 40]) near the critical point, in the presence of noise which drives fluctuations.

The following is a summary of our results. See section 3.4 for details. We find that this critical point belongs to a completely different universality class than the equilibrium liquid-vapor critical point. Indeed, even the *upper critical dimension* d_{LC} of the polar ordered active fluids critical point, defined in the usual way as the spatial dimension below which fluctuations change the scaling behavior of the transition, is different: it is $d_{LC} = 5$. In contrast, for equilibrium phase separation, the upper critical dimension is $d_{LC} = 4$.

While it might at first glance seem unsurprising that our non-equilibrium phase transition should belong to a different universality class than equilibrium phase separation, it becomes more surprising when one notes that active phase separation in systems lacking polar order belongs to the same universality class as equilibrium phase separation, as shown by [8]. Thus, the new universality class we find is not an inevitable consequence of the activity of our system; it also requires the presence of polar order (i.e., a non-zero mean velocity).

We have calculated a number of universal exponents characterizing the scaling behavior near the critical point using the DRG in an $\epsilon = 5 - d$ expansion. The first of these is the usual exponent β giving the width $\delta\rho$ of the binodal and spinodal curves in figure 21. Those widths both scale as a power law in the distance $M_c - M$ from the critical point:

$$\delta\rho \propto |M - M_C|^{\beta} , \tag{3.1.1}$$

We find

$$\beta = \frac{1}{2} - \frac{\epsilon}{6} + \mathcal{O}(\epsilon^2) . \tag{3.1.2}$$

In addition, we have calculated the correlation length exponent ν. Or, to be more precise, we find *two* correlation length exponents $\nu_{\perp,\parallel}$ for the divergences of the correlation lengths $\xi_{\perp,\parallel}$ perpendicular and parallel to the direction of mean flock motion, respectively. These are defined by

$$\xi_{\perp,\parallel} \propto |M - M_C|^{\nu_{\perp,\parallel}} . \tag{3.1.3}$$

We find

$$\nu_\perp = \frac{1}{2} + \frac{\epsilon}{12} + \mathcal{O}(\epsilon^2)\,, \tag{3.1.4}$$

and

$$\nu_\parallel = 1 + \frac{\epsilon}{6} + \mathcal{O}(\epsilon^2)\,. \tag{3.1.5}$$

See the caluclation leading up to 3.4.77 for more details.

In addition to this anisotropy in correlation lengths, which does not occur for equilibrium phase separation, the interpretation of the correlation lengths in phase separating flocks is also different. In equilibrium phase separation, the correlation length is the length scale on which density correlations decay exponentially; that is

$$C_{\rho\rho}^{\text{equilibrium}}(\mathbf{r}) \equiv \langle \delta\rho(\mathbf{r}+\mathbf{R})\delta\rho(\mathbf{R})\rangle \propto e^{-r/\xi}, \tag{3.1.6}$$

where $\delta\rho(\mathbf{r},t) \equiv \rho(\mathbf{r},t) - \rho_c$ is the departure of the local number density $\rho(\mathbf{r},t)$ at position $\mathbf{r}$ and time t from its mean value ρ_c.

In contrast, in phase separating flocks, the correlation lengths $\xi_{\perp,\parallel}$ are the length scales at which the density-density correlation function $C_{\rho\rho}(\mathbf{r})$ crosses over from one power law decay to another. That is

$$C_{\rho\rho}(\mathbf{r}_\perp, r_\parallel = 0) \propto \begin{cases} r_\perp^{2\chi_\perp^c} & ,\ r_\perp << \xi_\perp \\ \\ r_\perp^{2\chi_\perp} & ,\ r_\perp >> \xi_\perp \end{cases} \tag{3.1.7}$$

for points separated in the direction perpendicular to the direction "($\parallel$)" of mean flock motion, and

$$C_{\rho\rho}(\mathbf{r}_\perp = \mathbf{0}, r_\parallel) \propto \begin{cases} r_\parallel^{2\chi_\parallel^c} & ,\ r_\parallel << \xi_\parallel \\ \\ r_\parallel^{2\chi_\parallel} & ,\ r_\parallel >> \xi_\parallel \end{cases} \tag{3.1.8}$$

for points separated along the direction of mean flock motion. This behavior is illustrated in figure (22).

Thus, it would be more accurate to describe $\xi_{\perp,\parallel}$ as "crossover lengths" rather than "correlation lengths".

Our ϵ-expansion results for the critical "roughness exponents" $\chi^c_{\perp,\parallel}$ in spatial dimensions $d = 5-\epsilon$ are

$$\chi^c_\perp = -2 + \frac{\epsilon}{2} + \mathcal{O}(\epsilon^2) \tag{3.1.9}$$

$$\chi^c_\parallel = -4 + \epsilon + \mathcal{O}(\epsilon^2) \tag{3.1.10}$$

These exponents follow from the linearized version of our theory of the critical point, in particular 3.4.17, coupled with the observation that the only correction to these exponents arising from non-linearities comes in at $O(\epsilon^2)$.

In $5-\epsilon$ dimensions, the *non*-critical roughness exponents are given by

$$\chi_\perp = \frac{3-d}{2} = -1 + \frac{\epsilon}{2} \tag{3.1.11}$$

$$\chi_\parallel = 3 - d = -2 + \epsilon \tag{3.1.12}$$

exactly.

Note that these are *not* the same as the corresponding exponents in equilibrium liquid-vapor phase separation. This is because, in contrast to liquids and vapors, the polar ordered fluid away from the critical point spontaneously breaks a continuous symmetry (rotation invariance), which leads to Goldstone modes, which in turn make the exponents non-trivial. This point is discussed more in section 3.3 below.

Once the spatial dimension goes below $d = 4$ (which is obviously true for all physically relevant cases), the exact results (3.1.11) and (3.1.12) cease to hold. The χ's that apply then are simply those of the ordered state of a polar active fluid (i.e., a "flock") in that particular dimension of space. These exponents are known only from simulation[28], and are given in three dimensions by

$$\chi_\perp \approx \chi_\parallel \approx -.62\,, \tag{3.1.13}$$

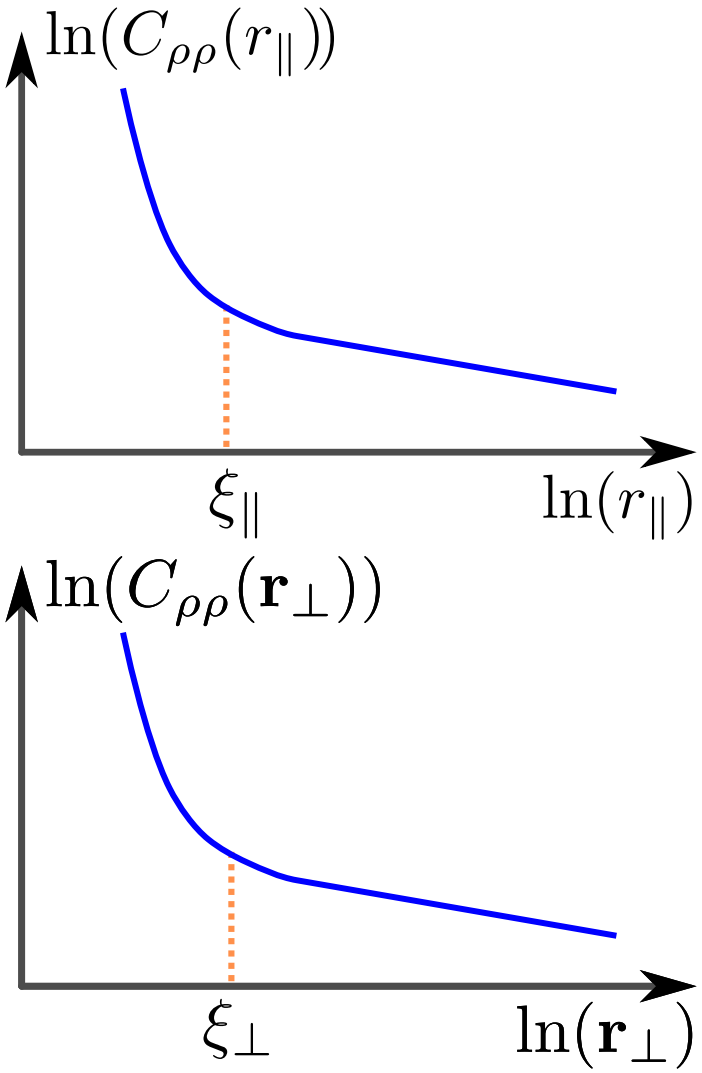

FIGURE 22. Schematic log-log plots of the density autocorrelation functions against distance in the direction of mean flock motion (top), and perpendicular to the mean direction of flock motion (bottom). In contrast to equilibrium phase separation, the density correlation decay does not drop off exponentially for distances greater than the correlation lengths. Instead, there are crossover lengths between these two regions with different power law decays. We identify those crossover lengths as the correlation lengths $\xi_{\perp,\parallel}$

and in two dimensions by

$$\chi_\perp \approx \chi_\parallel \approx -.31\,. \tag{3.1.14}$$

The remainder of this chapter is organized as follows. In section (3.2), we present the hydrodynamic theory of phase separating flocks near the critical point. We solve the linearized version of this theory in section (3.3). In section (3.4), we analyze the full model, including non-linearities, using the DRG, and thereby show that this linear theory breaks down for spatial dimensions $d \leq 5$, in contrast to equilibrium phase separation, for which this breakdown only occurs for $d \leq 4$. Additionally in section (3.4), we find the fixed point that controls the new universality class of phase separating flocks, and determine the critical exponents β, $\nu_{\perp,\parallel}$, and $\chi^c_{\perp,\parallel}$ to linear order in $\epsilon = 5 - d$. Section (3.5) summarizes our results. In the appendix we show that a *potentially* dangerously irrelevant parameter is, in fact, harmlessly irrelevant.

3.2 Hydrodynamics

This section may appear, at first glace, to be a retreading of our discussion of Toner-Tu theory and that is because the beginning part is; however, some subtle, yet important, details (e.g., some notational changes) are covered in the later half of this section. So convince your palate that it is not burdensome retreading that you taste, but notes of a light refreshing reminder deep within in this full-bodied cocktail (i.e., non-alcoholic, of course).

Our hydrodynamic model of a generic polar active fluid near the critical point for phase separation is the Toner-Tu theory of flocks [43, 46, 42, 44, 40], with a few small but important modifications. The most crucial difference is that we consider the case in which the inverse compressibility (defined precisely below) of the flock is tuned through zero to negative values.

The theory is a continuum model for two fields: the number density of boids $\rho(\mathbf{r}, t)$, and the boid velocity field $\mathbf{v}(\mathbf{r}, t)$. The equations of motion for these fields are:

$$\partial_t \mathbf{v} + \lambda_1(\mathbf{v}\cdot\nabla)\mathbf{v} + \lambda_2(\nabla\cdot\mathbf{v})\mathbf{v} + \lambda_3\nabla(|\mathbf{v}|^2) =$$
$$U(|\mathbf{v}|,\rho)\mathbf{v} - \nabla P_1(|\mathbf{v}|,\rho) - \mathbf{v}(\mathbf{v}\cdot\nabla P_2(|\mathbf{v}|,\rho)) + D_B\nabla(\nabla\cdot\mathbf{v})$$
$$+ D_T\nabla^2\mathbf{v} + D_2(\mathbf{v}\cdot\nabla)^2\mathbf{v} + \mathbf{f} \tag{3.2.1}$$
$$\partial_t\rho + \nabla\cdot(\mathbf{v}\rho) = \nabla\cdot\mathbf{f}_\rho \tag{3.2.2}$$

The significance of these terms is as follows:

The terms involving the parameters λ_i are analogs of the convective derivative of the coarse grained velocity field from the Navier-Stokes equations. If our system respected Galilean invariance, we would have $\lambda_1 = 1$ and $\lambda_{2,3} = 0$. However, because our flock is on a frictional substrate, which provides a special reference frame, we have neither Galilean invariance nor momentum conservation.

The $U(|\mathbf{v}|,\rho)$ term, which is similar in form to a dissipative term, clearly therefore also breaks both Galilean invariance and momentum conservation. However, because our system is active $U(|\mathbf{v}|,\rho)$ need not be negative for all $|\mathbf{v}|$; indeed, if we are to model a system in which the steady state is a *moving* flock, we must take it to have the form illustrated in figure 1. In earlier literature, the special choice $U(|\mathbf{v}|,\rho) = A - u|\mathbf{v}|^2$ is often made. This is by no means necessary, however.

The P_1 term is perfectly analogous to the isotropic pressure in the Navier-Stokes equations. The P_2 term is an "anisotropic pressure", and is allowed because our system breaks rotation invariance locally, which means that there is no reason that the response to density gradients *along* the local velocity $\mathbf{v}$ should be the same as that to gradients perpendicular to $\mathbf{v}$. Note that this term also breaks Galilean invariance.

The velocity diffusion constants D_B and D_T are precise analogs of the bulk and shear viscosities, respectively, in the Navier-Stokes equations. The diffusion constant D_2 is an anisotropic viscosity which has no analog in the Navier-Stokes equation, because it violates Galilean invariance. Since we lack Galilean invariance here, it is allowed in our problem. All of these viscosities have the effect of suppressing fluctuations of the velocity away from spatial uniformity.

The quantities $P_{1,2}(|\mathbf{v}|,\rho)$, $U(|\mathbf{v}|,\rho)$, $D_{B,T,2}$, and $\lambda_{1,2,3}$ are in general functions of $|\mathbf{v}|$ and ρ. They can *not* depend of the *direction* of $\mathbf{v}$ due to rotation invariance.

We will expand these parameters in powers of $\delta\rho(\mathbf{r},t) \equiv \rho(\mathbf{r},t) - \rho_c$, where $\delta\rho(\mathbf{r}) \equiv \rho(\mathbf{r},t) - \rho_c$ is the departure of the local number density of flockers $\rho(\mathbf{r},t)$ at position $\mathbf{r}$ and time t from its "critical" value ρ_c, and $\delta|\mathbf{v}(\mathbf{r},t)| \equiv |\mathbf{v}(\mathbf{r},t)| - v_0$ is likewise the departure of the local speed of the flockers $|\mathbf{v}(\mathbf{r},t)|$ at position $\mathbf{r}$ and time t from its mean value v_0.

Particularly crucial is the expansion of the isotropic pressure $P_1(\rho, |\mathbf{v}|)$. This can be written

$$P_1 = P_0 + \frac{m}{\rho_c}\delta\rho + u\delta\rho^3 - K\nabla_\perp^2\delta\rho\,. \tag{3.2.3}$$

This expansion differs from that considered in reference [41] in a few details, because our interest here is in the critical point, whereas [41] dealt with the ordered phase. These differences are:
1) We do not have a quadratic term (i.e., a $\delta\rho^2$ term) in the isotropic pressure P_1, because we are expanding around the critical point at which that term vanishes. Reference [41] had such a term, because it was studying flocks away from the critical point. In [33], it was shown that the special density around which the expansion of the pressure lacks this quadratic term is the critical density of the phase separation.

Thus, our leading order non-linearity in density is $\mathcal{O}(\delta\rho^3)$.
2) We will explicitly consider the limit in which the coefficient m of the linear term in P_1 vanishes; that is, the limit $m \to 0$, which was not considered in [41]. We consider this limit because phase separation occurs when the parameter m is tuned from positive to negative values. As mentioned in the introduction, there are many mechanisms that can lead to phase separation by driving this coefficient to zero. In addition to all of the mechanisms that can do so in equilibrium systems (e.g., direct attractive interactions between the particles), in active systems, auto-chemotaxis can also do this, as happens in, e.g., the Keller-Segel equations[25, 24, 38], and in our earlier work[32, 33].
3) The term $K\nabla^2\delta\rho$ was not considered in [41], because this term is negligible at long wavelengths in the ordered phase. This is because it scales in Fourier space like $q_\perp^3\delta\rho$, while the $\nu_x\partial_x\nabla_\perp\delta\rho$ scales like $q_x q_\perp\delta\rho$. Since the important regime of wavevectors in the ordered phase is $q_x \sim q_\perp^\zeta$ with $\zeta < 1$, the ν_x term dominates throughout the dominant regime of wavevector. Near the critical point, however, as we show in this chapter, the dominant regime of wavevector has $q_x \sim q_\perp^2$ (to one loop order), and so the ν_x and K terms are both of order $q_\perp^3\delta\rho$. Hence the K term must be kept.

As shown in ref [33], the coefficient m of the linear term in this expression can be driven from positive to negative values in autochemotaxic systems by increasing the strength of the

autochemotaxis[33], as well as a variety of other mechanisms. Here we will simply treat m as an experimentally tunable parameter that plays a role closely analogous to that of temperature in the liquid-gas phase diagram.

The noise terms $\mathbf{f}$ and $\mathbf{f}_\rho$ are assumed to be Gaussian white noise with the correlations:

$$\langle f_i(\mathbf{r},t) f_j(\mathbf{r}',t')\rangle = \Delta\delta_{ij}\delta^d(\mathbf{r}-\mathbf{r}')\delta(t-t') \tag{3.2.4}$$

$$\langle f_{\rho i}(\mathbf{r},t) f_{\rho j}(\mathbf{r}',t')\rangle = \Delta_\rho\delta_{ij}\delta^d(\mathbf{r}-\mathbf{r}')\delta(t-t') \tag{3.2.5}$$

We remind reader that the divergence of the $\mathbf{f}_\rho$ is taken in equation (3.2.2) to ensure that the inclusion of this noise term does not violate conservation of boid number. This is not a "Malthusian" flock[12].

In reference [33], the noises were set to zero. In a real system, they will always be non-zero. This causes fluctuations, which, as we'll show below, invalidate, for all spatial dimensions $d \leq 5$, the "linear" or, equivalently, "mean-field", approach used in reference [33].

We begin by expanding these equations of motion about a homogeneous moving flock state at the critical density. In a homogeneous state, both of our fields are constants, so we have

$$\rho(\mathbf{r},t) \quad = \rho_c\,, \tag{3.2.6}$$

$$\mathbf{v} \quad = v_0\hat{x}\,. \tag{3.2.7}$$

Note that the direction of $\mathbf{v}$ is completely arbitrary, due to the rotation invariance of our model. We will henceforth choose our coordinate system so that the x-axis is the direction of the spontaneous velocity.

Inserting these constant ansätze (3.2.6) and (3.2.7), into our equations of motion (3.2.1) and (3.2.2), it is clear that all terms involving spatial or temporal derivatives vanish. It is easy to see that this implies that the density equation (3.2.2) is automatically satisfied. The velocity equation reduces to

$$U(v_0,\rho_c) = 0\,. \tag{3.2.8}$$

This is a scalar algebraic equation for the unknowns ρ_c and v_0. We clearly need one more condition. This can be obtained by fixing ρ_c to be the value of ρ at which the expansion of the isotropic pressure P_1 takes the form 3.2.3; that is, that there is no term quadratic in $\delta\rho$.

With these values of ρ_c in hand, we can then in principle use (3.2.8) to determine the steady-state speed v_0. We will also assume that the solution of (3.2.8) is unique, which it clearly will be if $U(v_0, \rho_c)$ looks like figure 1.

We now expand our equations of motion about this steady state solution. That is, we will write

$$\rho(\mathbf{r}, t) = \rho_c + \delta\rho(\mathbf{r}, t), \tag{3.2.9}$$

$$\mathbf{v}(\mathbf{r}, t) = v_0\hat{x} + \delta\mathbf{v}(\mathbf{r}, t) = (v_0 + \delta v_x(\mathbf{r}, t))\hat{x} + \mathbf{v}_\perp(\mathbf{r}, t), \tag{3.2.10}$$

and then expand our equations of motion to cubic order in the fluctuation $\delta\rho(\mathbf{r}, t)$ of the density, and quadratic order in the fluctuation $\delta\mathbf{v}(\mathbf{r}, t)$ of $\mathbf{v}(\mathbf{r}, t)$. The DRG analysis that we will perform in section (3.4) shows that this order is sufficient to obtain the universal scaling laws of the transition.

The expansion process of linearization begins by expanding all of the $|\mathbf{v}|$ and ρ dependent parameters in the equations of motion. One also needs to eliminate the "fast" mode δv_x. This process is done explicitly in excruciating detail in reference [33]. The only differences between our analysis here and that done in reference [33] are the differences in the starting model discussed above. The result is the following closed set of equations of motion for $\delta\rho$ and $\mathbf{v}_\perp$:

$$\begin{aligned}\partial_t\mathbf{v}_\perp + v_v\partial_x\mathbf{v}_\perp + \lambda\left(\mathbf{v}_\perp\cdot\nabla_\perp\right)\mathbf{v}_\perp &= -g_1\delta\rho\partial_x\mathbf{v}_\perp - g_2\mathbf{v}_\perp\partial_x\delta\rho \\ &- \nabla_\perp\left(\frac{m}{\rho_c}\delta\rho + u\delta\rho^3 - K\nabla_\perp^2\delta\rho\right) + D_B\nabla_\perp(\nabla_\perp\cdot\mathbf{v}_\perp) + D_T\nabla_\perp^2\mathbf{v}_\perp \\ &+ D_x\partial_x^2\mathbf{v}_\perp + \nu_x\partial_x\nabla_\perp\delta\rho + \nu_t\partial_t\nabla_\perp\delta\rho + \mathbf{f}_\perp\,,\end{aligned} \tag{3.2.11}$$

$$\begin{aligned}\partial_t\delta\rho + \rho_c\nabla_\perp\cdot\mathbf{v}_\perp + \gamma\nabla_\perp\cdot(\mathbf{v}_\perp\delta\rho) + v_\rho\partial_x\delta\rho &= D_{\rho x}\partial_x^2\delta\rho + D_{\rho\perp}\nabla_\perp^2\delta\rho \\ &+ D_{\rho v}\partial_x\left(\nabla_\perp\cdot\mathbf{v}_\perp\right) + \phi\partial_t\partial_x\delta\rho + w_2\partial_x(\delta\rho^2) + \frac{\rho_c}{2v_0}\partial_x(|\mathbf{v}_\perp|^2) + \nabla\cdot\mathbf{f}_\rho\,,\end{aligned} \tag{3.2.12}$$

where we've defined $\lambda \equiv \lambda_1(\rho_c, v_0)$.

Strictly speaking, the coefficient γ of the $\nabla_\perp \cdot (\mathbf{v}_\perp \delta\rho)$ term in the equation of motion 3.2.12 for $\delta\rho$ is $\gamma = 1$ at this point. We have introduced γ because this coefficient will *not* remain equal to 1 upon renormalization, as we will see when we perform the DRG in section 3.4.

3.3 Linear Analysis

As a first step towards understanding the effect of fluctuations, we will solve these equations of motion to *linear* order. Our goal is to solve for $\mathbf{v}$ in terms of the forces $\mathbf{f}$ and $\mathbf{f}_\rho$. Once we have these solutions, we can obtain the correlations of the fields $\delta\rho$ and $\mathbf{v}_\perp$ from the known correlations (3.2.4) and (3.2.5) of the forces. These linear results are necessary for the DRG analysis performed later in this chapter.

To linear order, the equations of motion read:

$$\begin{aligned}\frac{\partial \delta\rho}{\partial t} =& D_{\rho\perp}\nabla_\perp^2 \delta\rho + D_{\rho x}\partial_x^2 \delta\rho - v_\rho \partial_x \delta\rho - \rho_c \nabla_\perp \cdot \mathbf{v}_\perp + D_{\rho v}\partial_x(\nabla_\perp \cdot \mathbf{v}_\perp) \\ &+ \phi \partial_t \partial_x \delta\rho + \nabla \cdot \mathbf{f}_\rho \,, \end{aligned} \tag{3.3.1}$$

$$\begin{aligned}\frac{\partial \mathbf{v}_\perp}{\partial t} =& - v_v \partial_x \mathbf{v}_\perp - \frac{m}{\rho_c}\nabla_\perp \delta\rho + K\nabla_\perp \nabla_\perp^2 \delta\rho + D_B \nabla_\perp(\nabla_\perp \cdot \mathbf{v}_\perp) + D_T \nabla_\perp^2 \mathbf{v}_\perp \\ &+ D_x \partial_x^2 \mathbf{v}_\perp + \nu_x \partial_x \nabla_\perp \delta\rho + \nu_t \partial_t \nabla_\perp \delta\rho + \mathbf{f}_\perp \,, \end{aligned} \tag{3.3.2}$$

where all coefficients can be written in terms of the original model parameters, as shown in great detail in [33].

We then proceed by Fourier transforming these equations of motion, using the following convention for Fourier transforms:

$$f(\mathbf{q},\omega) = \int_t \int_{\mathbf{r}} e^{-i(\mathbf{q}\cdot\mathbf{r} - \omega t)} f(\mathbf{r},t), \tag{3.3.3}$$

where $\int_t \equiv \int dt$ and $\int_{\mathbf{r}} \equiv d^d r$. The inverse transform is then given by

$$f(\mathbf{r},t) = \int_\omega \int_{\mathbf{q}} f(\mathbf{q},\omega) e^{i(\mathbf{q}\cdot\mathbf{r} - \omega t)} \,, \tag{3.3.4}$$

where, here and throughout this chapter, we will use the shorthand notation $\int_\omega \equiv \frac{d\omega}{2\pi}$ and $\int_{\mathbf{q}} \equiv \int \frac{d^d q}{(2\pi)^d}$.

The Fourier transformed equations of motion are:

$$\Big[-i(\omega - v_\rho q_x) + D_{\rho\perp} q_\perp^2 + D_{\rho x} q_x^2 - \phi\omega q_x \Big] \delta\rho = -i\rho_c \mathbf{q}_\perp \cdot \mathbf{v}_\perp - D_{\rho v} q_x (\mathbf{q}_\perp \cdot \mathbf{v}_\perp) + i\mathbf{q} \cdot \boldsymbol{f}_\rho, \tag{3.3.5}$$

$$\Big[-i(\omega - v_v q_x) + D_T q_\perp^2 + D_x q_x^2 \Big] \mathbf{v}_\perp + D_B \mathbf{q}_\perp (\mathbf{q}_\perp \cdot \mathbf{v}_\perp) = \Big[-i\Big(\frac{m}{\rho_c} + K q_\perp^2 \Big) + \nu_t \omega - \nu_x q_x \Big] \mathbf{q}_\perp \delta\rho + \boldsymbol{f}_\perp. \tag{3.3.6}$$

We decouple these by projecting (3.3.6) perpendicular to and along $\mathbf{q}_\perp$. That is, we write

$$\mathbf{v}_\perp = v_L \hat{q}_\perp + \mathbf{v}_T \,, \tag{3.3.7}$$

with the "transverse" components $\mathbf{v}_T$, by definition, perpendicular to $\mathbf{q}_\perp$. That is

$$\mathbf{v}_T \cdot \hat{q}_\perp = 0, \tag{3.3.8}$$

and the single "longitudinal" component

$$v_L = \frac{\mathbf{q}_\perp \cdot \mathbf{v}_\perp}{|q_\perp|}, \tag{3.3.9}$$

is the projection of $\mathbf{v}_\perp$ onto $\mathbf{q}_\perp$.

We preform a similar decomposition of the noise $\mathbf{f}_\perp$:

$$\mathbf{f}_\perp = f_L \hat{q}_\perp + \mathbf{f}_T \,, \tag{3.3.10}$$

with

$$\mathbf{f}_T \cdot \hat{q}_\perp = 0 \,, \tag{3.3.11}$$

and

$$f_L \equiv \frac{\mathbf{q}_\perp \cdot \mathbf{f}_\perp}{|q_\perp|}, \tag{3.3.12}$$

These expressions can also be conveniently rewritten in terms of the "transverse" and "longitudinal" projection operators[2]:

$$L_{ij}^\perp(\mathbf{q}_\perp) \equiv \frac{q_i^\perp q_j^\perp}{q_\perp^2}, \tag{3.3.13}$$

$$P_{ij}^\perp(\mathbf{q}_\perp) \equiv \delta_{ij}^\perp - L_{ij}^\perp, \tag{3.3.14}$$

where $\delta_{ij}^\perp = 1$ if $i = j$ *and* $i \neq x \neq j$, and $\delta_{ij}^\perp = 0$ otherwise. The tensor $\delta_{ij}^\perp$ projects any vector perpendicular to the direction of mean flock motion $\hat{x}$, while $P_{ij}^\perp(\mathbf{q}_\perp)$ projects any vector simultaneously perpendicular to *both* $\hat{x}$ *and* the projection $\mathbf{q}_\perp$ of $\mathbf{q}$ perpendicular to $\hat{x}$. The tensor $L_{ij}^\perp(\mathbf{q}_\perp)$ simply projects any vector along $\mathbf{q}$.

In terms of these operators,

$$v_{Ti} = P_{ij}^\perp v_j^\perp, \tag{3.3.15}$$

$$v_L \hat{q}_i^\perp = L_{ij}^\perp v_j^\perp \tag{3.3.16}$$

$$f_{Ti} = P_{ij}^\perp f_j^\perp, \tag{3.3.17}$$

$$f_L \hat{q}_i^\perp = L_{ij}^\perp f_j^\perp \,. \tag{3.3.18}$$

This split decouples $\delta\rho$ and v_L from the $d-2$ transverse modes $\mathbf{v}_T$, as can be seen by projecting equation (3.3.5) and (3.3.6) in the transverse and longitudinal directions, which gives:

$$\Big[-i(\omega - v_\rho q_x) + \Gamma_\rho(\mathbf{q}) - \phi\omega q_x \Big] \delta\rho = -(i\rho_c + D_{\rho v} q_x) q_\perp v_L + i\mathbf{q}\cdot\mathbf{f}_\rho \,, \tag{3.3.19}$$

$$\Big[-i(\omega - v_v q_x) + \Gamma_L(\mathbf{q}) \Big] v_L = \Big[-i\left(\frac{m}{\rho_c} + K q_\perp^2\right) + \nu_t \omega - \nu_x q_x \Big] q_\perp \delta\rho + f_L, \tag{3.3.20}$$

$$\Big[-i(\omega - v_v q_x) + \Gamma_T(\mathbf{q}) \Big] \mathbf{v}_T = \boldsymbol{f}_T \,. \tag{3.3.21}$$

Here we've defined

$$\begin{aligned}
\Gamma_T(\mathbf{q}) &\equiv D_T q_\perp^2 + D_x q_x^2 \,, \\
\Gamma_L(\mathbf{q}) &\equiv D_{L\perp} q_\perp^2 + D_x q_x^2 \,, \\
D_{L\perp} &\equiv D_T + D_B \,, \\
\Gamma_\rho(\mathbf{q}) &\equiv D_{\rho\perp} q_\perp^2 + D_{\rho x} q_x^2 \,.
\end{aligned} \tag{3.3.22}$$

Because $\mathbf{v}_T$ decouples from v_L and $\delta\rho$, we can immediately read off the solution for the field $\mathbf{v}_T$ in terms of the forces $\mathbf{f}_T$:

$$\mathbf{v}_T(\mathbf{q},\omega) = G_{TT}(\mathbf{q},\omega)\mathbf{f}_T \tag{3.3.23}$$

where we've defined the "transverse propagator"

$$G_{TT}(\mathbf{q},\omega) \equiv \frac{1}{-i(\omega - v_v q_x) + \Gamma_T(\mathbf{q})} \,. \tag{3.3.24}$$

We can simplify the remaining equations for $\delta\rho$ and v_L considerably by restricting our attention to the regime of wavevector $\mathbf{q}$ and frequency ω that dominates the fluctuations near the critical point; i.e., at small values of the parameter m in the expansion 3.2.3 of the isotropic pressure. As we will show below, and in more detail in Appendix A.1, in this regime, $\omega \sim q_x \sim q_\perp^2$, and $q_\perp$ is very small (specifically, of order $\sqrt{m}$). In this limit, the $D_{\rho x} q_x^2$ and $\phi\omega q_x$ terms in 3.3.19 are clearly both of order $q_\perp^4$, and, hence, negligible, for small $q_\perp$, relative to the $D_{\rho\perp} q_\perp^2$ term. We'll therefore drop those $D_{\rho x}$ and ϕ terms. Comparing the remaining terms in equation (3.3.20) it is straightforward to see that v_L scales like $q_\perp \delta\rho$.

Likewise, the $D_x q_x^2$ term in 3.3.20 is also of order $q_\perp^4$, and hence negligible relative to the $D_{L\perp} q_\perp^2$ term. We'll therefore drop the $D_x q_x^2$ term in 3.3.20 as well. The $D_{\rho v} q_x q_\perp v_L$ term is order $q_\perp^4$ and is also negligible relative to the $D_{L\perp} q_\perp^2$ term.

The restriction of being near the critical point will also make the noise $\mathbf{f}_\rho$ term negligible; however, this is not obvious and thus is demonstrated below.

With these simplifications, the longitudinal velocity v_L and density $\delta\rho$ equations of motion can be rewritten in matrix form:

$$\boldsymbol{M}(\mathbf{q},\omega)\begin{pmatrix}\delta\rho\\ v_L\end{pmatrix}=\begin{pmatrix}i\mathbf{q}\cdot\mathbf{f}_\rho\\ f_L\end{pmatrix}, \tag{3.3.25}$$

where we've defined the matrix

$$\boldsymbol{M}(\mathbf{q},\omega)\equiv\begin{pmatrix}[-i(\omega-v_\rho q_x)+D_{\rho\perp}q_\perp^2] & i\rho_c q_\perp\\ \left[i\left(\frac{m}{\rho_c}+Kq_\perp^2\right)+\nu_x q_x-\nu_t\omega\right]q_\perp & [-i(\omega-v_v q_x)+D_{L\perp}q_\perp^2]\end{pmatrix}.$$

The solution to this linear system of equations is clearly:

$$\begin{pmatrix}\delta\rho\\ v_L\end{pmatrix}=\boldsymbol{G}\begin{pmatrix}i\mathbf{q}\cdot\mathbf{f}_\rho\\ f_L\end{pmatrix} \tag{3.3.26}$$

where we've defined the propagator matrix:

$$\begin{aligned}\boldsymbol{G}\equiv\boldsymbol{M}^{-1}&\equiv\begin{pmatrix}G_{\rho\rho} & G_{\rho L}\\ G_{L\rho} & G_{LL}\end{pmatrix}\\ &=\frac{1}{Det[\boldsymbol{M}]}\begin{pmatrix}[-i(\omega-v_v q_x)+D_{L\perp}q_\perp^2] & -i\rho_c q_\perp\\ -\left[i\left(\frac{m}{\rho_c}+Kq_\perp^2\right)+\nu_x q_x-\nu_t\omega\right]q_\perp & [-i(\omega-v_\rho q_x)+D_{\rho\perp}q_\perp^2]\end{pmatrix},\end{aligned} \tag{3.3.27}$$

with the determinant given by

$$Det[M]=\mu(\mathbf{q},\omega)+i\kappa(\mathbf{q},\omega)+mq_\perp^2\,, \tag{3.3.28}$$

where we've defined

$$\mu(\mathbf{q},\omega) \equiv -\omega^2 + (v_v + v_\rho)\omega q_x + (D_{L\perp}D_{\rho\perp} + K\rho_c)q_\perp^4 - v_\rho v_v q_x^2, \tag{3.3.29}$$

$$\kappa(\mathbf{q},\omega) \equiv \left[(v_\rho D_{L\perp} + v_v D_{\rho\perp} - \rho_c\nu_x)q_x - (D_{L\perp} + D_{\rho\perp} - \rho_c\nu_t)\omega\right]q_\perp^2 \,. \tag{3.3.30}$$

Note that at the critical point - that is where $m = 0$ - μ and κ are both of order $q_\perp^4$ if $\omega \lesssim \sqrt{D_{L\perp}D_{\rho\perp}}q_\perp^2$ and $q_x \lesssim \sqrt{\frac{D_{L\perp}D_{\rho\perp}}{v_\rho v_v}}q_\perp^2$, and both much greater than order $q_\perp^2$ if either ω or q_x are much greater than those limits. We will see in a moment that the fluctuations in both velocity and density are proportional to $\frac{1}{\mu^2(\mathbf{q},\omega)+\kappa^2(\mathbf{q},\omega)}$. Hence, the regime

$$\omega \lesssim \sqrt{D_{L\perp}D_{\rho\perp}}q_\perp^2 \quad , \quad q_x \lesssim \sqrt{\frac{D_{L\perp}D_{\rho\perp}}{v_\rho v_v}}q_\perp^2 \tag{3.3.31}$$

dominates the fluctuations. We will use this fact later to help us assess the relative importance of various terms in our model, and thereby eliminate many of them.

Note also that $\mu(\mathbf{q},\omega)$ and $\kappa(\mathbf{q},\omega)$ are both independent of m; we will make much use of this fact in the RG analysis of section 3.4.

Using (3.3.23), (3.3.26) and (3.3.27), we can summarize our solutions for the velocity and density fields in terms of the noises as follows:

$$v_L(\mathbf{q},\omega) = G_{LL}(\mathbf{q},\omega)f_L(\mathbf{q},\omega) + G_{L\rho}(\mathbf{q},\omega)i\mathbf{q}\cdot\mathbf{f}_\rho(\mathbf{q},\omega)\,, \tag{3.3.32}$$

$$v_{Ti}(\mathbf{q},\omega) = G_{TT}(\mathbf{q},\omega)P_{ij}^\perp(\hat{q}_\perp)f_j^\perp(\mathbf{q},\omega)\,, \tag{3.3.33}$$

and, most importantly, the solution for $\delta\rho(\mathbf{q},\omega)$:

$$\delta\rho(\mathbf{q},\omega) = G_{\rho L}(\mathbf{q},\omega)f_L(\mathbf{q},\omega) + G_{\rho\rho}(\mathbf{q},\omega)i\mathbf{q}\cdot\mathbf{f}_\rho(\mathbf{q},\omega)\,. \tag{3.3.34}$$

Using equation 3.3.12, we can rewrite this as:

$$\delta\rho(\mathbf{q},\omega) = G_{\rho j}(\mathbf{q},\omega)f_j^\perp(\mathbf{q},\omega) + G_{\rho\rho}(\mathbf{q},\omega)i\mathbf{q}\cdot\mathbf{f}_\rho(\mathbf{q},\omega)\,, \tag{3.3.35}$$

where we've defined

$$G_{\rho j}(\mathbf{q},\omega) \equiv \frac{q_j^\perp}{q_\perp} G_{\rho L}(\mathbf{q},\omega) = -\frac{i\rho_c q_j^\perp}{Det[M]} \tag{3.3.36}$$

Combining our solutions 3.3.32 and 3.3.33 for v_L and $\mathbf{v}_T$, and using the projection operators 3.3.13 and 3.3.14 introduced earlier, we can obtain the solution for the velocity field:

$$\begin{aligned} v_i^\perp &= [G_{LL}(\mathbf{q},\omega) L_{ij}^\perp + G_{TT}(\mathbf{q},\omega) P_{ij}^\perp] f_i \\ &\quad + iG_{L\rho}(\mathbf{q},\omega)\left[L_{ij}^\perp q_\perp f_j^\rho(\mathbf{q},\omega) + X_{ij} q_x f_j^\rho(\mathbf{q},\omega)\right] \\ &\equiv G_{ij}(\mathbf{q},\omega) f_j + G_{ij}^\rho(\mathbf{q},\omega) f_j^\rho \,, \end{aligned} \tag{3.3.37}$$

where we've defined

$$G_{ij}(\mathbf{q},\omega) \equiv G_{LL}(\mathbf{q},\omega) L_{ij}^\perp + G_{TT}(\mathbf{q},\omega) P_{ij}^\perp \,, \tag{3.3.38}$$

$$X_{ij} \equiv \frac{q_i^\perp \delta_{jx}}{q_\perp} \tag{3.3.39}$$

and

$$\begin{aligned} G_{ij}^\rho &\equiv iG_{L\rho}\left(\frac{q_i^\perp q_j^\perp}{q_\perp} + \frac{q_i^\perp \delta_{jx}}{q_\perp} q_x\right) \\ &= \left[\frac{\frac{m}{\rho_c} + Kq_\perp^2 + i(\nu_t\omega - \nu_x q_x)}{\mu(\mathbf{q},\omega) + i\kappa(\mathbf{q},\omega) + mq_\perp^2}\right](q_i^\perp q_j^\perp + q_i^\perp \delta_{jx} q_x) \,. \end{aligned} \tag{3.3.40}$$

To avoid any potential confusion, we remind the reader that the subscript x on q_x is a label and not an index.

We can now autocorrelate our fields with themselves and cross-correlate them with each other. Doing so for the velocity fields gives:

$$\begin{aligned}\langle v_i^\perp(\mathbf{q},\omega)v_j^\perp(-\mathbf{q},-\omega)\rangle = &\Big[G_{LL}(\mathbf{q},\omega)G_{LL}(-\mathbf{q},-\omega)L_{ik}^\perp L_{jl}^\perp \\ &+ G_{TT}(\mathbf{q},\omega)G_{TT}(-\mathbf{q},-\omega)P_{ik}^\perp P_{jl}^\perp\Big]\langle f_k(\mathbf{q},\omega)f_l(-\mathbf{q},-\omega)\rangle \\ &+ G_{L\rho}(\mathbf{q},\omega)G_{L\rho}(-\mathbf{q},-\omega)\Big[L_{ik}^\perp L_{jl}^\perp q_\perp^2 + X_{ik}X_{jl}q_x^2\Big]\langle f_k^\rho(\mathbf{q},\omega)f_l^\rho(-\mathbf{q},-\omega)\rangle \end{aligned} \tag{3.3.41}$$

We now use the noise correlations (3.2.4) and (3.2.5) in this expression, along with the identities

$$\begin{aligned} P_{ik}^\perp P_{jk}^\perp = P_{ij}^\perp \quad &, \quad L_{ik}^\perp L_{jk}^\perp = L_{ij}^\perp\,, \\ L_{ik}X_{jk} = 0 \quad &, \quad X_{ik}X_{jk} = L_{ij}^\perp\,, \end{aligned} \tag{3.3.42}$$

obeyed by the projection operators. We also note that the $X_{ik}X_{jl}q_x^2$ term is order $q_\perp^4$ and thus negligible compared to the $L_{ik}L_{jl}q_\perp^2$ term; we therefore drop it. Then further using our earlier results (3.3.24) and (3.3.27) for the propagators $G_{LL}(-\mathbf{q},-\omega)$, $G_{L\rho}(\mathbf{q},\omega)$, and $G_T(\mathbf{q},\omega)$, we obtain

$$C_{ij}(\mathbf{q},\omega) = \langle v_i^\perp(\mathbf{q},\omega)v_j^\perp(\mathbf{q}',\omega')\rangle = C_L(\mathbf{q},\omega)L_{ij}^\perp + C_T(\mathbf{q},\omega)P_{ij}^\perp \tag{3.3.43}$$

where we've defined

$$C_T(\mathbf{q},\omega) \equiv \frac{\Delta}{[(\omega - v_v q_x)^2 + \Gamma_T(\mathbf{q})^2]} \tag{3.3.44}$$

$$\begin{aligned} C_L(\mathbf{q},\omega) \equiv &\left(\frac{\omega^2 - 2v_\rho\omega q_x + v_\rho^2 q_x^2 + D_{\rho\perp}^2 q_\perp^4}{(\mu(\mathbf{q},\omega) + mq_\perp^2)^2 + \kappa^2(\mathbf{q},\omega)}\right)\Delta \\ &+ \left(\frac{\nu_x^2 q_x^2 q_\perp^2 - 2\nu_x\nu_t\omega q_x q_\perp^2 + \nu_t^2\omega^2 q_\perp^2}{(\mu(\mathbf{q},\omega) + mq_\perp^2)^2 + \kappa^2(\mathbf{q},\omega)}\right)\Delta_\rho \end{aligned} \tag{3.3.45}$$

Once again we can leverage the scaling of the wavevectors and frequencies near the critical point to simplify $C_L(\mathbf{q},\omega)$. Note that, since, in the dominant regime of wavevector and frequency, $\omega \sim q_x \sim q_\perp^2$, the Δ term in 3.3.45 is (near the critical point $m = 0$) of order $\frac{q_\perp^4}{(\mu^2(\mathbf{q},\omega)+\kappa^2(\mathbf{q},\omega))}$, while the Δ_ρ term is of order $\frac{q_\perp^6}{(\mu^2(\mathbf{q},\omega)+\kappa^2(\mathbf{q},\omega))}$; that is, smaller by a factor of $q_\perp^2$. Hence, this term is negligible, and we shall drop it.

This leaves us with:

$$C_{ij}(\mathbf{q},\omega) = \langle v_i^{\perp}(\mathbf{q},\omega) v_j^{\perp}(\mathbf{q}',\omega')\rangle = \left(\frac{\omega^2 - 2v_\rho\omega q_x + v_\rho^2 q_x^2 + D_{\rho\perp}^2 q_\perp^4}{(\mu(\mathbf{q},\omega) + mq_\perp^2)^2 + \kappa^2(\mathbf{q},\omega)}\right)\Delta L_{ij}^{\perp} + \frac{\Delta}{[(\omega - v_v q_x)^2 + \Gamma_T(\mathbf{q})^2]} P_{ij}^{\perp} \tag{3.3.46}$$

Equation 3.3.46 is the final form of our velocity autocorrelation.

Now, we will autocorrelate the density field $\delta\rho$ with itself. This is simpler, since $\delta\rho$ is a scalar rather than a vector.

$$\begin{aligned} C_{\rho\rho}(\mathbf{q},\omega) &= G_{\rho L}(\mathbf{q},\omega) G_{\rho L}(-\mathbf{q},-\omega)\langle |f_L(\mathbf{q},\omega)|^2\rangle \\ &\quad + G_{\rho\rho}(\mathbf{q},\omega) G_{\rho\rho}(-\mathbf{q},-\omega)\langle |f_\rho(\mathbf{q},\omega)|^2\rangle \qquad (3.3.47) \\ &= \left(\frac{\rho_c^2 q_\perp^2}{(\mu(\mathbf{q},\omega) + mq_\perp^2)^2 + \kappa^2(\mathbf{q},\omega)}\right)\Delta \\ &\quad + \left(\frac{\omega^2 - 2v_v\omega q_x + v_v^2 q_x^2 + D_{L\perp}^2 q_\perp^4}{(\mu(\mathbf{q},\omega) + mq_\perp^2)^2 + \kappa^2(\mathbf{q},\omega)}\right)\Delta_\rho \qquad (3.3.48) \end{aligned}$$

Once again power counting in the dominant regime of wavevector and frequency $\omega \sim q_x \sim q_\perp^2$, we see that the Δ term in 3.3.48 is of order $q_\perp^2/(\mu^2(\mathbf{q},\omega) + \kappa^2(\mathbf{q},\omega))$, while the Δ_ρ term is of order $q_\perp^4/(\mu^2(\mathbf{q},\omega) + \kappa^2(\mathbf{q},\omega))$; that is, smaller by a factor of $q_\perp^2$. Hence, this term is also negligible, and we shall henceforth drop it as well. This means that the noise $\mathbf{f}_\rho$ in the density equation has dropped out of the problem. The fate of the noise $\mathbf{f}_\rho$ is similar in the DRG, where we will show that it is irrelevant. Thus our the final form of our density field autocorrelation function is:

$$C_{\rho\rho}(\mathbf{q},\omega) = \frac{\rho_c^2 q_\perp^2 \Delta}{(\mu(\mathbf{q},\omega) + mq_\perp^2)^2 + \kappa^2(\mathbf{q},\omega)}. \tag{3.3.49}$$

Note that all of the correlation functions we've just found are controlled entirely by the model parameters D_T, $D_{L\perp}$, $D_{\rho\perp}$, v_v, v_ρ, ρ_c, ν_x, ν_t, and Δ. We will exploit this fact in our DRG treatment in the next section, where will assess the importance of the *non-linear* terms in the equations of motion by choosing our DRG rescaling factors to keep all of the above parameters fixed upon rescaling.

With the above results 3.3.44, 3.3.45, and 3.3.49 for the spatiotemporally Fourier transformed correlation functions in hand, we can now Fourier transform back to real space and time to obtain the position and time dependent correlation functions. We will focus here on the *critical* correlation functions; that is, those when the linear coefficient m in the expansion 3.2.3 for the isotropic pressure P_1 vanishes; that is, when $m = 0$.

In this limit, the density-density correlation function $C_{\rho\rho}(\mathbf{r}, t) \equiv \langle \delta\rho(\mathbf{r}, t)\delta\rho(\mathbf{0}, 0)\rangle$ in real space $\mathbf{r}$ and time t is given by:

$$C_{\rho\rho}(\mathbf{r}, t) = \int \frac{d^{d-1}q_\perp}{(2\pi)^{d-1}} \int_{-\infty}^{\infty} \frac{dq_x}{2\pi} \int_{-\infty}^{\infty} \frac{d\omega}{2\pi} C_{\rho\rho}(\mathbf{q}, \omega) e^{i(\mathbf{q}\cdot\mathbf{r} - \omega t)} \tag{3.3.50}$$

$$= \rho_c^2 \Delta \int \frac{d^{d-1}q_\perp}{(2\pi)^{d-1}} \int_{-\infty}^{\infty} \frac{dq_x}{2\pi} \int_{-\infty}^{\infty} \frac{d\omega}{2\pi} \frac{\exp[i(\mathbf{q}_\perp \cdot \mathbf{r}_\perp + q_x r_x - \omega t)] q_\perp^2}{\mu^2(\omega, \mathbf{q}_\perp, q_x) + \kappa^2(\omega, \mathbf{q}_\perp, q_x)} \tag{3.3.51}$$

We can now tease out the dependence of this correlation function on $\mathbf{r}_\perp$, x, and t by rescaling variables of integration from ω and q_x to new variables of integration Ω and Q_x defined by

$$\omega \equiv D_T q_\perp^2 \Omega \quad , \quad q_x \equiv \frac{D_T q_\perp^2}{\sqrt{v_v v_\rho}} Q_x \,, \tag{3.3.52}$$

where we've defined

$$D_T \equiv \sqrt{D_{L\perp} D_{\rho\perp} + K\rho_c} \,. \tag{3.3.53}$$

Making these changes of variable in our expressions 3.3.29 and 3.3.30 for $\mu(q_x, \mathbf{q}_\perp, \omega)$ and $\kappa(q_x, \mathbf{q}_\perp, \omega)$ gives

$$\mu(q_x, \mathbf{q}_\perp, \omega) = D_T^2 q_\perp^4 \alpha(\Omega, Q_x) \,, \tag{3.3.54}$$

$$\kappa(q_x, \mathbf{q}_\perp, \omega) = D_T^2 q_\perp^4 \sigma(\Omega, Q_x) \,, \tag{3.3.55}$$

where we've defined

$$\alpha(Q_x, \Omega) \equiv -\Omega^2 + \Theta\Omega Q_x - Q_x^2 + 1 \,, \tag{3.3.56}$$

$$\sigma(Q_x, \Omega) \equiv \Xi Q_x - \Upsilon\Omega \,, \tag{3.3.57}$$

with the dimensionless parameters

$$\Theta \equiv \sqrt{\frac{v_v}{v_\rho}} + \sqrt{\frac{v_\rho}{v_v}} \tag{3.3.58}$$

$$\Xi \equiv \frac{(v_\rho D_{L\perp} + v_v D_{\rho\perp} - \rho_c \nu_x)}{D_T \sqrt{v_v v_\rho}} \tag{3.3.59}$$

$$\Upsilon \equiv \frac{(D_{L\perp} + D_{\rho\perp} - \rho_c \nu_t)}{D_T} \tag{3.3.60}$$

Note that Θ is bounded below by 2, while Ξ and Υ can take on any positive value.

With the change of variables 3.3.52, our expression (3.3.51) for the real space density-density correlation function becomes

$$C_{\rho\rho}(\mathbf{r},t) = \frac{\rho_c^2 \Delta}{D_T^2} \int \frac{d^{d-1}q_\perp}{(2\pi)^{d-1}} \int_{-\infty}^{\infty} \frac{dQ_x}{2\pi} \int_{-\infty}^{\infty} \frac{d\Omega}{2\pi} \frac{\exp[i(\mathbf{q}_\perp \cdot \mathbf{r}_\perp + aQ_x q_\perp^2 r_x - \Omega D_T q_\perp^2 t)]}{q_\perp^2 \Big(\alpha^2(Q_x,\Omega) + \sigma^2(Q_x,\Omega)\Big)} . \tag{3.3.61}$$

where $a \equiv \frac{D_T}{\sqrt{v_v v_\rho}}$ is a non-universal microscopic length. Now making one further change of variables

$$\mathbf{q}_\perp \equiv \frac{\mathbf{Q}_\perp}{|\mathbf{r}_\perp|} , \tag{3.3.62}$$

gives

$$C_{\rho\rho}(\mathbf{r}_\perp, r_x, t) = |r_\perp|^{3-d} F_{\rho\rho}(u,\tau) \tag{3.3.63}$$

where we've defined:

$$u \equiv \frac{r_x}{|r_\perp|^2}, \quad \tau \equiv \frac{|t|}{|r_\perp|^2}, \tag{3.3.64}$$

and the scaling function

$$F_{\rho\rho}(u,\tau) = \frac{\rho_c^2 \Delta}{D_T^2} \int \frac{d^{d-1}Q_\perp}{(2\pi)^{d-1}} \int_{-\infty}^{\infty} \frac{dQ_x}{2\pi} \int_{-\infty}^{\infty} \frac{d\Omega}{2\pi} \left(\frac{\exp[i(\mathbf{Q}_\perp \cdot \hat{\mathbf{r}}_\perp + aQ_x Q_\perp^2 u - \Omega Q_\perp^2 \tau)]}{Q_\perp^2 \left(\alpha^2(Q_x,\Omega) + \sigma^2(Q_x,\Omega)\right)} \right) . \tag{3.3.65}$$

Note that if define a "roughness exponent" χ_ρ, an "anisotropy exponent" ζ, and a "dynamical scaling exponent" z, via the definition

$$C_{\rho\rho}(\mathbf{r}_\perp, r_x, t) = |r_\perp|^{2\chi_\rho} f_{\rho\rho}\left(\frac{r_x}{|r_\perp|^\zeta}, \frac{|t|}{|r_\perp|^z}\right), \tag{3.3.66}$$

then equation 3.3.63 implies that the linear theory predicts that $\chi_\rho = \chi_{\rho\,\mathrm{lin}}$, $\zeta = \zeta_{\mathrm{lin}}$, and $z = z_{\mathrm{lin}}$, with

$$\chi_{\rho\,\mathrm{lin}} = \frac{3-d}{2} \quad , \quad \zeta_{\mathrm{lin}} = z_{\mathrm{lin}} = 2\,. \tag{3.3.67}$$

We will show in the next section that, while the scaling *form* 3.3.66 continues to hold for spatial dimensions $d < 5$, the true values of the exponents χ_ρ, ζ, and z are all changed by non-linearities in that range of dimension.

3.4 Nonlinear Regime: Rg analysis

Identifying the relevant vertex, and determining the critical dimension

Now we wish to go beyond the linear theory presented in the last section, and include the effects of the non-linear terms in the full equations of motion (3.2.11) and (3.2.12). We'll do so using a dynamical renormalization group (DRG) analysis. Readers interested in a more complete and pedagogical discussion of the DRG are referred to [17] for the details of this general approach, including the use of Feynman graphs in it.

For convenience of reference all involved, we recall the original full hydrodynamic equations:

$$\begin{aligned}\partial_t \mathbf{v}_\perp + v_v \partial_x \mathbf{v}_\perp + \lambda\left(\mathbf{v}_\perp\cdot\nabla_\perp\right)\mathbf{v}_\perp &= -g_1\delta\rho\partial_x\mathbf{v}_\perp - g_2\mathbf{v}_\perp\partial_x\delta\rho \\ &- \nabla_\perp\left(\frac{m}{\rho_c}\delta\rho + u\delta\rho^3 - K\nabla_\perp^2\delta\rho\right) + D_B\nabla_\perp(\nabla_\perp\cdot\mathbf{v}_\perp) + D_T\nabla_\perp^2\mathbf{v}_\perp \\ &+ D_x\partial_x^2\mathbf{v}_\perp + \nu_x\partial_x\nabla_\perp\delta\rho + \nu_t\partial_t\nabla_\perp\delta\rho + \mathbf{f}_\perp\,,\end{aligned} \tag{3.4.1}$$

$$\begin{aligned}\partial_t\delta\rho + \rho_c\nabla_\perp\cdot\mathbf{v}_\perp + \gamma\nabla_\perp\cdot(\mathbf{v}_\perp\delta\rho) + v_\rho\partial_x\delta\rho &= D_{\rho x}\partial_x^2\delta\rho + D_{\rho\perp}\nabla_\perp^2\delta\rho \\ &+ D_{\rho v}\partial_x\left(\nabla_\perp\cdot\mathbf{v}_\perp\right) + \phi\partial_t\partial_x\delta\rho + w_2\partial_x(\delta\rho^2) + \frac{\rho_c}{2v_0}\partial_x(|\mathbf{v}_\perp|^2) + \nabla\cdot\mathbf{f}_\rho\,,\end{aligned} \tag{3.4.2}$$

First we decompose the Fourier modes $\mathbf{v}_\perp(\mathbf{q},\omega)$ and $\rho(\mathbf{q},\omega)$ into rapidly varying parts $\mathbf{v}_\perp^>(\mathbf{q},\omega)$ and $\rho^>(\mathbf{q},\omega)$ and slowly varying parts $\mathbf{v}_\perp^<(\mathbf{q},\omega)$ and $\rho^<(\mathbf{q},\omega)$ in the equations of motion (3.4.1) and (3.4.2). The rapidly varying part is supported in the momentum shell $-\infty < k_x < \infty$, $\Lambda b^{-1} < k_\perp < \Lambda$, where $\mathrm{d}\ell$ is an infinitesimal and Λ is the ultraviolet cutoff. The slowly varying part is supported in $-\infty < k_x < \infty$, $0 < k_\perp < b^{-1}\Lambda$, where b is an arbitrary rescaling factor that we will ultimately take to be $b = 1 + d\ell$, with $d\ell$ differential. We separate the noise $\mathbf{f}$ in exactly the same way.

The DRG procedure then consists of two steps. In step 1, we eliminate $\mathbf{v}_\perp^>(\mathbf{q},\omega)$ and $\rho^>(\mathbf{q},\omega)$ from (3.4.1) and (3.4.2). We do this by solving iteratively for $\mathbf{v}_\perp^<(\mathbf{q},\omega)$ and $\rho^<(\mathbf{q},\omega)$. This solution is a perturbative expansion in $\mathbf{v}_\perp^>(\mathbf{q},\omega)$ and $\rho^>(\mathbf{q},\omega)$, as well as the fast components $\mathbf{f}^>$ of the noise. As usual, the perturbation theory can be represented by Feynman graphs. We substitute these solutions into (3.4.1) and (3.4.2) and average over the short wavelength components $\mathbf{f}^>(\mathbf{q},\omega)$ of the noise $\mathbf{f}$, which gives a closed EOM for $\mathbf{v}_\perp^<(\mathbf{q},\omega)$.

In step 2, we rescale the *real space* fields $\mathbf{v}_\perp^<(\mathbf{r},t)$ and $\rho^<(\mathbf{r},t)$, time t, and coordinates $\mathbf{r}_\perp$ and r_x as follows:

$$\begin{aligned} \mathbf{v}_\perp &= b^\chi \mathbf{v}'_\perp \quad , \quad \delta\rho = b^{\chi_\rho}\delta\rho' \quad , \quad t = b^z t' \quad , \quad \mathbf{r}_\perp = b\mathbf{r}'_\perp \\ r_x &= b^\zeta r'_x \,. \end{aligned} \tag{3.4.3}$$

The rescaling of $\mathbf{r}_\perp$ restores the ultraviolet cutoff back to Λ. The velocity and density rescaling exponents χ and χ_ρ, the "dynamical" exponent z, and the "anisotropy" exponent ζ, are all, at this point, completely arbitrary. We will show below that, as usual in RG calculations, there is a particular choice of all of these exponents that makes it particularly simple to determine which non-linearities are important.

After these two RG steps, we reorganize the resultant EOMs so that they have the same form as (3.4.1) and (3.4.2), but with various coefficients renormalized. This reorganization amounts to multiplying the EOM by a power of b chosen to restore the coefficient of $\partial_t \mathbf{v}_\perp$ and $\partial_t \delta\rho$ in (3.4.1) and (3.4.2) to unity.

We focus first on the coefficients that control the size of the fluctuations in the linear theory. Upon performing the two steps on our equation of motion (3.4.1) and (3.4.2), and the aforementioned reorganization (which amounts to multiplying the EOM by a power of b chosen to restore the coefficient of $\partial_t \mathbf{v}_\perp$ and $\partial_t \delta\rho$ in (3.4.1) and (3.4.2) to unity), we find:

$$v_v' = b^{z-\zeta}(v_v + \text{graphs})\,, \tag{3.4.4}$$

$$v_\rho' = b^{z-\zeta}(v_\rho + \text{graphs})\,, \tag{3.4.5}$$

$$D_{L\perp}' = b^{z-2}(D_{L\perp} + \text{graphs})\,, \tag{3.4.6}$$

$$D_{\rho\perp}' = b^{z-2}(D_{\rho\perp} + \text{graphs})\,, \tag{3.4.7}$$

$$D_T' = b^{z-2}(D_T + \text{graphs})\,, \tag{3.4.8}$$

$$\nu_t' = b^{\chi_\rho-\chi-1}(\nu_t + \text{graphs})\,, \tag{3.4.9}$$

$$\nu_x' = b^{z-\zeta-1-\chi+\chi_\rho}(\nu_x + \text{graphs})\,, \tag{3.4.10}$$

$$\rho_c' = b^{z+\chi-\chi_\rho-1}\rho_c\,, \tag{3.4.11}$$

$$K' = b^{-3-2\xi+\chi_\rho-\chi+z}(K + \text{graphs})\,, \tag{3.4.12}$$

$$\Delta' = b^{z-2\chi-\zeta-d+1}(\Delta + \text{graphs})\,, \tag{3.4.13}$$

$$\Delta_\rho' = b^{-2}(\Delta_\rho + \text{graphs})\,, \tag{3.4.14}$$

$$D_x' = b^{z-2\zeta}(D_x + \text{graphs})\,, \tag{3.4.15}$$

where "graphs" denote the "graphical" corrections coming from the first, perturbative step of the RG.

Now we'll make the convenient choice of the rescaling exponents χ, χ_ρ, z, and ζ mentioned above. Our choice will be to choose them so that we keep the parameters listed in 3.4.4-3.4.15fixed. Doing so means we keep the size of the fluctuations fixed, since, as we showed in the previous section, that size, at least in the linear approximation, is controlled entirely by the set of parameters listed in 3.4.4-3.4.15.

This means that we can determine whether any of the non-linear terms in equations (3.4.1) and (3.4.2) become more important as we renormalize simply by asking whether their coefficients grow or shrink upon renormalization.

We will simplify the argument further by assuming that the bare values of those non-linear coefficients are so small that the "graphs" in equation 3.4.4-3.4.15are negligible. Once we neglect those corrections, keeping the parameters in 3.4.4-3.4.15fixed can obviously be achieved simply by choosing the rescaling exponents χ, χ_ρ, z, and ζ so as to make the exponents of the rescaling factor

b in (3.4.4)-(3.4.14) vanish. Doing so for v_v and v_ρ clearly leads to $z = \zeta$. Keeping $D_{L\perp}$ and $D_{\rho\perp}$ fixed requires $z = 2$. Keeping ν_t fixed implies $\chi_\rho = \chi + 1$, while keeping Δ fixed requires $z - 2\chi - \zeta - d + 1 = 0$. To summarize, keeping these six parameters fixed requires the simultaneous conditions

$$z = \zeta \quad , \quad z = 2 \quad , \quad \chi_\rho = \chi + 1 \quad , \quad z - 2\chi - \zeta - d + 1 = 0\,. \tag{3.4.16}$$

These four simultaneous linear equations for the four unknown exponents can be easily solved, with the result:

$$z = \zeta = 2\,, \quad \chi = \frac{1-d}{2}\,, \quad \chi_\rho = \frac{3-d}{2}\,. \tag{3.4.17}$$

It is straightforward to check that this choice of exponents will keep all of the other parameters listed in 3.4.4-3.4.15fixed, *except* for K, D_x and Δ_ρ, whose recursion relations, with the choice 3.4.17 become

$$\begin{aligned} K' &= b^{-4}(K + \text{graphs})\,, \\ \Delta'_\rho &= b^{-2}(\Delta_\rho + \text{graphs})\,, \\ D'_x &= b^{-2}(D_x + \text{graphs})\,. \end{aligned} \tag{3.4.18}$$

The recursion relation for Δ_ρ shows that it is irrelevant, as we'd already concluded in our linear analysis of section 3.3 3.4.4-3.4.15 during our calculation of the autocorrelation of the fields.

The fact that D_x will flow to zero upon renormalization is more problematic. Since the fluctuations of the transverse velocity $\mathbf{v}_T$ diverge as $D_x \to 0$, D_x is a "dangerously irrelevant" variable in the renormalization group sense. That is, it is not adequate to simply *set* it to zero, rather, we must keep track of *how fast* it scales to zero. We do so in Appendix A.2, where we show that this dangerous irrelevance does not affect our conclusion below that *only* the $u\delta\rho^3$ non-linearity is relevant near $d = 5$. More precisely, the effect of the dangerous irrelevance of D_x is only to raise the critical dimension of the velocity-dependent non-linearities λ, g_1, g_2, γ, and $\frac{\rho_c}{2v_0}$ to $d = 4$; hence, they all remain *irrelevant* near $d = 5$, as does the w_2 non-linearity. Therefore, the only relevant non-linearity near $d = 5$ is $u\delta\rho^3$. This tremendously simplifies our analysis.

The nonlinear terms in the equations of motion (3.4.1) and (3.4.2) scale as:

$$u' = b^{3\chi_\rho + z - \chi - 1}(u + \text{graphs}) = b^{5-d}(u + \text{graphs}), \tag{3.4.19}$$

$$\lambda' = b^{\chi + z - 1}(\lambda + \text{graphs}) = b^{(3-d)/2}(\lambda + \text{graphs}), \tag{3.4.20}$$

$$g_1' = b^{\chi_\rho + z - \zeta}(g_1 + \text{graphs}) = b^{(3-d)/2}(g_1 + \text{graphs}), \tag{3.4.21}$$

$$g_2' = b^{\chi_\rho + z - \zeta}(g_2 + \text{graphs}) = b^{(3-d)/2}(g_2 + \text{graphs}), \tag{3.4.22}$$

$$w_2' = b^{\chi_\rho + z - \zeta}(w_2 + \text{graphs}) = b^{(3-d)/2}(w_2 + \text{graphs}), \tag{3.4.23}$$

$$\left(\frac{\rho_c}{2v_0}\right)' = b^{2\chi - \chi_\rho + z - \zeta}\left(\frac{\rho_c}{2v_0} + \text{graphs}\right) = b^{-(1+d)/2}\left(\frac{\rho_c}{2v_0} + \text{graphs}\right), \tag{3.4.24}$$

$$\gamma' = b^{\chi + z - 1}(\gamma + \text{graphs}) = b^{(3-d)/2}(\gamma + \text{graphs}), \tag{3.4.25}$$

where the second equality in each case comes from using the exponents 3.4.17 in the first equality in each case.

We see from these relations that, as lower spatial dimension d from very high values, all of the non-linearities are irrelevant, until we reach the "upper critical dimension" $d_c = 5$. At and near this point - that is, for $d = 5 - \epsilon$ with $\epsilon \ll 1$, u - *and only* u, is relevant. All other non-linearities are *irrelevant*, and can hence be ignored in a $5 - \epsilon$-expansion, to which we will turn in the next section.

We'll see later that we'll also need the scaling behavior of the "mass" m:

$$\left(\frac{m}{\rho_c}\right)' = b^{\chi_\rho - \chi + z - 1}\left(\frac{m}{\rho_c} + graphs\right) = b^2\left(\frac{m}{\rho_c} + graphs\right), \tag{3.4.26}$$

where in the second equality we have again used the values 3.4.17 of the exponents.

5-ϵ-expansion

We demonstrated in the last subsection3.4 that the upper critical dimension for our problem is $d_c = 5$, and that only the u vertex is relevant near five dimensions. To proceed further, we need to

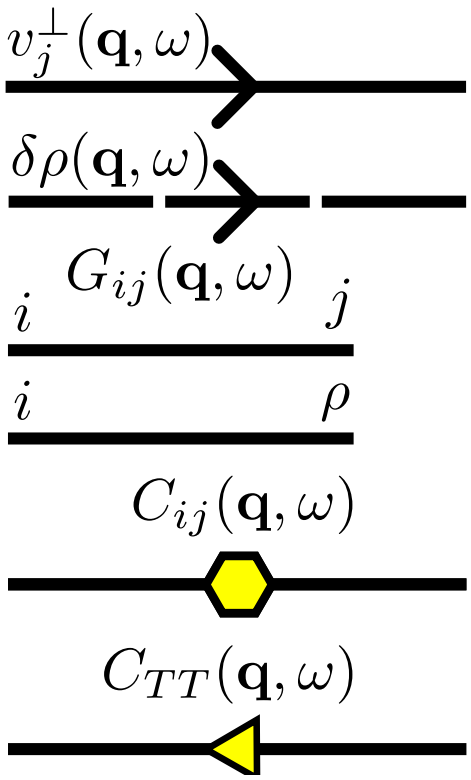

FIGURE 23. Graphical representation of propagators, fields, and correlation functions: The top two lines adorned with arrows and labeled with $v_i^{\perp}(\mathbf{q},\omega)$ and $\delta\rho(\mathbf{q},\omega)$ represent the fields. The next two lines down embellished with i,j and i,ρ and labeled with $G_{ij}(\mathbf{q},\omega)$ are the propagators. The final two lines represent the correlation of our propagators. We note that i,j are indexes that span the space perpendicular to the mean flock direction $\hat{x}$; additionally we allow these indexes to assume the "value" of ρ. So the first correlation function, ornamented with a hexagon, $C_{ij}(\mathbf{q},\omega)$ may represent $C_{i\rho}, C_{\rho j}$, or $C_{\rho\rho}$. The second correlation function, garnished with a triangle, includes only the transverse velocity field and is only used in appendix A.2.

actually evaluate the graphical corrections. In this section, we do a full RG treatment accurate to linear order in ϵ.

The basic rules for the graphical representation are illustrated in Fig. 23.

The u vertex can be represented graphically by the Feynman graph shown in figure 24. The only one loop graphs that can be made from this vertex are the two shown in figures 25 and 26. Since the first graph generates a term in the equation of motion for $\mathbf{v}_{\perp}$ that is proportional to $\partial_i\delta\rho$, it represents a renormalization of the mass m, since m is the coefficient of precisely such a term in that EOM. Likewise, the graph in figure 26 is clearly a renormalization of u itself.

None of the parameters other than m and u receive any graphical corrections at one loop order.

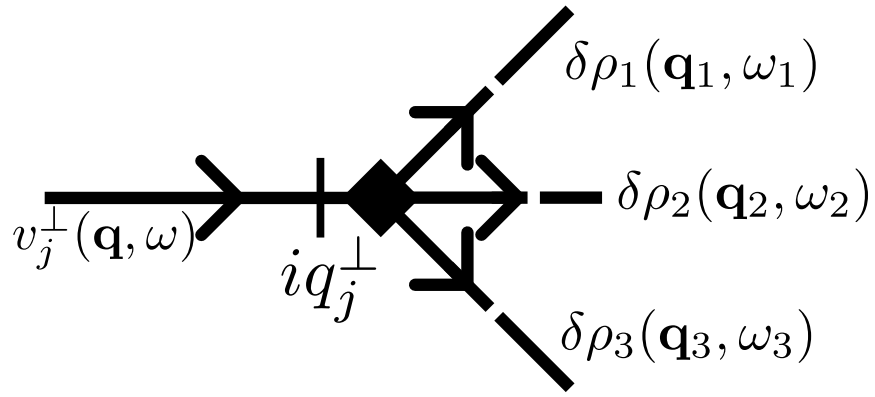

FIGURE 24. Graphical representation of the u vertex. The incoming leg on the left labelled $v_i^\perp$ tells us that this represents a term in the v_i equation of motion. The tick mark on that leg represents the q_i in the $uq_i\delta\rho^3$ term, and each of the three outgoing legs represents one of those $\delta\rho$'s. See[17] for a more detailed description of the Feynman graph representation of equations of motion, and their use in perturbation theory and the DRG.

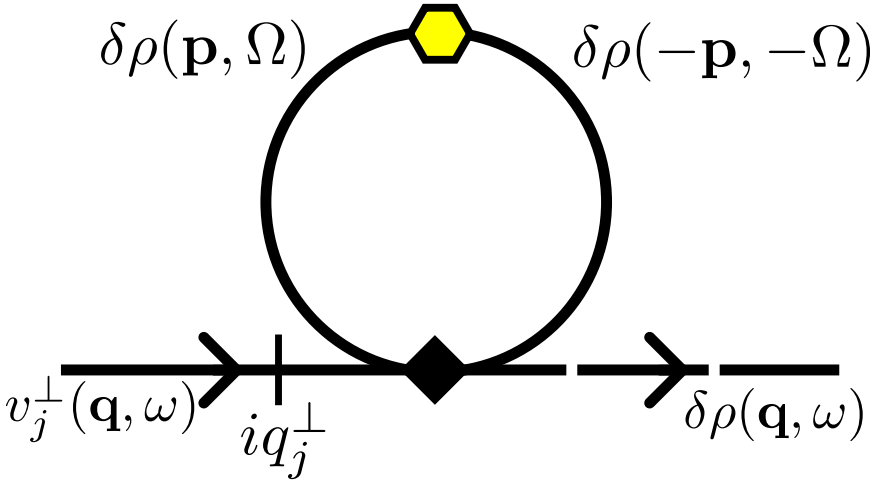

FIGURE 25. Graphical correction to m from one u vertices. This graph can be made a total of 3 different ways.

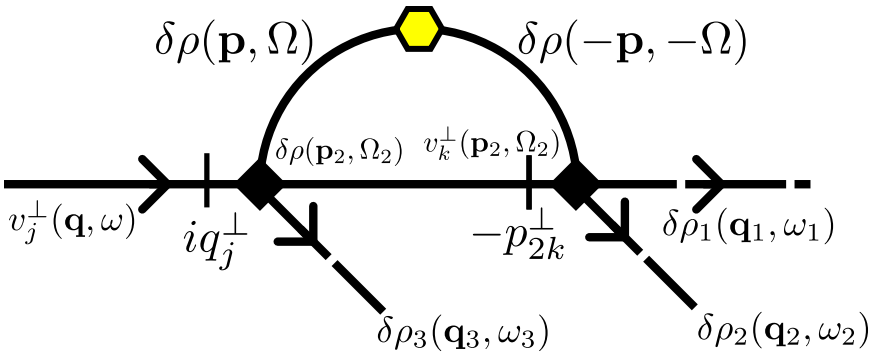

FIGURE 26. Graphical correction to u from two u verticies. This graph can be made a total of 18 different ways.

We'll now evaluate these one loop graphical corrections, starting with figure 25. This generates an extra term in the equation of motion for v_i given by

$$\delta\Big[\partial_t v_i\Big] = \mathrm{FT}\Big\{ -3uiq_i\delta\rho(\mathbf{q},\omega)\int^{>}_{\mathbf{p},\Omega} C_{\rho\rho}(\mathbf{p},\Omega)\Big\}, \tag{3.4.27}$$

where $\mathrm{FT}\{x(\mathbf{q},\omega)\}$ denotes a Fourier transform of $x(\mathbf{q},\omega)$ back to real space and time; i.e., $\mathrm{FT}\{x(\mathbf{q},\omega)\} = x(\mathbf{r},t)$, and the ">" superscript implies that the integral over $\mathbf{p}$ is over the the region $b^{-1}\Lambda < |\mathbf{p}_\perp| < \Lambda$, $-\infty < p_x < \infty$ and $-\infty < \Omega < \infty$, which is the region over which we average out the degrees of freedom in each step of our RG. Note the Ω used here is *not* the same as the Ω used in the rescaling of ω for the purposing of extracting scaling behavior of the correlation functions in equation (3.3.52).

The form of this generated term is exactly the same as that of the $\frac{m}{\rho_c}$ term already present in the equation of motion (3.4.1). Hence, this can be interpreted as a graphical correction $\delta\big[\frac{m}{\rho_c}\big]$ to $\big[\frac{m}{\rho_c}\big]$ given by

$$\delta\left[\frac{m}{\rho_c}\right] = 3u\int^{>}_{\mathbf{p},\Omega} C_{\rho\rho}(\mathbf{p},\Omega) = 3u\rho_c^2\Delta\int^{>}_{\mathbf{p},\Omega}\frac{p_\perp^2}{(\mu(\mathbf{p},\Omega)+mp_\perp^2)^2+\kappa^2(\mathbf{p},\Omega)}\,. \tag{3.4.28}$$

Since only the ratio $\frac{m}{\rho_c}$ appears in the equation of motion, it is completely arbitrary how much of this renormalization we attribute to a renormalization of m and ρ_c individually. We will henceforth make the entirely arbitrary choice of attributing all of it to renormalization of m; that is, we'll treat ρ_c as a constant.

Because we are interested in the behavior around the critical point, which occurs at small m, we will expand (3.4.28) to linear order in m. It is straightforward to show that higher order terms in m only change the critical exponents we find here at $\mathcal{O}(\epsilon^2)$, which is beyond the order to which we are working. This expansion in m gives

$$\delta\left[\frac{m}{\rho_c}\right] = 3u\rho_c^2\Delta\int^{>}_{\mathbf{p},\Omega}\left[\frac{p_\perp^2}{\mu^2(\mathbf{p},\Omega)+\kappa^2(\mathbf{p},\Omega)} - \frac{2\mu(\mathbf{p},\Omega)p_\perp^4 m}{\big(\mu^2(\mathbf{p},\Omega)+\kappa^2(\mathbf{p},\Omega)\big)^2} + \mathcal{O}(m^2)\right] \tag{3.4.29}$$

Making the same change of variables (3.3.52) that we made earlier when evaluating the space-time density correlation function - that is, replacing Ω and p_x with new variables of integration ϖ

and P_x defined via:

$$\Omega \equiv D_T p_\perp^2 \varpi \quad , \quad p_x \equiv \frac{D_T q_\perp^2}{\sqrt{v_v v_\rho}} P_x \,, \tag{3.4.30}$$

we can rewrite this as

$$\delta\left[\frac{m}{\rho_c}\right] = \frac{3u\rho_c^2\Delta}{\sqrt{v_v v_\rho}}\left(\frac{1}{D_T^2}\int_{\mathbf{p}_\perp}^{>}\frac{1}{p_\perp^2} I_1(\Theta,\Xi,\Upsilon) - \frac{2m}{D_T^4}\int_{\mathbf{p}_\perp}^{>}\frac{1}{p_\perp^4} I_2(\Theta,\Xi,\Upsilon) + \mathcal{O}(m^2)\right), \tag{3.4.31}$$

where we've defined the two dimensionless, $\mathcal{O}(1)$ integrals

$$\begin{aligned} I_1(\Theta,\Xi,\Upsilon) &\equiv \int_{-\infty}^{\infty}\frac{dP_x}{2\pi}\int_{-\infty}^{\infty}\frac{d\varpi}{2\pi}\left[\frac{1}{\alpha^2(P_x,\varpi)+\sigma^2(P_x,\varpi)}\right] \\ I_2(\Theta,\Xi,\Upsilon) &\equiv \int_{-\infty}^{\infty}\frac{dP_x}{2\pi}\int_{-\infty}^{\infty}\frac{d\varpi}{2\pi}\frac{\alpha(P_x,\varpi)}{\left(\alpha^2(P_x,\varpi)+\sigma^2(P_x,\varpi)\right)^2}\,, \end{aligned} \tag{3.4.32}$$

where $\alpha(P_x,\varpi)$ and $\sigma(P_x,\varpi)$ are defined (with different names for their arguments) in 3.3.56 and 3.3.57.

Very fortunately, it proves to be unnecessary to evaluate these integrals in order to calculate the critical exponents to $\mathcal{O}(\epsilon)$. It is sufficient for our purposes to know that $I_1(\Theta,\Xi,\Upsilon)$ and $I_2(\Theta,\Xi,\Upsilon)$ are finite and positive for *some* range of the three dimensionless parameters Θ, Ξ, and Υ. One can show that both $I_1(\Theta,\Xi,\Upsilon)$ and $I_2(\Theta,\Xi,\Upsilon)$ are finite provided that $\alpha(P_x,\varpi)$ and $\sigma(P_x,\varpi)$ do not vanish at the same point in the (P_x,ϖ) plane. We can show that this does not happen by noting that σ only vanishes on the line in the P_x-ϖ plane given by:

$$P_x = \frac{\Upsilon\Omega}{\Xi}\,. \tag{3.4.33}$$

Hence, if we can show that $\alpha(P_x,\varpi)$ does not vanish on this line, we will have established that $I_1(\Theta,\Xi,\Upsilon)$ and $I_2(\Theta,\Xi,\Upsilon)$ are both finite.

To establish that $\alpha(P_x,\varpi)$ does not vanish on the line 3.4.33, we simply evaluate $\alpha(P_x,\varpi)$ on that line by plugging 3.4.33 into 3.3.56 (with Q_x and Ω replaced with P_x and ϖ respectively). This gives

$$\alpha = 1 + \varpi^2\left[\frac{\Upsilon\Theta}{\Xi} - \frac{\Upsilon^2}{\Xi^2} - 1\right], \tag{3.4.34}$$

which is clearly positive definite if and only if the condition

$$\Theta\Xi\Upsilon > \Xi^2 + \Upsilon^2\,, \tag{3.4.35}$$

is satisfied. Equation 3.4.35 is easily satisfied (indeed, since Θ is always greater than 2, this condition is *always* satisfied when $\Xi = \Upsilon$).

The integral $I_1(\Theta, \Xi, \Upsilon)$ is clearly positive definite, since the integrand is. We have established that there is some range of Θ, Ξ, and Υ in which $I_2(\Theta, \Xi, \Upsilon)$ is positive by brute force numerical integration for a few specific sets of values of the dimensionless parameters Θ, Ξ, and Υ.

Note also that, since we will be choosing our arbitrary DRG rescaling exponents to keep the parameters of the linear theory fixed, and since Θ, Ξ, and Υ depend *only* on the parameters of the linear theory, Θ, Ξ, and Υ will themselves be constant under the RG. Hence, so will $I_1(\Theta, \Xi, \Upsilon)$ and $I_2(\Theta, \Xi, \Upsilon)$.

The integrals over $\mathbf{p}_\perp$ in 3.4.31, on the other hand, can be readily evaluated, especially in the limit

$$b = 1 + d\ell\,, \tag{3.4.36}$$

with $d\ell$ differential. Recalling that the superscript "$>$" on the integral over $\mathbf{p}_\perp$ implies that $\mathbf{p}_\perp$ lies in the thin shell $b^{-1}\Lambda < |\mathbf{p}_\perp| < \Lambda$, and taking the limit of $d\ell \ll 1$, it is easy to see that

$$\int_{\mathbf{p}_\perp}^{>} \frac{1}{p_\perp^2} = K_{d-1}\Lambda^{d-3}d\ell \quad , \quad \int_{\mathbf{p}_\perp}^{>} \frac{1}{p_\perp^4} = K_{d-1}\Lambda^{d-5}d\ell \tag{3.4.37}$$

where we've defined

$$K_{d-1} \equiv \frac{S_{d-1}}{(2\pi)^{d-1}}\,, \tag{3.4.38}$$

with S_{d-1} the surface area of a unit $d-1$-dimensional ball. This factor cancels out of all physical observables (e.g., critical exponents), so there is no need for us to give an explicit form for it (although we *could*, of course!).

Summarizing these results, the graphical corrections δm to m at one loop order are given by:

$$\delta m = \frac{3K_{d-1}u\rho_c^3\Delta}{\sqrt{v_v v_\rho}}\left(\frac{\Lambda^{d-3}I_1(\Theta, \Xi, \Upsilon)}{D_T^2} - \frac{2m\Lambda^{d-5}I_2(\Theta, \Xi, \Upsilon)}{D_T^4} + \mathcal{O}(m^2)\right)d\ell\,, \tag{3.4.39}$$

with $I_1(\Theta, \Xi, \Upsilon)$ and $I_2(\Theta, \Xi, \Upsilon)$ given by 3.4.32. Keep in mind that both of these integrals are constant under the RG.

Using this result for the term "graphs" in equation 3.4.26 gives us the complete RG recursion relation for m:

$$\begin{aligned} m' &= b^{\chi_\rho - \chi + z - 1}(m + \delta m) \\ &= b^{\chi_\rho - \chi + z - 1}\left[m + \frac{3K_{d-1}u\rho_c^3\Delta}{\sqrt{v_v v_\rho}}\left(\frac{\Lambda^{d-3}I_1(\Theta, \Xi, \Upsilon)}{D_T^2} - \frac{2m\Lambda^{d-5}I_2(\Theta, \Xi, \Upsilon)}{D_T^4} + \mathcal{O}(m^2)\right)d\ell\right]. \end{aligned} \tag{3.4.40}$$

The RG now proceeds by iterating this process. The result can be summarized by a differential recursion relation in the following (by now very standard) manner: as already mentioned, we choose $b = 1 + d\ell$ with $d\ell$ differential. Instead of keeping track of the number n of iterations of the renormalization group, we introduce a "renormalization group time" ℓ defined as $\ell \equiv nd\ell$. Then applying the recursion relation 3.4.41 after a renormalization group time ℓ, we must evaluate all of the parameters on the right hand side at RG time ℓ; the result $m' = m(\ell + d\ell)$. Hence, after expanding the right hand side of (3.4.41) to linear order in $d\ell$, we can rewrite (3.4.41) as

$$\begin{aligned} m(\ell + d\ell) = m(\ell) + \Bigg[&(\chi_\rho - \chi + z - 1)m(\ell) + \\ &\frac{3K_{d-1}u(\ell)\rho_c^3\Delta}{\sqrt{v_v v_\rho}}\left(\frac{\Lambda^{d-3}I_1}{D_T^2} - \frac{2m(\ell)\Lambda^{d-5}I_2}{D_T^4} + \mathcal{O}(m^2)\right)\Bigg]d\ell. \end{aligned} \tag{3.4.41}$$

Subtracting $m(\ell)$ from both sides of this expression and dividing by $d\ell$ gives us the differential recursion relation

$$\frac{dm}{d\ell} = (\chi_\rho - \chi + z - 1)m + \frac{3K_{d-1}u\rho_c^3\Delta}{\sqrt{v_v v_\rho}}\left(\frac{\Lambda^{d-3}I_1}{D_T^2} - \frac{2m\Lambda^{d-5}I_2}{D_T^4}\right) + \mathcal{O}(m^2)\,. \tag{3.4.42}$$

We now turn to the graphical corrections to u, which arise from the graph shown in figure 26. This graph generates a correction to the right hand side of the spatially Fourier transformed equation of motion (3.4.1) for v_i of the form

$$\delta\left[\partial_t v_i\right] = -\mathrm{FT}\{18iu^2 q_i\}\int_{\mathbf{p},\Omega}^{>} C_{\rho\rho}(\mathbf{p},\Omega)G_{\rho v}(-\mathbf{p},-\Omega)(ip_\perp)\}\delta\rho^3(\mathbf{r},t)\,. \tag{3.4.43}$$

Because this is of precisely the same form as the u term already present in the equation of motion 3.4.1, we can identify this as a contribution $\delta[u]$ to u given by

$$\delta[u] = 18u^2\int_{\mathbf{p},\Omega}^{>} C_{\rho\rho}(\mathbf{p},\Omega)G_{\rho v}(-\mathbf{p},-\Omega)(ip_\perp)\,. \tag{3.4.44}$$

We can simplify this expression somewhat by noting, as we'll show *a posteriori*, that both m and u are of $\mathcal{O}(\epsilon)$. Hence, this correction to u is already of $\mathcal{O}(\epsilon^2)$; keeping the dependence of $C_{\rho\rho}$ and $G_{\rho v}$ on m will only add corrections of $\mathcal{O}(\epsilon^3)$, which are negligible at the order to which we are working. A slightly more elaborate argument shows that keeping those m terms in $C_{\rho\rho}$ and $G_{\rho v}$ only changes the critical exponents to $\mathcal{O}(\epsilon^2)$, which is again higher order than that to which we are working. Therefore, we can drop the dependence on m of $C_{\rho\rho}$ and $G_{\rho v}$ in 3.4.44. Doing so, and using our earlier expressions 3.3.49 and 3.3.36 for $C_{\rho\rho}$ and $G_{\rho v}$ gives

$$\delta[u] = -18u^2\rho_c^3\Delta\int_{\mathbf{p},\Omega}^{>}\frac{p_\perp^4\mu(\mathbf{p},\Omega)}{(\mu^2(\mathbf{p},\Omega)+\kappa^2(\mathbf{p},\Omega))^2} \tag{3.4.45}$$

The alert reader will recognize the integral on the right hand side as that which already appeared in our expression (3.4.31) for the linear in m term in the renormalization of m. Indeed, making the change of variables (3.4.30), we quickly find

$$\delta[u] = -\frac{18u^2\rho_c^3 K_{d-1}\Lambda^{d-5}I_2}{\sqrt{v_v v_\rho}D_T^4}d\ell\,. \tag{3.4.46}$$

Using this result for the "graphs" in the first equality of our general RG recursion relation 3.4.19 for u, and converting that recursion relation into a differential equation as we did the recursion relation for m, we find

$$\frac{du}{d\ell} = (3\chi_\rho - \chi + z - 1)u - u^2 \left(\frac{18 K_{d-1} \rho_c^3 \Delta \Lambda^{d-5} I_2}{\sqrt{v_v v_\rho} D_T^4} \right) . \tag{3.4.47}$$

To completely close these recursion relations, we need to determine the rescaling exponents χ. χ_ρ, and z. These are, of course, arbitrary. However, to make the analysis simple, it is very convenient to chose those exponents so as to keep the parameters of the linear theory (aside from m) fixed, because then we can treat the unknown integrals I_1 and I_2 as constants. To determine the choice of those exponents that accomplishes this, we turn to the recursion relations (3.4.4)-(3.4.14) for the linear parameters, and note that, to one loop order, there are no graphical corrections to any of the linear parameters (aside from m). Hence, *to one loop order*, the choice of exponents that keeps those linear parameters fixed is the same as the choice we made in the previous subsection, in which we ignored those graphical corrections altogether; that is,

$$z = \zeta = 2 , \tag{3.4.48}$$

$$\chi = \frac{1-d}{2} , \tag{3.4.49}$$

$$\chi_\rho = \frac{3-d}{2} . \tag{3.4.50}$$

We expect there to be $\mathcal{O}(\epsilon^2)$ corrections to all of these exponents.

With these choices, our recursion relations for m and u become

$$\frac{dm}{d\ell} = 2m + \frac{3 K_{d-1} u \rho_c^3 \Delta}{\sqrt{v_v v_\rho}} \left(\frac{\Lambda^{d-3} I_1}{D_T^2} - \frac{2m \Lambda^{d-5} I_2}{D_T^4} \right) \tag{3.4.51}$$

$$\frac{du}{d\ell} = \epsilon u - u^2 \left(\frac{18 K_{d-1} \rho_c^3 \Delta \Lambda^{d-5} I_2}{\sqrt{v_v v_\rho} D_T^4} \right) , \tag{3.4.52}$$

where we remind the reader that we've defined $\epsilon \equiv 5 - d$. The flows implied by these equations, which are illustrated in figure (27), are extremely similar in *form* to those for equilibrium phase separation (that is, the equilibrium Ising model), but with ϵ being $5 - d$ for our problem, while it is $4 - d$ for the equilibrium problem.

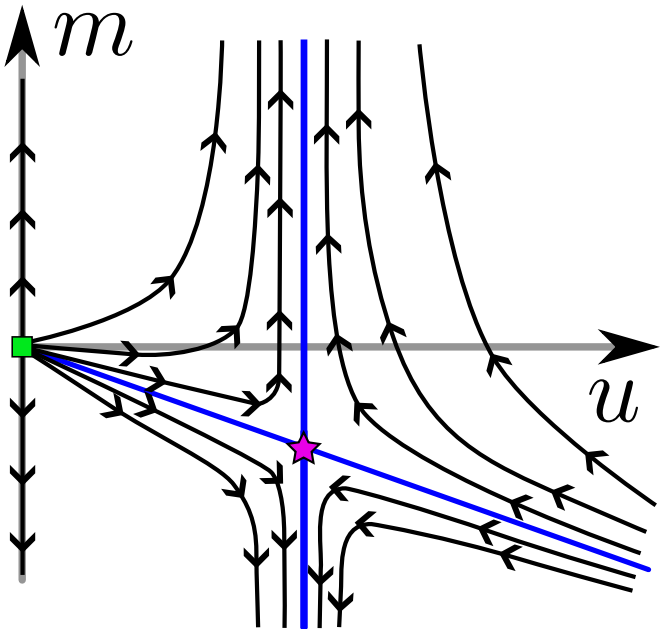

FIGURE 27. Renormalization group flows of the parameters m and u on the $u - m$ manifold of parameter space. The Gaussian fixed point is located at the origin and is marked by a green square. The linear fixed point is located at (u^*, m^*), with u^* and m^* given by (3.4.53) and (3.4.54), and is marked by a pink five pointed star. The illustrated flow lines are those of equations (3.4.51) and (3.4.52). The solid blue lines intersecting the linear fixed point run in the directions of the eigenvectors given in equations (3.4.66) and (3.4.67).

The fixed points of these recursion relations can be determined by setting $\frac{dm}{d\ell} = 0 = \frac{du}{d\ell}$, which leads to two equations for the two unknowns (m^*, u^*), where the superscript $*$ denotes the fixed point values. Aside from the trivial Gaussian fixed point $(m^*, u^*) = (0, 0)$, which is doubly unstable for $\epsilon > 0$ - that is, for $d < 5$, and hence does not control the transition, there is a single stable analog of the familiar Wilson-Fisher fixed point at

$$m^* = -\left(\frac{\Lambda^2 D_T^2 I_1}{12 I_2}\right)\epsilon\,, \tag{3.4.53}$$

$$u^* = \left(\frac{\sqrt{v_v v_\rho} D_T^4 \Lambda^{5-d}}{18 \rho_c^3 \Delta K_{d-1} I_2}\right)\epsilon\,. \tag{3.4.54}$$

This is the "critical fixed point", which controls the transition for $d < 5$. Linearizing the recursion relations 3.4.51 and 3.4.52 around this fixed point by taking

$$m(\ell) = m^* + \delta m(\ell)\,, \tag{3.4.55}$$

$$u(\ell) = u^* + \delta u(\ell) \tag{3.4.56}$$

gives

$$\frac{d\delta m}{d\ell} = \left(2 - \frac{6 K_{d-1} \rho_c^3 \Delta \Lambda^{d-5} I_2}{\sqrt{v_v v_\rho} D_T^4} u^*\right)\delta m + C_u \delta u\,, \tag{3.4.57}$$

$$\frac{d\delta u}{d\ell} = \left(\epsilon - \left(\frac{36 K_{d-1} \rho_c^3 \Delta \Lambda^{d-5} I_2}{\sqrt{v_v v_\rho} D_T^4}\right)\right)\delta u\,. \tag{3.4.58}$$

where the constant

$$C_u = \frac{3 K_{d-1} u \rho_c^3 \Delta \Lambda^{d-3} I_1}{\sqrt{v_v v_\rho} D_T^2} + \mathcal{O}(\epsilon)\,. \tag{3.4.59}$$

Inserting the fixed point value 3.4.53 of u into these recursion relations, we see that massive cancellations occur; in particular, the unevaluated integral I_2 cancels out. This leaves the recursion relations in the very simple form:

$$\frac{d\delta m}{d\ell} = (2 - \frac{1}{3}\epsilon)\delta m + C_u \delta u\,, \tag{3.4.60}$$

$$\frac{d\delta u}{d\ell} = -\epsilon \delta u\,. \tag{3.4.61}$$

Seeking solutions to this linearized system of an exponential form; i.e.,

$$\begin{pmatrix} \delta m(\ell) \\ \delta u(\ell) \end{pmatrix} = \mathbf{S} e^{\lambda \ell} \tag{3.4.62}$$

where $\mathbf{S}$ is a constant eigenvector, and λ a constant growth rate (which should not be confused with the parameter λ in our original equations of motion!), we see that there are two eigenvalues for λ:

$$\lambda_1 = -\epsilon \tag{3.4.63}$$

$$\lambda_2 \equiv \lambda_t = 2 - \frac{1}{3}\epsilon \tag{3.4.64}$$

We identify λ_t, which is the only positive eigenvalue, as the "thermal" eigenvalue. We use this term in the usual RG sense, which is that it determines the dependence of the correlation length on the departure of the control parameter (which is usually temperature in equilibrium problems, hence the term "thermal eigenvalue") from its critical value.

We can see this by the following completely standard RG analysis:

Note that, as usual for a system of coupled linear ODE's, the general solution of our linearized recursion relations is

$$\begin{pmatrix} \delta u(\ell) \\ \delta m(\ell) \end{pmatrix} = a(m_0)\hat{\mathbf{s}}_1 e^{-\epsilon \ell} + c(m_0)\hat{\mathbf{s}}_2 e^{\lambda_t \ell}\,, \tag{3.4.65}$$

where $\hat{\mathbf{s}}_{1,2}$ are the unit eigenvectors associated with the two eigenvalues $\lambda_{1,2}$ respectively, and the scalar constants $a(m_0)$ and $c(m_0)$ are determined by the initial (i.e., bare) parameters of the model, and hence, in particular, the bare value m_0 of m.

The unit eigenvectors are given to leading order in ϵ by by:

$$s_1 = \frac{1}{\sqrt{4 + C_u^2}} \begin{pmatrix} -C_u \\ 2 \end{pmatrix}, \tag{3.4.66}$$

$$s_2 = \begin{pmatrix} 0 \\ 1 \end{pmatrix}. \tag{3.4.67}$$

These eigenvectors are depicted in figure 27 as the blue lines emanating from the linear fixed point.

Now it is easy to see that, in order for the initial parameters of our system to be such that the system flows under renormalization into the critical fixed point (3.4.53) and (3.4.54), we clearly must have $\delta m(\ell \to \infty) \to 0$, $\delta u(\ell \to \infty) \to 0$, which can clearly only occur at a value of m_0 such that $c(m_0) = 0$, so that the exponentially growing part of the general solution (3.4.72) vanishes. We'll call this special value of m_0 m_c, that is, we'll define m_c by the condition $c(m_c) = 0$. It clearly then follows by analyticity that, for m_0 near m_c,

$$c(m_0) \approx A(m_0 - m_c)\,, \tag{3.4.68}$$

with A a constant. This implies that, if $A > 0$, $c(m_0)$ will be positive for $m_0 > m_c$. As a result, as RG time $\ell \to \infty$, the renormalized $m(\ell)$ will go to large, positive values (since the exponentially growing c term in (3.4.72) will inevitably eventually dominate over the exponentially decaying a term). This clearly corresponds to the *non*-phase separated region, in which the state of uniform density is stable. Likewise, if $m_0 < m_c$, (continuing for now to assume $A > 0$), $c(m_0)$ will be negative. As a result, as RG time $\ell \to \infty$, the renormalized $m(\ell)$ will go to large, negative values. This clearly corresponds to the phase separated region, in which the state of uniform density is unstable.

Hence, m_c clearly corresponds to the critical value of m at which the critical point occurs.

Recognizing this, we can now use the expansion 3.4.68 to obtain the behavior of the correlation length near the critical point by the following very standard RG argument

Starting with any m_0 near m_c, we run the renormalization group until we reach a value $\ell^*(m_0)$ of ℓ at which the renormalized $\delta m(\ell^*)$ takes on some particular "$\mathcal{O}(1)$" reference value which we'll call δm_r. By "$\mathcal{O}(1)$", which is literally meaningless in this context, since δm is a dimensionful quantity, what we really mean is a value small enough that the linearized recursion relations (3.4.60) and (3.4.61) , and, therefore, their solution (3.4.72), remain valid, but as big as it can be consistent with that requirement.

For m_0 close to m_c, therefore, the value of ℓ^* required to reach such a large $\delta m(\ell^*)$ will clearly be large, since the coefficient $c(m_0)$ of the exponentially growing part of the solution (3.4.72) of our linearized recursion relations is small in that case. It follows that, by the time ℓ reaches ℓ^*, the

exponentially decaying a term in the solution (3.4.72) will have become negligible, so that

$$\delta m(\ell^*) \approx c(m_0) e^{\lambda_t \ell^*} = \delta m_r \,, \tag{3.4.69}$$

where in the last equality we have applied our condition on ℓ^* that it make $\delta m(\ell^*) = \delta m_r$. It is clearly straightforward to solve 3.4.69 for ℓ^*; we'll instead solve it for e^{ℓ^*}, which, as we'll see in a moment, proves to be the more useful quantity:

$$e^{\ell^*} = \left(\frac{\delta m_r}{c(m_0)} \right)^{\nu} \propto |m_0 - m_c|^{-\nu_\perp} \,, \tag{3.4.70}$$

where we've defined the "correlation length exponent"

$$\nu_\perp \equiv \frac{1}{\lambda_2} = \frac{1}{2} + \frac{\epsilon}{12} + \mathcal{O}(\epsilon^2) \,. \tag{3.4.71}$$

Note that, in the limit $m_c \to m_0$, all of our starting systems have been mapped onto the same point

$$\begin{pmatrix} \delta u(\ell^*) \\ \delta m(\ell^*) \end{pmatrix} = \begin{pmatrix} 0 \\ \delta m_r \end{pmatrix} \,, \tag{3.4.72}$$

since the exponentially decaying part of the solution (3.4.72) will have vanished in this limit. Hence, all of these systems are mapped onto the same model, and, hence, onto a model with the same correlation lengths in the perpendicular and parallel direction.

Note that this does *not* imply that all of these systems have the same correlation lengths. On the contrary, since each of them will have to have been renormalized for a different, strongly $(m_0 - m_c)$-dependent RG time as implied by (3.4.70), they will have very different correlation lengths. Indeed, since, on every time step, we rescale lengths in the $\perp$-directions by a factor of $b = 1 + d\ell$, while directions in the $\|$-direction are rescaled (at the one loop order to which we've worked here) by a factor of b^2, the actual correlation lengths in the $\perp$ and $\|$ directions $\xi_{\|,\perp}$ are related to those at the

"reference point $\begin{pmatrix} \delta u(\ell^*) \\ \delta m(\ell^*) \end{pmatrix}$ by

$$\begin{aligned} \xi_\perp(m_0) &= b^{n^*}\xi_\perp(\delta m_r) = e^{\ell^*}\xi_\perp(\delta m_r) \propto |m_0 - m_C|^{-\nu_\perp} , \\ \xi_\parallel(m_0) &= b^{2n^*}\xi_\parallel(\delta m_r) = e^{\ell^*}\xi_\parallel(\delta m_r) \propto |m_0 - m_C|^{-2\nu_\perp} \\ &\equiv |m_0 - m_C|^{-\nu_\parallel} . \end{aligned} \tag{3.4.73}$$

(3.4.74)

Here $n^* = \ell^*/d\ell$ is the number of RG steps required to reach ℓ^*, and we've used the fact that, for $d\ell$ differential and $\ell^* = nd\ell$ finite, $b^{n^*} = (1 + d\ell^*)^{n^*} = (e^{d\ell^*})^{n^*} = e^{n^* d\ell^*} = e^{\ell^*}$. We've also used our earlier expression (3.4.70) for e^{ℓ^*}, and defined

$$\nu_\parallel = 2\nu_\perp . \tag{3.4.75}$$

Since everything in our expressions 3.4.74 for these two correlation lengths is independent of the bare m_0 except for the terms explicitly displayed, which arise from the singular m_0-dependence of the RG time ℓ^*, that explicitly displayed dependence is the entire dependence of the correlation lengths on m_0. Thus we have

$$\xi_\perp(m_0) \propto |m_0 - m_C|^{-\nu_\perp} \quad , \quad \xi_\parallel(m_0) \propto |m_0 - m_C|^{-\nu_\parallel} , \tag{3.4.76}$$

with the universal critical exponents $\nu_{\perp,\parallel}$ given by

$$\nu_\perp = \frac{1}{\lambda_2} = \frac{1}{2} + \frac{\epsilon}{12} + \mathcal{O}(\epsilon^2) \quad , \quad \nu_\parallel = 1 + \frac{\epsilon}{6} + \mathcal{O}(\epsilon^2) . \tag{3.4.77}$$

Note that the 2 to 1 ratio of the exponents $\nu_\parallel$ to $\nu_\perp$ will not persist to higher order in ϵ; it is an artifact of the fact that the anisotropy exponent $\zeta = 2$ up to and including linear order in ϵ. At $\mathcal{O}(\epsilon^2)$ and higher, there will be graphical corrections to, e.g., $D_{L\perp,\rho\perp}$ and various other parameters of the linear model, which will in turn make $\zeta \neq 2$. The general *form* of 3.4.76 will continue to hold

at higher order in ϵ, but the relation between $\nu_\parallel$ and $\nu_\perp$ will become

$$\nu_\parallel = \zeta \nu_\perp \tag{3.4.78}$$

with ζ given by

$$\zeta = 2 + \mathcal{O}(\epsilon^2)\,. \tag{3.4.79}$$

We can compute one more exponent: the critical exponent β, which gives the shape of the phase boundary in figure(21). The argument, which is very similar to that just presented, proceeds as follows:

Because we rescale density by a factor of b^{χ_ρ} on each RG time step, the density difference $\delta\rho$ between the two coexisting densities in figure (21) at some $m_0 < m_c$ can be related to the corresponding difference at a *negative* reference value δm_r via

$$\Delta\rho(\delta m_0; \ell = 0) = e^{\ell_* \chi_\rho} \Delta\rho(\delta m_r)\,. \tag{3.4.80}$$

As we argued for the correlation length, so here the quantity $\Delta\rho(\delta m_r)$ will be independent of our starting value δm_0. Hence, all of the dependence of $\Delta\rho$ on m_0 comes again from the factor $e^{\ell_* \chi_\rho} = \left(e^{\ell_*}\right)^{\chi_\rho}$. The relation (3.4.70) relating e^{ℓ_*} to m_0 continues to hold, so we have

$$\delta\rho \propto |m_0 - m_c|^\beta \tag{3.4.81}$$

with

$$\beta = -\nu_\perp \chi_\rho\,. \tag{3.4.82}$$

This relation is exact. We can use it to generate an ϵ-expansion for β by using our earlier expansion (3.4.77) for $\nu_\perp$, along with our earlier argument that χ_ρ is unchanged from its linear value 3.4.50 to first order in ϵ, in 3.4.82 to obtain

$$\begin{aligned}\beta &= -\nu\chi_\rho = \left(\frac{1}{2}+\frac{\epsilon}{12}+\mathcal{O}(\epsilon^2)\right)\left(\frac{3-d}{2}+\mathcal{O}(\epsilon^2)\right)\\ &= \left(\frac{1}{2}+\frac{\epsilon}{12}+\mathcal{O}(\epsilon^2)\right)\left(-1+\frac{\epsilon}{2}+\mathcal{O}(\epsilon^2)\right)\\ &= \frac{1}{2}-\frac{\epsilon}{6}+\mathcal{O}(\epsilon^2)\,.\end{aligned} \tag{3.4.83}$$

As mentioned earlier, there are no one loop corrections to the rescaling exponents z, ζ, χ, and χ_ρ. We *do* expect them to pick up $\mathcal{O}(\epsilon^2)$ corrections when going beyond one loop order.

This concludes our dynamical renormalization group calculation of the order parameter exponents $\nu_\perp, \nu_\parallel$ and β to $\mathcal{O}(\epsilon)$ in a $d = 5-\epsilon$ expansion.

3.5 Discussion and Summary

We have shown that phase separation in polar ordered active fluids ("flocks")belongs to a new universality class, radically different from that of equilibrium phase separation. Even the critical dimension of the problem is different: flocks have a critical dimension of five, while for equilibrium phase separation, the critical dimension is four.

The well-informed reader will have noticed that, to leading order in ϵ, our results for the thermal eigenvalue λ_t and the order parameter exponent β are identical, *when expressed in terms of* $\epsilon = d_c - d$, to those for the equilibrium problem. The only difference, *at this order*, is that d_c is larger by 1 for the flocking problem that in equilibrium.

One might therefore be tempted to speculate that this property holds to all orders; that is, that $\lambda_t^{\rm flock}(d) = \lambda_t^{\rm equil}(d-1)$. However, this speculation is almost certainly incorrect. There is, in fact, at least one known problem in which, as in ours, the critical dimension differs from that for equilibrium phase separation by 1, and the exponents, to leading order in ϵ, are the same as those of the equilibrium short-ranged Ising model. That problem is the Ising model with dipolar interactions[3, 6], for which $d_c = 3$. For that problem, a second order in ϵcalculation[6] finds different results from the second order in ϵ calculation for the short-ranged problem. This dipolar problem has many features in common with ours, including a two to one anisotropy of scaling at the linear level, and the fact that correlations do not decay exponentially even beyond the correlation length.

Hence, we strongly suspect that our problem does *not* map on to the equilibrium problem in one lower dimension.

Our ϵ-expansion results are, of course, *not* expected to be accurate for the physically relevant cases of $d = 3$ ($\epsilon = 2$) or $d = 2$ ($\epsilon = 3$). The significance of our calculation, and, in particular, our demonstration of the existence of a non-Gaussian fixed point in $d = 5 - \epsilon$, is that he shows the existence of a critical point in a new universality class for phase separation in flocks. The fact that the critical dimension for our problem is $d_c = 5$, in contrast to the value $d_c = 4$ that one finds for equiblibrium phase separation[10, 27] implies that this universality class is *very* different from that of equilibrium phase separation. In particular, it implies that the critical exponents characterizing this transition should be very far from their equilibrium values.

What can we say about the exponents in $d = 3$ and $d = 2$? One thing that we know is that, at higher loop order, linear coefficients like the diffusion constants $D_{L\perp}$ and so on will get graphical corrections. This will make the anisotropy exponent ζ differ from 2, although it will remain universal. Thus we will continue to have two correlation lengths, one for correlations of points in space separated along ($\parallel$) the direction of mean flock motion, and one for correlations of points in space separated perpendicular to ($\perp$) the direction of mean flock motion. These will diverge as the control parameter m_0, defined via the pressure expansion (3.2.3), approaches its critical value m_c, according to

$$\xi_\perp(m_0) \quad \propto |m_0 - m_C|^{-\nu_\perp} \quad , \quad \xi_\parallel(m_0) \propto |m_0 - m_C|^{-\nu_\parallel} \, , \tag{3.5.1}$$

with the universal critical exponents $\nu_{\perp,\parallel}$ obeying

$$\nu_\parallel = \zeta \nu_\perp \, , \tag{3.5.2}$$

with

$$\zeta = 2 + \mathcal{O}(\epsilon^2) \, . \tag{3.5.3}$$

This ϵ-expansion obviously tells us nothing quantitative about the universal anisotropy exponent ζ in $d = 2$ or $d = 3$, other than that it does not equal 2.

One very big remaining open question is: what is the *lower* critical dimension d_{LC}, below which the critical point disappears, for our problem? For equilibrium phase separation, that lower critical dimension is one. The "$d \to d-1$" argument described above would then suggest that $d_{LC} = 2$ for our problem. But, as discussed earlier, we do not believe that argument, so the question of the lower critical dimension remains open. Thus, we cannot unambiguously claim that our new universality class persists down to the physically relevant spatial dimensions $d = 2, 3$. This is a question that will have to be answered by experiment. What we can be quite confident of in light of our work is that, if such a critical point *does* exist, it will certainly belong to a universality class very different from that of equilibrium phase separation.

APPENDIX

A POTENTIALLY DANGEROUS IRRELEVANT COEFFICIENT

This work was published in volume 110 of the journal Physical Review E in November 2024.

A.1 Demonstration of anisotropic scaling at the critical point

Consider first the case $q_x = 0$. The linearized equation of motion (III.19) for $\delta\rho$ then reads exactly:

$$(-i\omega + D_{\rho\perp}q_\perp^2)\delta\rho + i\rho_c q_\perp v_L = 0\,, \tag{A.1.1}$$

where we've set the density noise to zero since, as we show in the paper, its effects are negligible.

Equation (A.1.1) is readily solved for v_L in terms of $\delta\rho$:

$$v_L = \frac{1}{\rho_c}\left(\frac{\omega}{q_\perp} + iD_{\rho\perp}q_\perp\right)\delta\rho\,. \tag{A.1.2}$$

Inserting this into the equation of motion (III.20) for v_L then gives a closed equation for $\delta\rho$ in terms of f_L, whose solution is

$$\delta\rho(\mathbf{q},\omega) = \frac{\rho_c q_\perp f_L(\mathbf{q},\omega)}{B\omega q_\perp^2 + i(Aq_\perp^4 - \omega^2)}\,, \tag{A.1.3}$$

where we've defined

$$A \equiv K\rho_c + D_{L\perp}D_{\rho\perp}, \quad B \equiv D_{\rho\perp} + D_{L\perp} - \nu_t\,. \tag{A.1.4}$$

Now autocorrelating (A.1.3) with itself, and using equation (II.4) for the f_L correlations, gives

$$\langle|\delta\rho(\mathbf{q},\omega)|^2\rangle = \frac{\rho_c^2 q_\perp^2\,\Delta}{(\omega^2 - Aq_\perp^4)^2 + B^2\omega^2 q_\perp^4} \tag{A.1.5}$$

Integrating this over all frequencies ω then gives the equal-time correlation function

$$\langle|\delta\rho(\mathbf{q},t)\delta\rho(-\mathbf{q},t)|\rangle \equiv C_\rho^{ET}(\mathbf{q}) = \rho_c^2 q_\perp^2 \Delta \int_{-\infty}^{\infty} \frac{d\omega}{2\pi[(\omega^2 - Aq_\perp^4)^2 + B^2\omega^2 q_\perp^4]} \,. \tag{A.1.6}$$

Changing variables of integration from ω to u, where u is defined via

$$\omega = u\sqrt{A}q_\perp^2 \,, \tag{A.1.7}$$

gives

$$C_\rho^{ET}(\mathbf{q}) = \frac{\rho_c^2 \Delta}{A^{3/2} q_\perp^4} f\left(\frac{B^2}{A}\right), \tag{A.1.8}$$

with

$$f\left(\frac{B^2}{A}\right) = \int_{-\infty}^{\infty} \frac{du}{2\pi\left[(u^2-1)^2 + \frac{B^2}{A}u^2\right]} \tag{A.1.9}$$

an $O(1)$ dimensionless constant that depends only on the dimensionless ratio $\frac{B^2}{A}$, but *not* on wavenumber $q_\perp$. Hence, equation (A.1.8) shows that $C_\rho(\mathbf{q}) \sim \frac{1}{q^4}$ when $q_x = 0$.

We'll now show that when q_x and $q_\perp$ are comparable, $C_\rho^{ET}(\mathbf{q}) \sim \frac{1}{q^2}$. This will thereby confirm the 2 to 1 anisotropy of scaling between q_x and $q_\perp$ in the dominant regime of wavevector for the ρ fluctuations.

To begin our analysis of the case $q_x \sim q_\perp$, we'll determine the eigenfrequencies $\omega(\mathbf{q})$ in this range of wavevector for small q. We'll assume (and verify a posteriori) that these take the form

$$\omega(\mathbf{q}) = c(\theta_\mathbf{q})q - i\epsilon(\theta_\mathbf{q})q^2 \tag{A.1.10}$$

where $c(\theta_q)$ and $\epsilon(\theta_q)$ depend only on the *direction* of $\mathbf{q}$, but *not* its magnitude. (Here we define $\theta_\mathbf{q}$ as the angle between $\mathbf{q}$ and the x-axis.)

Inserting the ansatz (A.1.10) into the equations of motion for (III.19) and (III.20), and keeping only terms of $O(q)$, leads to

$$\begin{aligned} -i(cq - v_\rho q_x)\delta\rho + i\rho_c q_\perp v_L &= 0\,, \\ (cq - v_v q_x)v_L &= 0\,, \end{aligned} \tag{A.1.11}$$

where we have set the forces to zero on the right hand side, because we're trying to determine eigenfrequencies. It is clear from (A.1.11) that the two possible eigenvalues of c are

$$c = v_\rho \frac{q_x}{q} = v_\rho \cos\theta_q \equiv c_\rho(\theta_q) \tag{A.1.12}$$

and

$$c = v_v \frac{q_x}{q} = v_v \cos\theta_q \equiv c_v(\theta_q)\,. \tag{A.1.13}$$

We now need to determine the ϵ's in equation (A.1.10) associated with each of these sound speeds.

Consider the c_ρ root first. Inserting the ansatz (A.1.10) with $c = c_\rho$ into equation (A.1.10) and keeping terms up to $O(q^2)$ in both equations leads to

$$[-\epsilon_\rho q^2 + \Gamma_\rho(\mathbf{q}) - \phi v_\rho q_x^2]\delta\rho + i\rho_c q_\perp v_L = 0\,, \tag{A.1.14}$$

and

$$(\nu_x - \nu_t v_\rho)q_x q_\perp \delta\rho - i(v_\rho - v_v)q_x v_L = 0\,. \tag{A.1.15}$$

Thiese two equations are an eigenvalue condition on ϵ_ρ, and lead to

$$\epsilon_\rho = \frac{1}{q^2}\left[-\phi v_\rho q_x^2 - \rho_c \frac{\nu_t v_\rho - \nu_x}{v_\rho - v_v} q_\perp^2 + \Gamma_\rho(\mathbf{q})\right]. \tag{A.1.16}$$

Note that, as asserted in our ansatz (A.1.10), ϵ_ρ depends only on the direction of $\theta_\mathbf{q}$ of $\mathbf{q}$, not on its magnitude, since every term inside the square brackets is proportional to q^2.

A similar analysis for the c_v mode gives

$$\epsilon_v = +\frac{1}{q^2}\left[\Gamma_L(\mathbf{q}) + \frac{\nu_x - \nu_t v_v}{v_v - v_\rho}\rho_c q_\perp^2\right] \tag{A.1.17}$$

which also depends only on the direction of $\theta_{\mathbf{q}}$ of $\mathbf{q}$.

Note, importantly, that for $q_x \ll q_\perp$, both ϵ_ρ and ϵ_v go to finite non-zero limits:

$$\epsilon_\rho \to \left[D_{\rho\perp} + \left(\frac{\nu_x - \nu_t v_v}{v_\rho - v_v}\right)\rho_c\right] \equiv D_1\,, \tag{A.1.18}$$

$$\epsilon_v \to \left[D_{L\perp} + \left(\frac{\nu_x - \nu_t v_v}{v_v - v_\rho}\right)\rho_c\right] \equiv D_2\,. \tag{A.1.19}$$

To summarize, for $q_x \sim q_\perp$, the eigenfrequencies are given by

$$\omega_\rho(\mathbf{q}) = v_\rho q_x - i\epsilon_\rho q^2\,, \tag{A.1.20}$$

and

$$\omega_v(\mathbf{q}) = v_v q_x - i\epsilon_v q^2\,. \tag{A.1.21}$$

Note that these do not have a simple scaling form; that is, the eigenfrequencies are not proportional to a simple power of q. Instead, the real parts scale linearly with q, while the imaginary parts scale quadratically. This can lead to confusion when attempting to power count, so care must be taken. We'll now proceed with that in mind.

With these eigenvalues in hand, its a straightforward exercise in linear algebra to find $\langle|\rho(\mathbf{q},\omega)|^2\rangle$. First, we note that the equations of motion can be written in matrix form as

$$\underset{\sim}{M}(\mathbf{q},\omega)\begin{bmatrix}\delta\rho\\ v_L\end{bmatrix} = \begin{bmatrix}0\\ f_L\end{bmatrix}\,, \tag{A.1.22}$$

where the 2×2 matrix $\underset{\sim}{M}$ is

$$\underset{\sim}{M} = \begin{bmatrix}a & b\\ c & d\end{bmatrix}\,, \tag{A.1.23}$$

with

$$a = -i(\omega - v_\rho q_x) + \Gamma_\rho - \phi\omega q_x \,, \tag{A.1.24}$$

$$b = i\rho_c q_\perp + D_{\rho v} q_x q_\perp \,, \tag{A.1.25}$$

$$c = (\nu_x q_x - \nu_t \omega) q_\perp + iK q_\perp^3 \,, \tag{A.1.26}$$

$$d = -i(\omega - v_v q_x) + \Gamma_L \,. \tag{A.1.27}$$

The solution of A.1.22 is clearly

$$\begin{bmatrix} \delta\rho \\ v_L \end{bmatrix} = \underset{\sim}{M}^{-1} \begin{bmatrix} 0 \\ f_L \end{bmatrix} \,. \tag{A.1.28}$$

One can easily verify that

$$\underset{\sim}{M}^{-1} = \frac{1}{det\underset{\sim}{M}(\mathbf{q},\omega)} \begin{pmatrix} d & -b \\ -c & a \end{pmatrix} \,. \tag{A.1.29}$$

Using equation A.1.28, we see that

$$\delta\rho = -\frac{b f_L}{det\underset{\sim}{M}(\mathbf{q},\omega)} \tag{A.1.30}$$

The determinant of $\underset{\sim}{M}$ is clearly a quadratic function of ω, with its ω^2 term equal to $-\omega^2$. Furthermore, the two roots of this quadratic function are clearly the eigenvalues $\omega_{\rho,v}(\mathbf{q})$ given by equations A.1.20 and A.1.21.

Taking these two facts together it follows that

$$det\underset{\sim}{M}(\mathbf{q},\omega) = -(\omega - \omega_\rho(\mathbf{q}))(\omega - \omega_v(\mathbf{q})) = [(\omega - v_v q_x) + i\epsilon_v q^2][(\omega - v_\rho q_x) + i\epsilon_\rho q^2] \tag{A.1.31}$$

Using this equation A.1.30 gives

$$\delta\rho(\mathbf{q},\omega) = -\frac{i\rho_c q_\perp f_L(\mathbf{q},\omega)}{[(\omega - v_v q_x) + i\epsilon_v q^2][(\omega - v_\rho q_x) + i\epsilon_\rho q^2]} \tag{A.1.32}$$

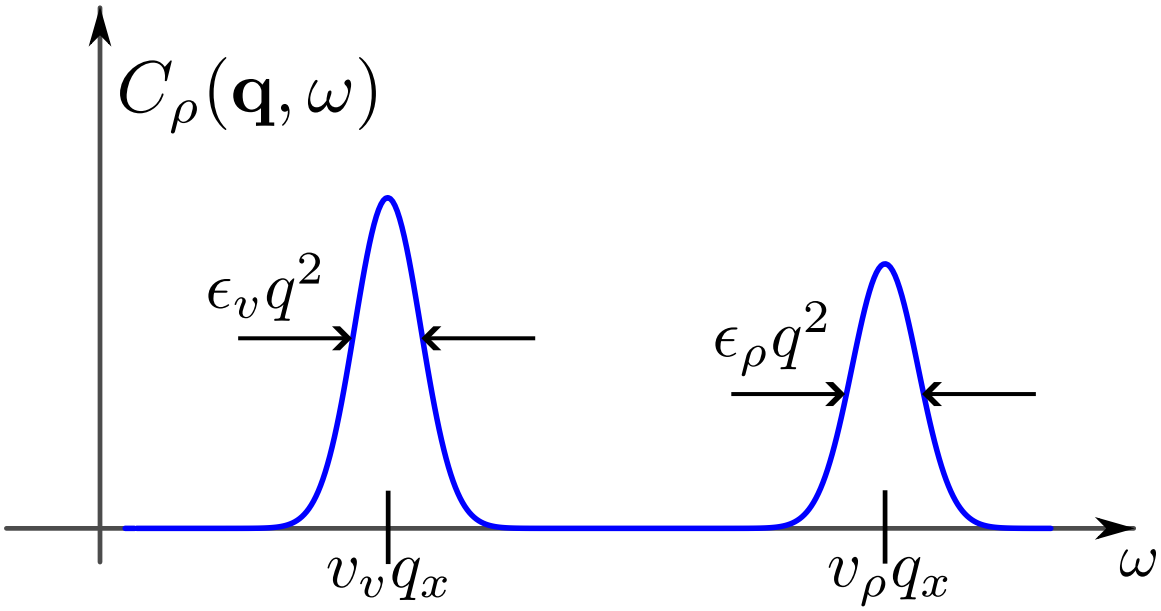

FIGURE 28. Plot of $C_\rho(\mathbf{q},\omega)$versus frequency ω for fixed $\mathbf{q}$ with $q_x \sim q_\perp$. Note that as $q \to 0$, the width of the peaks, which vanishes like q^2, becomes infinitely narrower than the separation between them, which only vanishes like q.

Taking the squared magnitude of this, and averaging over the noise $f_L(\mathbf{q},\omega)$ using

$$\langle |f_L(\mathbf{q},\omega)|^2 \rangle = \Delta \tag{A.1.33}$$

then gives

$$\langle |\delta\rho(\mathbf{q},\omega)|^2 \rangle \equiv C_\rho(\mathbf{q},\omega) = \frac{\rho_c^2 q_\perp^2 \Delta}{[(\omega - v_v q_x)^2 + \epsilon_v^2 q^4)][(\omega - v_\rho q_x)^2 + \epsilon_\rho^2 q^4]} \,. \tag{A.1.34}$$

Keep in mind that ϵ_v and ϵ_ρ depend on the direction of $\theta_\mathbf{q}$ of $\mathbf{q}$ via equations A.1.16 and A.1.17, but do not depend on the magnitude of q, as can be seen from A.1.16 and A.1.17.

A plot of $C_\rho(\mathbf{q},\omega) \equiv \langle |\rho(\mathbf{q},\omega)|^2 \rangle$ as a function of ω clearly consists of two sharp peaks, one at $\omega = v_v q_x$, the other at $\omega = v_\rho q_x$, as illustration in figure 28. We call these peaks "sharp" because their width is $O(q^2)$, while their separation in $O(q)$, and, hence, much greater than their width in the limit of $q \to 0$.

This helps us to evaluate the integral of $C_\rho(\mathbf{q},\omega)$ over all ω, which, of course, gives the equal time correlation function

$$C_\rho^{ET}(\mathbf{q}) = \int_{-\infty}^{\infty} C_\rho(\mathbf{q},\omega)\frac{d\omega}{2\pi}\,. \tag{A.1.35}$$

Because the sharpness of the two peaks in $C_\rho(\mathbf{q},\omega)$, we can evaluate the contribution of each of them separately. For the peak near $\omega = v_v q_x$, we write

$$\omega = v_v q_x + \delta\omega \tag{A.1.36}$$

and consider $\delta\omega << |v_v - v_\rho| q_x$. In this limit, the two factors in the denominator of A.1.34 become

$$(\omega - v_v q_x)^2 + \epsilon_v^2 q^4 = \delta\omega^2 + \epsilon_v^2 q^4 \tag{A.1.37}$$

and

$$(\omega - v_\rho q_x)^2 + \epsilon_\rho^2 q^4 = (v_v - v_\rho)^2 q_x^2\,. \tag{A.1.38}$$

Using these in A.1.34 gives

$$C_\rho(\mathbf{q},\omega) \approx \frac{\rho_c^2 q_\perp^2 \Delta}{(v_v - v_\rho)^2 q_x^2}\left(\frac{1}{\delta\omega^2 + \epsilon_v^2 q^4}\right)\,. \tag{A.1.39}$$

Inserting this into A.1.35 and integrating over $\delta\omega$ gives the contribution from ω's near the $v_x q_x$ peak:

$$[C_\rho^{ET}(\mathbf{q})]_{v_\rho q_x, peak} = \frac{\rho_c^2 q_\perp^2 \Delta}{(v_v - v_\rho)^2 q_x^2}\int_{-\infty}^{\infty}\frac{d\delta\omega}{2\pi(\delta\omega^2 + \epsilon_v^2 q^4)} = \frac{\rho_c^2 q_\perp^2 \Delta}{2(v_v - v_\rho)^2 q_x^2 \epsilon_v(\theta_q) q^2}\,. \tag{A.1.40}$$

An almost identical calculation by writing

$$\omega = v_\rho q_x + \delta\omega\,. \tag{A.1.41}$$

and expanding around the other peak gives

$$[C_\rho^{ET}(\mathbf{q})]_{v_\rho q_x, peak} = \frac{\rho_c^2 q_\perp^2 \Delta}{2(v_v - v_\rho)^2 q_x^2 \epsilon(\theta_q) q^2} \,. \tag{A.1.42}$$

Adding these two together gives the total equal-time density correlation function:

$$C_\rho^{ET}(\mathbf{q}) = \frac{\rho_c^2 \Delta}{2(v_v - v_\rho)^2} \left(\frac{q_\perp^2}{q_x^2 q^2} \right) \left(\frac{1}{\epsilon_v(\theta_q)} + \frac{1}{\epsilon_\rho(\theta_q)} \right) . \tag{A.1.43}$$

Remember we've derived this for $q_x \sim q_\perp$. Therefore, we see that in that regime of wavevectors,

$$C_\rho^{ET}(\mathbf{q}) \propto \frac{1}{q^2} \,. \tag{A.1.44}$$

Recalling that our result when $q_x = 0$ for $C_\rho^{ET}(\mathbf{q})$ was $C_\rho^{ET}(\mathbf{q}) \propto \frac{1}{q^4}$, we see that there is, as we claimed, a 2 to 1 anisotropy of scaling between q_x and $q_\perp$.

To make this more precise, we can ask when does the $q_x \sim q_\perp$ result A.1.43 cross over to the $q_x = 0$ result A.1.8. This will clearly happen when the two results become comparable, that is, when

$$\frac{\rho_c^2 \Delta}{A^{3/2} q_\perp^4} \sim \frac{\rho_c^2 \Delta}{(v_v - v_\rho)^2} \left(\frac{q_\perp^2}{q_x^2 q^2} \right) \left(\frac{1}{\epsilon_v(\theta_q)} + \frac{1}{\epsilon_\rho(\theta_q)} \right) . \tag{A.1.45}$$

Let's assume, and verify a posteriori, that this happens at a value of q_x that is $<< q_\perp$; this means that $\theta_\mathbf{q} \to \frac{\pi}{2}$, and also means that $q^2 \approx q_\perp^2$.

Thus our crossover condition A.1.45 becomes

$$A^{3/2} q_\perp^4 \sim (v_v - v_\rho)^2 q_x^2 \left(\frac{1}{\epsilon_v(\theta_q)} + \frac{1}{\epsilon_\rho(\theta_q)} \right)^{-1} . \tag{A.1.46}$$

As we noted earlier, $\epsilon_v(\frac{\pi}{2})$ and $\epsilon(\frac{\pi}{2})$ are both finite, and of order typical diffusion constants. From A.1.4, we see that A is of order a typical diffusion constant squared. Hence, calling our typical diffusion constant D, A.1.46 reads

$$D^3 q_\perp^4 \sim (v_v - v_\rho)^2 q_x^2 D \,, \tag{A.1.47}$$

which implies that the corssover occurs at

$$q_x \sim \frac{D}{|v_v - v_\rho|} q_\perp^2 \,. \tag{A.1.48}$$

Thus the dominant fluctuations occur in the regime $q_x \sim q_\perp^2$, as we claimed in section 3.3.

A.2 Demonstration that the potentially dangerous irrelevance of D_x does not change the conclusion that only the u vertex is relevant near $d = 5$

In this appendix, we demonstration that the potentially dangerous irrelevance of D_x does not change the conclusion that only the u vertex is relevant near $d = 5$.

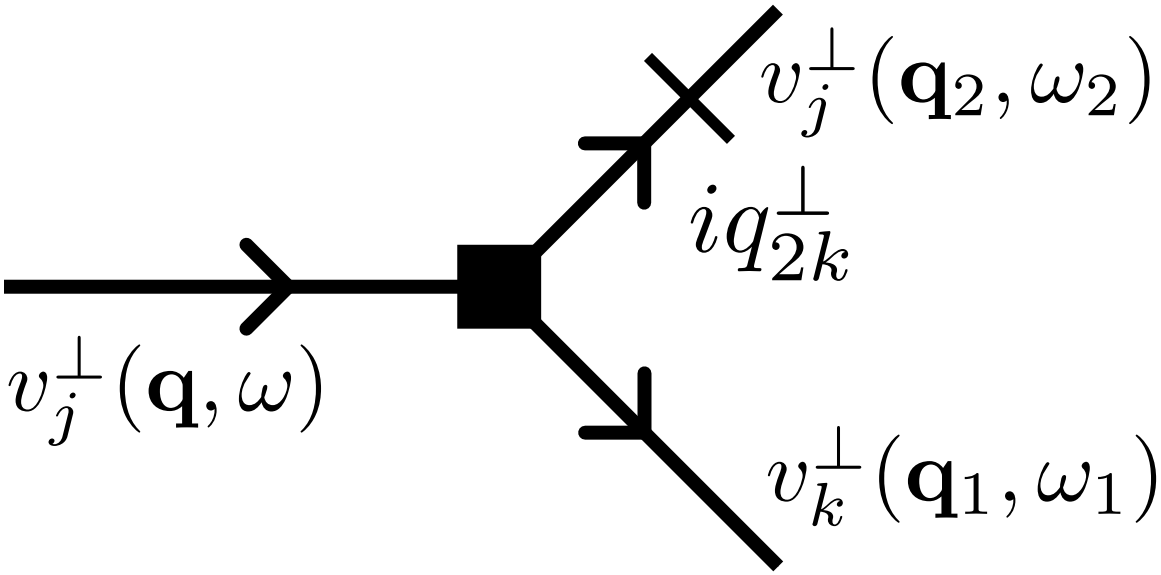

FIGURE 29. Graphical representation of the λ vertex. Unlike the u vertex, the tick mark is located after the vertex, rather than before it. In the λ term in equation 3.4.1, $\lambda(v_k q_k^\perp)v_j$, it represents the fact the $q_k^\perp$ is operating only on v_j.

We'll do this by calculating the graphical correction to $D_\perp$ coming from the λ vertex, see 29. This correction is represented by the Feynman graph shown in Figure 30, which gives for the correction to $D_\perp$: equation

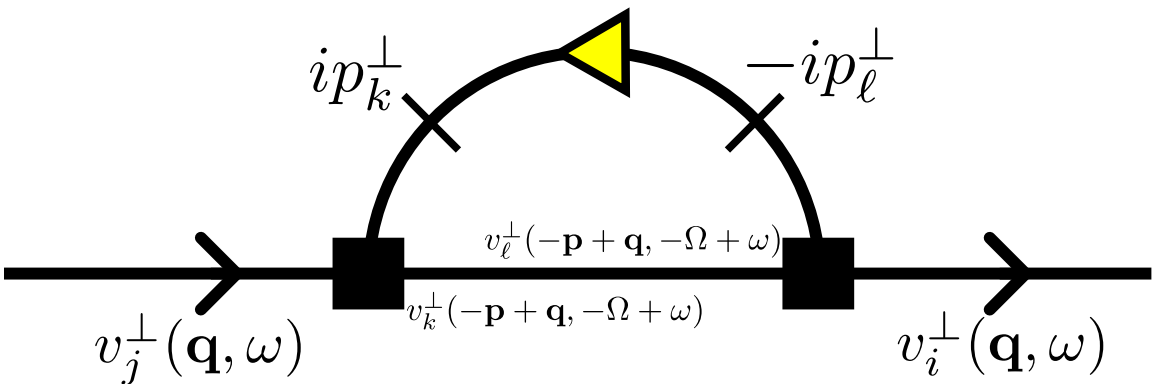

FIGURE 30. Graphical correction to D_T from two λ verticies. This graph can be made different ways.

$$\delta D_T = \lambda^2 \int_{\mathbf{q},\omega} G_{TT}(\mathbf{q},\omega) C_{TT}(\mathbf{q},\omega) \times \mathcal{O}(1) \tag{A.2.1}$$

$$= \lambda^2 \int_{\mathbf{q}_\perp} \int_{-\infty}^{\infty} \frac{dq_x}{2\pi} \int_{-\infty}^{\infty} \frac{d\omega}{2\pi} \left[\frac{1}{i(\omega - v_v q_x) + \Gamma_T} \right] \left[\frac{\Delta}{(\omega - v_v q_x)^2 + \Gamma_T^2} \right] \times \mathcal{O}(1) \tag{A.2.2}$$

$$\delta D_T = \Delta\lambda^2 \int_{\mathbf{q}_\perp} \int_{-\infty}^{\infty} \frac{dq_x}{2\pi} \int_{-\infty}^{\infty} \frac{d\omega}{2\pi} \frac{(-i(\omega - v_v q_x) + \Gamma_T)}{((\omega - v_v q_x)^2 + \Gamma_T^2)^2} \times \mathcal{O}(1) \tag{A.2.3}$$

The term proportional to ω in the numerator of this expression vanishes when integrated over ω , since it is odd in ω, while all other factors in that term are even in ω. Likewise, the term proportional to q_x in the numerator vanishes when integrated over q_x, since it is odd in q_x, while all other factors in that term are even in q_x. Thus we are left with

$$\delta D_T = \Delta\lambda^2 \int_{\mathbf{q}_\perp} \int_{-\infty}^{\infty} \frac{dq_x}{2\pi} \int_{-\infty}^{\infty} \frac{d\omega}{2\pi} \frac{\Gamma_T}{((\omega - v_v q_x)^2 + \Gamma_T^2)^2} \times \mathcal{O}(1) \tag{A.2.4}$$

The frequency integral in this expression is elementary, giving

$$\delta D_T = \Delta\lambda^2 \int_{\mathbf{q}_\perp} \int_{-\infty}^{\infty} \frac{dq_x}{\Gamma_T^2} \times \mathcal{O}(1) \tag{A.2.5}$$

$$= \Delta\lambda^2 \int_{\mathbf{q}_\perp} \int_{-\infty}^{\infty} \frac{dq_x}{(D_x q_x^2 + D_T q_\perp^2)^2} \times \mathcal{O}(1). \tag{A.2.6}$$

The q_x integral in this expression is also elementary; performing it gives:

$$\delta D_T = \frac{\Delta\lambda^2}{\sqrt{D_x D_T^3}} \int \frac{d^{d-1}q_\perp}{q_\perp^3} \times \mathcal{O}(1) \tag{A.2.7}$$

Evaluating the $dq_\perp$ integral then gives our final result:

$$\delta D_T = \frac{\Delta\lambda^2}{\sqrt{D_x D_T^3}} \Lambda^{d-4} d\ell \times \mathcal{O}(1) \tag{A.2.8}$$

This implies that the contribution to the recursion relation for D_T coming from this vertex is given by

$$\left(\frac{dD_T}{d\ell}\right)_\lambda = g_\lambda D_T \tag{A.2.9}$$

with

$$g_\lambda = \frac{\Delta\lambda^2}{\sqrt{D_x D_T^5}} \Lambda^{d-4} \times \mathcal{O}(1) \tag{A.2.10}$$

The recursion relation for g_λ can be obtained from the known recursion relations (3.4.8), (3.4.15), (3.4.13), and (3.4.20) for D_T, D_x, Δ, and λ, and is

$$g'_\lambda = b^{4-d}(g_\lambda + graphs) \tag{A.2.11}$$

from which we see that the critical dimension below which the contribution A.2.9 to D_T becomes relevant is $d = 4$. Hence, this contribution is *irrelevant* near $d = 5$.

It is straightforward to check by similar logic that all graphical corrections to all quantities coming from the fluctuations of the transverse components $\mathbf{v}_T$ of $\mathbf{v}$ are likewise irrelevant near $d = 5$, despite the potentially "dangerous irrelevance" of D_x. This completes our proof that the u vertex is the only relevant vertex near $d = 5$, and, hence, the only one we need to consider in our $5 - \epsilon$-expansion.

Bibliography

[1] Strictly speaking, we should also have included a term proportional to $\partial_x \Delta \rho^3$on the right hand side of the equation of motion for ρ.

[2] Note that the "longitudinal" and "tranverse" projection operators $L_{ij}^{\perp}(\mathbf{q}_{\perp}))$ and $P_{ij}^{\perp}(\mathbf{q}_{\perp}))$ that we define here are not quite the conventional longitudinal $(L_{ij}(\mathbf{q}))$ and transverse $(P_{ij}(\mathbf{q}))$ projection operators. The latter project along and perpendicular to the *full* wvavector $\mathbf{q}$ respectively. Our operators $L_{ij}^{\perp}(\mathbf{q}_{\perp}))$ and $(P^{\perp}(\mathbf{q}_{\perp}))_{ij}$ project *first* perpendicular to the mean velocity (i.e., perpendicular to $\hat{\boldsymbol{x}}$, or, equivalently, onto the the $\perp$ subspace), and then perpendicular to $\mathbf{q}_{\perp}$) within the $\perp$ subspace.

[3] Amnon Aharony. "Critical Behavior of Magnets with Dipolar Interactions. V. Uniaxial Magnets in d Dimensions". In: *Phys. Rev. B* 8 (7 Oct. 1973), pp. 3363–3370. DOI: 10.1103/PhysRevB.8.3363. URL: https://link.aps.org/doi/10.1103/PhysRevB.8.3363.

[4] P A Anderson and G O Mackie. "Electrically coupled, photosensitive neurons control swimming in a jellyfish". en. In: *Science* 197.4299 (July 1977), pp. 186–188.

[5] Thibault Bertrand and Chiu Fan Lee. "Diversity of phase transitions and phase separations in active fluids". In: *Phys. Rev. Res.* 4 (2 May 2022), p. L022046. DOI: 10.1103/PhysRevResearch.4.L022046. URL: https://link.aps.org/doi/10.1103/PhysRevResearch.4.L022046.

[6] E. Brézin and J. Zinn-Justin. "Critical behavior of uniaxial systems with strong dipolar interactions". In: *Phys. Rev. B* 13 (1 Jan. 1976), pp. 251–254. DOI: 10.1103/PhysRevB.13.251. URL: https://link.aps.org/doi/10.1103/PhysRevB.13.251.

[7] Antoine Bricard et al. "Emergence of macroscopic directed motion in populations of motile colloids". In: *Nature* 503.7474 (Nov. 2013), pp. 95–98. ISSN: 1476-4687. DOI: 10.1038/nature12673. URL: https://doi.org/10.1038/nature12673.

[8] Fernando Caballero and Michael E. Cates. "Stealth Entropy Production in Active Field Theories near Ising Critical Points". In: *Phys. Rev. Lett.* 124 (24 June 2020), p. 240604. DOI: 10.1103/PhysRevLett.124.240604. URL: https://link.aps.org/doi/10.1103/PhysRevLett.124.240604.

[9] Michael E. Cates and Julien Tailleur. "Motility-Induced Phase Separation". In: *Annual Review of Condensed Matter Physics* 6.1 (2015), pp. 219–244. DOI: 10.1146/annurev-conmatphys-031214-014710.

[10] P. M. Chaikin and T. C. Lubensky. *Principles of Condensed Matter Physics*. Cambridge University Press, 1995. DOI: 10.1017/CBO9780511813467.

[11] Hugues Chaté et al. "Collective motion of self-propelled particles interacting without cohesion". In: *Phys. Rev. E* 77 (4 Apr. 2008), p. 046113. DOI: 10.1103/PhysRevE.77.046113. URL: https://link.aps.org/doi/10.1103/PhysRevE.77.046113.

[12] Leiming Chen, Chiu Fan Lee, and John Toner. "Moving, Reproducing, and Dying Beyond Flatland: Malthusian Flocks in Dimensions $dgt;2$". In: *Phys. Rev. Lett.* 125 (9 Aug. 2020), p. 098003. DOI: 10.1103/PhysRevLett.125.098003. URL: https://link.aps.org/doi/10.1103/PhysRevLett.125.098003.

[13] I D Couzin and N R Franks. "Self-organized lane formation and optimized traffic flow in army ants". en. In: *Proc. Biol. Sci.* 270.1511 (Jan. 2003), pp. 139–146.

[14] Charles C Doane. *The Gypsy moth:research toward integrated pest management*. 1981.

[15] Dirk Dormann and Cornelis J Weijer. "Chemotactic cell movement during Dictyostelium development and gastrulation". In: *Current Opinion in Genetics & Development* 16.4 (2006), pp. 367–373. ISSN: 0959-437X. DOI: https://doi.org/10.1016/j.gde.2006.06.003. URL: https://www.sciencedirect.com/science/article/pii/S0959437X06001122.

[16] A Dussutour et al. "Noise improves collective decision-making by ants in dynamic environments". en. In: *Proc. Biol. Sci.* 276.1677 (Sept. 2009), pp. 4353–4361.

[17] Dieter Forster, David R. Nelson, and Michael J. Stephen. "Large-distance and long-time properties of a randomly stirred fluid". In: *Phys. Rev. A* 16 (2 Aug. 1977), pp. 732–749. DOI: 10.1103/PhysRevA.16.732. URL: https://link.aps.org/doi/10.1103/PhysRevA.16.732.

[18] Guillaume Grégoire and Hugues Chaté. "Onset of Collective and Cohesive Motion". In: *Phys. Rev. Lett.* 92 (2 Jan. 2004), p. 025702. DOI: 10.1103/PhysRevLett.92.025702. URL: https://link.aps.org/doi/10.1103/PhysRevLett.92.025702.

[19] E Hildebrand and U B Kaupp. "Sperm chemotaxis: a primer". en. In: *Ann. N. Y. Acad. Sci.* 1061 (Dec. 2005), pp. 221–225.

[20] T Hillen and K J Painter. “A user’s guide to PDE models for chemotaxis”. In: *Journal of Mathematical Biology* 58.1 (Jan. 2009), pp. 183–217.

[21] Dirk Horstmann. “From 1970 until present : the Keller-Segel model in chemotaxis and its consequences I.” In: *Jahresbericht der Deutschen Mathematiker-Vereinigung* 105.3 (2003), pp. 103–165. ISSN: 0012-0456.

[22] Patrick Jentsch and Chiu Fan Lee. “Critical phenomena in compressible polar active fluids: Dynamical and functional renormalization group studies”. In: *Phys. Rev. Res.* 5 (2 Apr. 2023), p. 023061. DOI: 10.1103/PhysRevResearch.5.023061. URL: https://link.aps.org/doi/10.1103/PhysRevResearch.5.023061.

[23] Mehran Kardar, Giorgio Parisi, and Yi-Cheng Zhang. “Dynamic Scaling of Growing Interfaces”. In: *Phys. Rev. Lett.* 56 (9 Mar. 1986), pp. 889–892. DOI: 10.1103/PhysRevLett.56.889. URL: https://link.aps.org/doi/10.1103/PhysRevLett.56.889.

[24] Evelyn F. Keller and Lee A. Segel. “Initiation of slime mold aggregation viewed as an instability”. In: *Journal of Theoretical Biology* 26.3 (1970), pp. 399–415. ISSN: 0022-5193. DOI: https://doi.org/10.1016/0022-5193(70)90092-5. URL: https://www.sciencedirect.com/science/article/pii/0022519370900925.

[25] Evelyn F. Keller and Lee A. Segel. “Model for chemotaxis”. In: *Journal of Theoretical Biology* 30.2 (1971), pp. 225–234. ISSN: 0022-5193. DOI: https://doi.org/10.1016/0022-5193(71)90050-6. URL: https://www.sciencedirect.com/science/article/pii/0022519371900506.

[26] Evelyn F. Keller and Lee A. Segel. “Traveling bands of chemotactic bacteria: A theoretical analysis”. In: *Journal of Theoretical Biology* 30.2 (1971), pp. 235–248. ISSN: 0022-5193. DOI: https://doi.org/10.1016/0022-5193(71)90051-8. URL: https://www.sciencedirect.com/science/article/pii/0022519371900518.

[27] S. K. Ma. *Modern Theory of Critical Phenomena*. Benjamin, Reading, Mass, 1995.

[28] Benoıt Mahault, Francesco Ginelli, and Hugues Chaté. “Quantitative Assessment of the Toner and Tu Theory of Polar Flocks”. In: *Phys. Rev. Lett.* 123 (21 Nov. 2019), p. 218001. DOI: 10.1103/PhysRevLett.123.218001. URL: https://link.aps.org/doi/10.1103/PhysRevLett.123.218001.

[29] M. C. Marchetti et al. “Hydrodynamics of soft active matter”. In: *Reviews of Modern Physics* 85.3 (July 2013), pp. 1143–1189. DOI: 10.1103/RevModPhys.85.1143.

[30] N. D. Mermin and H. Wagner. “Absence of Ferromagnetism or Antiferromagnetism in One- or Two-Dimensional Isotropic Heisenberg Models”. In: *Phys. Rev. Lett.* 17 (22 Nov. 1966). ; P. C. Hohenberg, Phys. Rev. **158**, 383 (1967); N. D. Mermin, J. Math. Phys. **8**, 1061 (1967)., pp. 1133–1136. DOI: 10.1103/PhysRevLett.17.1133. URL: https://link.aps.org/doi/10.1103/PhysRevLett.17.1133.

[31] R Mesibov and J Adler. “Chemotaxis toward amino acids in Escherichia coli”. en. In: *J. Bacteriol* 112.1 (Oct. 1972), pp. 315–326.

[32] Maxx Miller and John Toner. “Following Your Nose: Autochemotaxis and Other Mechanisms for Spinodal Decomposition in Flocks”. In: *Phys. Rev. Lett.* 132 (12 Mar. 2024), p. 128301. DOI: 10.1103/PhysRevLett.132.128301. URL: https://link.aps.org/doi/10.1103/PhysRevLett.132.128301.

[33] Maxx Miller and John Toner. “Spinodal decomposition and phase separation in polar active matter”. In: *Phys. Rev. E* 109 (3 Mar. 2024), p. 034606. DOI: 10.1103/PhysRevE.109.034606. URL: https://link.aps.org/doi/10.1103/PhysRevE.109.034606.

[34] Shradha Mishra, Aparna Baskaran, and M. Cristina Marchetti. “Fluctuations and pattern formation in self-propelled particles”. In: *Phys. Rev. E* 81 (6 June 2010), p. 061916. DOI: 10.1103/PhysRevE.81.061916. URL: https://link.aps.org/doi/10.1103/PhysRevE.81.061916.

[35] Claude-Louis Navier. “Sur les lois des mouvements des fluides, en ayant égard à l’adhésion des molecules”. In: *Annales de chimie et de physique* 19 (1821), pp. 244–260.

[36] M Pline, J A Diez, and D B Dusenbery. “Extremely Sensitive Thermotaxis of the Nematode Meloidogyne incognita”. en. In: *J Nematol* 20.4 (Oct. 1988), pp. 605–608.

[37] Sriram Ramaswamy. “The Mechanics and Statistics of Active Matter”. In: *Annual Review of Condensed Matter Physics* 1.1 (2010), pp. 323–345. DOI: 10.1146/annurev-conmatphys-070909-104101.

[38] Holger Stark. “Artificial Chemotaxis of Self-Phoretic Active Colloids: Collective Behavior”. en. In: *Acc. Chem. Res.* 51.11 (Oct. 2018), pp. 2681–2688.

[39] J.B. Stock and M.D. Baker. "Chemotaxis". In: *Encyclopedia of Microbiology (Third Edition)*. Ed. by Moselio Schaechter. (Academic Press, Oxford, 2009), pp.71-78. ISBN: 978-0-12-373944-5. DOI: https://doi.org/10.1016/B978-012373944-5.00068-7. URL: https://www.sciencedirect.com/science/article/pii/B9780123739445000687.

[40] John Toner. "Birth, Death, and Flight: A Theory of Malthusian Flocks". In: *Phys. Rev. Lett.* 108 (8 Feb. 2012), p. 088102. DOI: 10.1103/PhysRevLett.108.088102. URL: https://link.aps.org/doi/10.1103/PhysRevLett.108.088102.

[41] John Toner. "Reanalysis of the hydrodynamic theory of fluid, polar-ordered flocks". In: *Phys. Rev. E* 86 (3 Sept. 2012), p. 031918. DOI: 10.1103/PhysRevE.86.031918. URL: https://link.aps.org/doi/10.1103/PhysRevE.86.031918.

[42] John Toner and Yuhai Tu. "Flocks, herds, and schools: A quantitative theory of flocking". In: *Phys. Rev. E* 58 (4 Oct. 1998), pp. 4828–4858. DOI: 10.1103/PhysRevE.58.4828. URL: https://link.aps.org/doi/10.1103/PhysRevE.58.4828.

[43] John Toner and Yuhai Tu. "Long-Range Order in a Two-Dimensional Dynamical XY Model: How Birds Fly Together". In: *Phys. Rev. Lett.* 75 (23 Dec. 1995), pp. 4326–4329. DOI: 10.1103/PhysRevLett.75.4326. URL: https://link.aps.org/doi/10.1103/PhysRevLett.75.4326.

[44] John Toner, Yuhai Tu, and Sriram Ramaswamy. "Hydrodynamics and phases of flocks". In: *Annals of Physics* 318.1 (2005). Special Issue, pp. 170–244. ISSN: 0003-4916. DOI: https://doi.org/10.1016/j.aop.2005.04.011. URL: https://www.sciencedirect.com/science/article/pii/S0003491605000540.

[45] Chad M Topaz et al. "Locust dynamics: behavioral phase change and swarming". en. In: *PLoS Comput. Biol.* 8.8 (Aug. 2012), e1002642.

[46] Yuhai Tu, John Toner, and Markus Ulm. "Sound Waves and the Absence of Galilean Invariance in Flocks". In: *Phys. Rev. Lett.* 80 (21 May 1998), pp. 4819–4822. DOI: 10.1103/PhysRevLett.80.4819. URL: https://link.aps.org/doi/10.1103/PhysRevLett.80.4819.

[47] Tamás Vicsek et al. "Novel Type of Phase Transition in a System of Self-Driven Particles". In: *Phys. Rev. Lett.* 75 (6 Aug. 1995), pp. 1226–1229. DOI: 10.1103/PhysRevLett.75.1226. URL: https://link.aps.org/doi/10.1103/PhysRevLett.75.1226.